LA-9468-PR
Progress Report

Los Alamos National Laboratory is operated by the University of California for the United States Department of Energy under contract W-7405-ENG-36.

Applied Nuclear Data Research and Development

October 1, 1981—March 31, 1982

Los Alamos
Los Alamos National Laboratory
Los Alamos, New Mexico 87545

The four most recent reports in this series, unclassified, are LA-8757-PR, LA-8874-PR, LA-9060-PR and LA-9262-PR.

This work was performed under the auspices of the US Department of Energy's Division of Reactor Research and Technology, Office of Basic Energy Sciences, and Office of Fusion Energy; the Spent Fuel Project Office under the technical direction of the Savannah River Laboratory; the Electric Power Research Institute; and the Nuclear Regulatory Commission.

LA-9468-PR
Progress Report

UC-34c
Issued: August 1982

Applied Nuclear Data Research and Development

October 1, 1981—March 31, 1982

Compiled by
P. G. Young

Los Alamos
Los Alamos National Laboratory
Los Alamos, New Mexico 87545

CONTENTS

APPLIED NUCLEAR DATA RESEARCH AND DEVELOPMENT
SEMIANNUAL PROGRESS REPORT
October 1, 1981 - March 31, 1982

Compiled by

P. G. Young

ABSTRACT

This progress report describes the activities of the Los Alamos Nuclear Data Group for October 1, 1981, through March 31, 1982. The topical content is summarized in the Table of Contents.

I. THEORY AND EVALUATION OF NUCLEAR CROSS SECTIONS

A. Peripheral Effects in R-Matrix Theory (G. M. Hale)

The spinless, one-dimensional treatment of peripheral effects in R-matrix theory described in a previous report[1] has been generalized to the case of three dimensions and finite-mass transferred particles, including spin. As they do in the one-dimensional case, peripheral overlap effects in this case lead to "particle-exchange" poles in the R matrix for proper choice of the boundary conditions, which have the form

$$R_{12}^{x} = R_{21}^{x} = \frac{-(-1)^{\ell} C_1 C_2 d_s W_\ell(a_1,a_2)}{\varepsilon_x - \varepsilon} \quad .$$

Here W_ℓ is a projection of the overlapping bound states on the channel surface that acts as a sort of ℓ-dependent "width" for particle exchange; d_s is a spin-function overlap factor; C_1 and C_2 are dimensionless normalization constants

for the asymptotic tails of the bound-state wavefunctions; and ε_x is the position of the pole, which is always negative, and depends only on the binding energies and masses of the particles.

The type of term described above is unconventional in R-matrix theory for two reasons. In a reaction, it contributes only to the off-diagonal elements of the R matrix, whereas the usual resonance poles that contribute to a reaction necessarily have non-zero diagonal elements. For elastic scattering, due to the $(-1)^{\ell}$ factor that is characteristic of particle exchange, the residues of the pole alternate sign with ℓ, whereas the residues of conventional resonance poles all have the same sign for elastic scattering. These characteristics can give, in general, a different behavior of the collision matrix from that obtainable from conventional R-matrix theory, while preserving its properties of unitarity and symmetry. One result, for instance, would be more pronounced backward peaking in elastic differential cross sections at low energies than can be obtained from the conventional theory at a given radius.

We are currently applying the revised theory including peripheral effects to an analysis of reactions in the ^{7}Li system. The contribution of the deuteron exchange pole to the ^{6}Li(n,t) reaction appears to account for a significant amount of 1/v cross section at low energies. We plan next to consider the effects of the deuteron exchange pole on p-^{3}He and n-T elastic scattering where it may provide the increased backward peaking needed to describe adequately precise measurements of the p-^{3}He differential cross section at low energies, and possibly explain the rather poorly understood behavior of the s-waves for n-T scattering at low energies.

B. Charged-Particle Elastic Cross Sections [G. M. Hale, D. C. Dodder, and J. C. De Veaux (U. Illinois)]

The slowing down of charged particles in a plasma has, in the past, concerned particles with energies sufficiently low to assume that the dominant mechanism is Coulomb elastic scattering. However, current fusion studies are sometimes concerned with the slowing down of fast ions, in which the nuclear components of the scattering are important at large angles, and enter even at small angles through interference with the Coulomb amplitude. Using a format developed at Los Alamos that allows an exact Legendre polynomial representation of $\sigma_{NI}(\mu)$, the difference of the elastic scattering cross section and the Rutherford (or "pure Coulomb") cross section at $\mu = \cos\theta_{CM}$, we are constructing

a file of elastic cross sections for most of the possible interactions between light ions from protons through alpha particles, at energies up through several MeV.

The cross sections are calculated from parameters obtained over the years from the extensive Los Alamos program of R-matrix analyses of light systems, and are generally based on large data bases that contain many other measurements in addition to elastic cross sections. R-matrix theory provides an explicit separation of nuclear and Coulomb effects in the cross section, and reasonable extrapolations to low energies, particularly in the presence of low-lying resonances, as in the case of d-T scattering.

Figure 1 shows the results of various integrals involving $\sigma_{NI}(\mu)$ for d-T scattering, compared to evaluations at Livermore reported by Perkins and Cullen.[2]

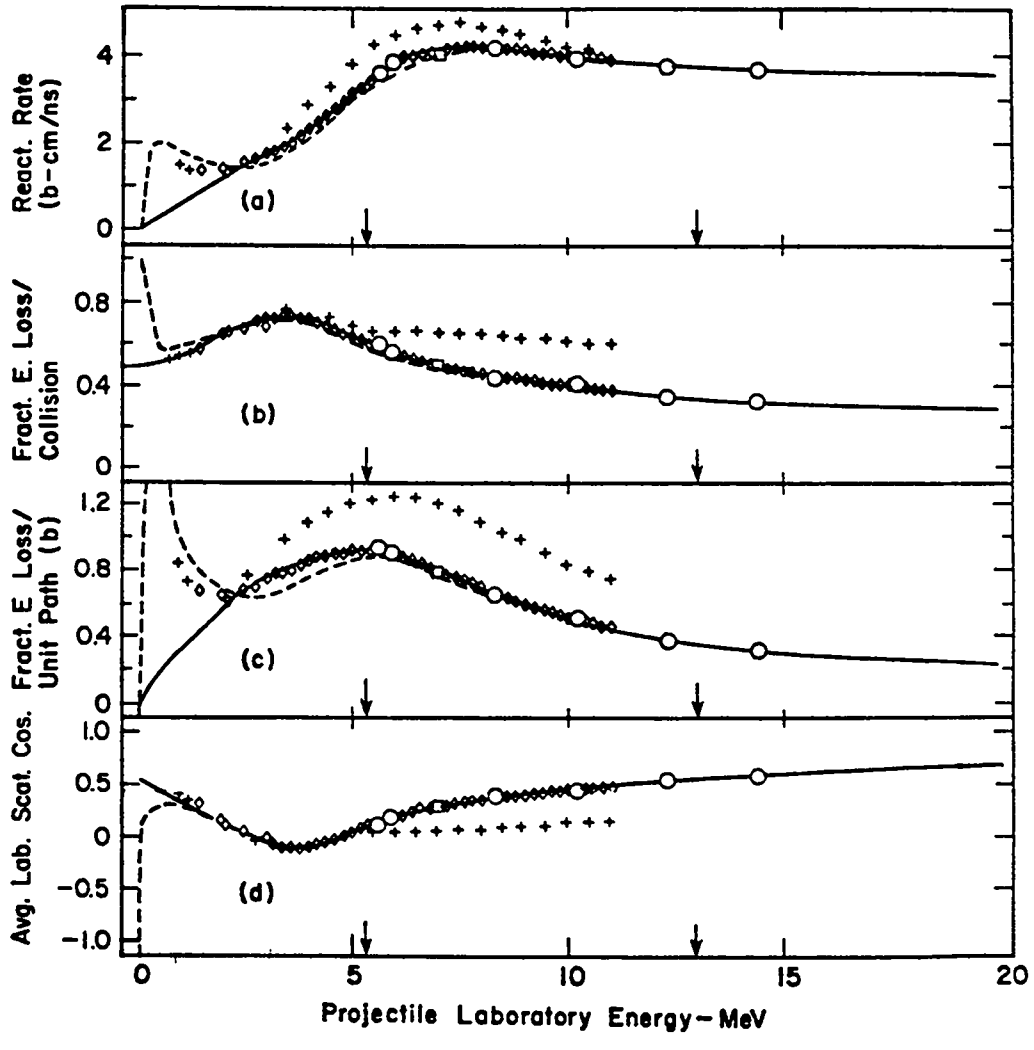

Fig. 1. Integrals of $\sigma_{NI}(\mu)$ for d-T scattering. The solid curves are the evaluations of Perkins and Cullen; the dashed curves are calculated from Los Alamos cross sections; and the points represent experimental data.

The solid curves are the Livermore results and the dashed curves are the Los Alamos calculations. In both cases, the upper limits of the integrals over μ are given by min (.94, μ_o), where $\sigma_{NI}(\mu_o) = 0$, in order to define values of the integrals that correspond to positive integrated cross sections. The integral quantities are seen to disagree substantially in the region of the low-energy d-T resonance where the Livermore extrapolations to zero energy are somewhat oversimplified owing to the lack of elastic cross-section data.

C. Energy-Angle Correlated Emission Spectra from the D(n,2n)P Reaction (P. G. Young)

The existing ENDF/B-V evaluation for neutron reactions on deuterium uses a representation for the D(n,2n)P reaction that ignores the pronounced energy-angle correlations in the secondary neutron spectra. This limitation is caused by format and processing code restrictions on Version V of ENDF/B. In order to investigate possible effects in applied problems from errors in the emission spectra, a modified version of the ENDF/B-V evaluation has been developed that uses a simple model to specify energy-angle correlations in the (n,2n) neutron emission spectra.

Using a technique first employed[3] to represent energy-angle data from the ^{9}Be(n,2n) reaction, the D(n,2n) reaction in the ENDF/B-V evaluation was recast into a special excitation-energy-bin format that uses the reaction designators MT = 51-87 to represent the data. In this formulation the MT = 4 cross section, which is the sum of MT = 51-87, actually represents the (n,2n) reaction. In computing an emission spectrum, however, each of the MT = 51-87 cross sections must be doubled because two neutrons are emitted per reaction. The NJOY processing code properly accounts for this effect, and the kinematic energy-angle correlations are automatically preserved in the processing because of the MT = 51-87 level representation.

The excitation-energy-bin representation was implemented using a simple 3-body phase space model to apportion the cross section among the MT = 51-87 reaction types. This model has been found to reasonably describe measured spectra from the D(n,2n) reaction and certainly approximates the kinematics of the reaction far better than does ENDF/B-V. Isotropic angular distributions were assumed in the center-of-mass system for each of the MT = 51-87 energy bins, and the sum of the reaction was normalized to the ENDF/B-V D(n,2n) cross section. All other data in the revised evaluation are taken from ENDF/B-V.

A comparison between neutron emission spectra calculated from the present work and ENDF/B-V is shown in Fig. 2 for an incident neutron energy of 15 MeV and for θ_{LAB} = 0°, 90°, and 180°. The peak at higher energy in each spectrum is elastic scattering, and the lower energy distribution results from the (n,2n) reaction. The problem with the energy-angle uncorrelated representation for ENDF/B-V is evident in Fig. 2.

Included in Table I is a comparison of the average neutron emission energies for E_n = 5, 10, 15 MeV and θ_{LAB} = 0°, 90°, 180°. Large differences between ENDF/B-V and the present work are evident, especially for the (n,2n) reaction but also for the total energy [elastic plus (n,2n)].

The new evaluation will be provided to the ENDF/A library at the National Nuclear Data Center in Brookhaven. The evaluation is being processed with the NJOY code[4] and will be made available in MATXS format at the National Magnetic Fusion Energy Computer Center at Livermore.

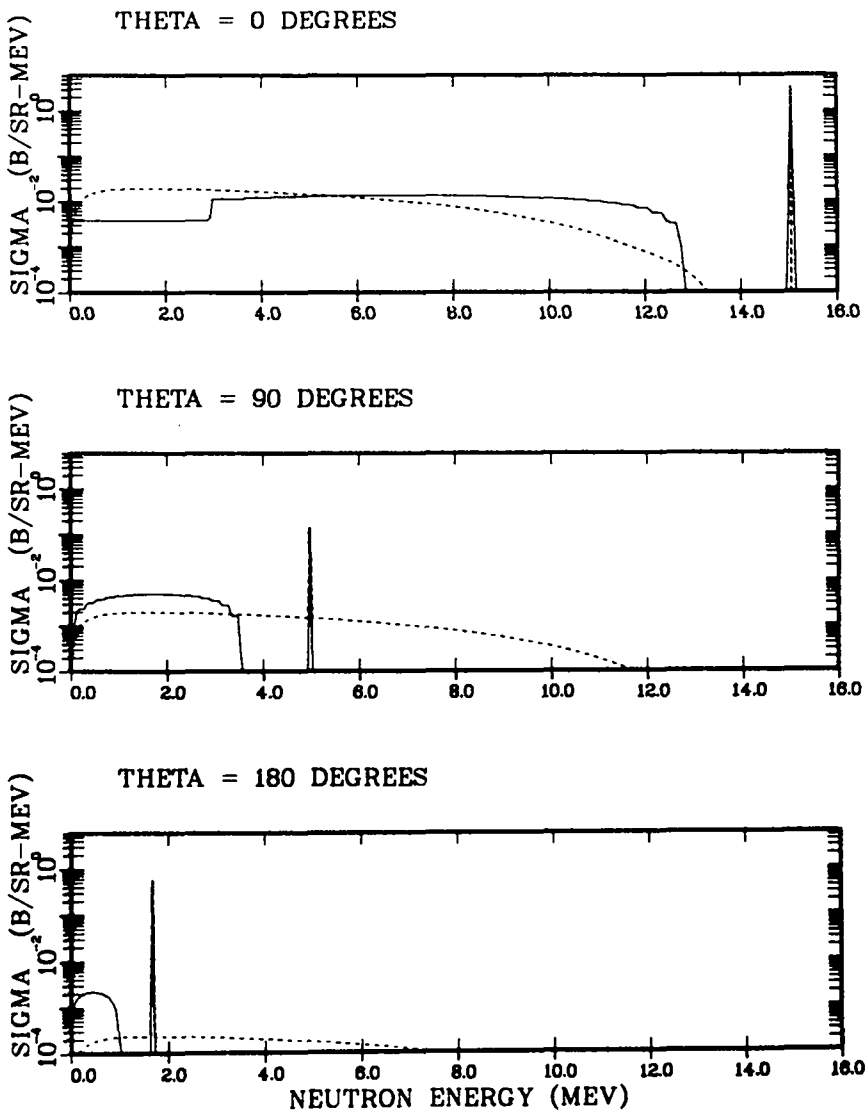

Fig. 2. Neutron emission spectra at 3 angles from the D(n,2n)P reaction with 15-MeV incident neutrons. The solid curve was calculated from the present evaluation and the dashed curve from ENDF/B-V.

TABLE I

COMPARISON OF AVERAGE SECONDARY NEUTRON ENERGIES FROM ENDF/B-V AND THE PRESENT EVALUATION FOR THE (n,2n) REACTION AND FOR THE TOTAL EMISSION SPECTRUM

		ENDF/B-V		LA-82			
E_n (MeV)	θ	$E_{n,2n}$ (MeV)	E_{total} (MeV)	$E_{n,2n}$ (MeV)	E_{total} (MeV)	$\Delta_{n,2n}$ (%)	Δ_{total} (%)
5	0°	0.955	4.684	1.301	4.716	36.2	0.7
	90°	0.955	1.673	0.092	1.662	-90.3	-0.7
	180°	0.0	0.575	0.025	0.575	—	0
10	0°	2.613	8.493	4.116	8.858	57.5	4.3
	90°	2.613	3.087	0.931	2.520	-64.4	-18.4
	180°	2.613	1.146	0.219	1.100	-91.6	-4.0
15	0°	4.273	11.863	6.895	12.739	61.4	7.4
	90°	4.273	4.509	1.760	2.839	-58.8	-37.0
	180°	4.273	1.819	0.477	1.606	-88.8	-11.7

D. New ENDF/B-V Evaluation of n+^{7}Li Reactions (P. G. Young)

A new evaluation of neutron-induced reactions on ^{7}Li has been completed and submitted to the National Nuclear Data Center at Brookhaven for Revision 2 of the ENDF/B-V evaluated data library. The new evaluation includes a variance-covariance analysis of the major reaction cross sections, a complete reanalysis of all elastic and inelastic angular distribution data, a division of the (n,nt) cross section into a series of excitation energy bins that permit inclusion of accurate energy-angle correlations for emission neutrons, and complete covariance files for all cross-section data and (n,nt) neutron emission spectra.

The variance-covariance analysis has been described previously[5,6] and will not be detailed here. Basically, the analysis utilized the GLUCS code system, developed at Oak Ridge National Laboratory,[7] to perform variance-covariance analyses of each of the major cross-section types for which experimental data exist. The results of this analysis were then combined using the Los Alamos code ALVIN[8] under the constraint that all partial reactions sum to the total cross section, with full account being taken of all covariances.

The evaluated elastic and inelastic neutron angular distributions were obtained from a Legendre coefficient analysis of all the available experimental data. The experiments of Lane et al.,[9] Knitter and Coppola,[10] Knox et al.,[11] Knox and Lane,[12] and Hogue et al.[13] were emphasized in the elastic angular distribution evaluation. Figure 3 compares the measurements of Hogue et al. at 4 energies to the new evaluation. Because there are no elastic angular distribution data above 14.1 MeV, a spherical optical model calculation was used to extrapolate the angular distributions to 20 MeV. The resulting parameters are given in Ref. 5.

Because the customary representations used for ENDF/B evaluations do not permit inclusion of energy-angle correlation effects in secondary neutron emission data from (n,xn) reactions, we used an excitation-energy binning technique to represent the ^{7}Li(n,nt) reaction. With this technique the continuum neutrons from (n,nt) reactions are described as a series of lumped, discrete scattering levels, each representing a bin of excitation energy in the residual nucleus and each with a separate energy-dependent cross section and angular distribution. When these data are processed into multigroup form, the kinematic energy-angle correlations are automatically preserved.

The evaluation of the (n,nt) data into excitation energy bins was based upon the neutron emission spectrum measurements of Lisowski et al.[14] using monoenergetic neutrons from the Los Alamos Tandem Van de Graaff at 6, 10, and 14 MeV. The results are compared in Fig. 4 to the spectra measured at the Oak Ridge Electron Linear Accelerator (ORELA) by Morgan[15] at 55° and 125° for an incident neutron energy bin of 12.45-14.95 ($\bar{E}$ = 13.7) MeV. The broad peaks at higher energy are from elastic scattering, and the lower energy spectra result from the (n,nt) reaction.

Complete covariance files for the major cross-section types and for the excitation energy bins are included in the evaluation. The latter data determine the correlated errors in the neutron emission spectra from the (n,nt) reaction. Covariances for the cross sections were taken directly from the GLUCS-ALVIN analysis, when possible, and are based on those results for all major reaction types. The errors and cross correlations for the emission spectra were estimated from the Lisowski[14] experimental errors, but the final results were adjusted via the ALVIN code to be consistent with results from the independent GLUCS-ALVIN cross-section analysis.

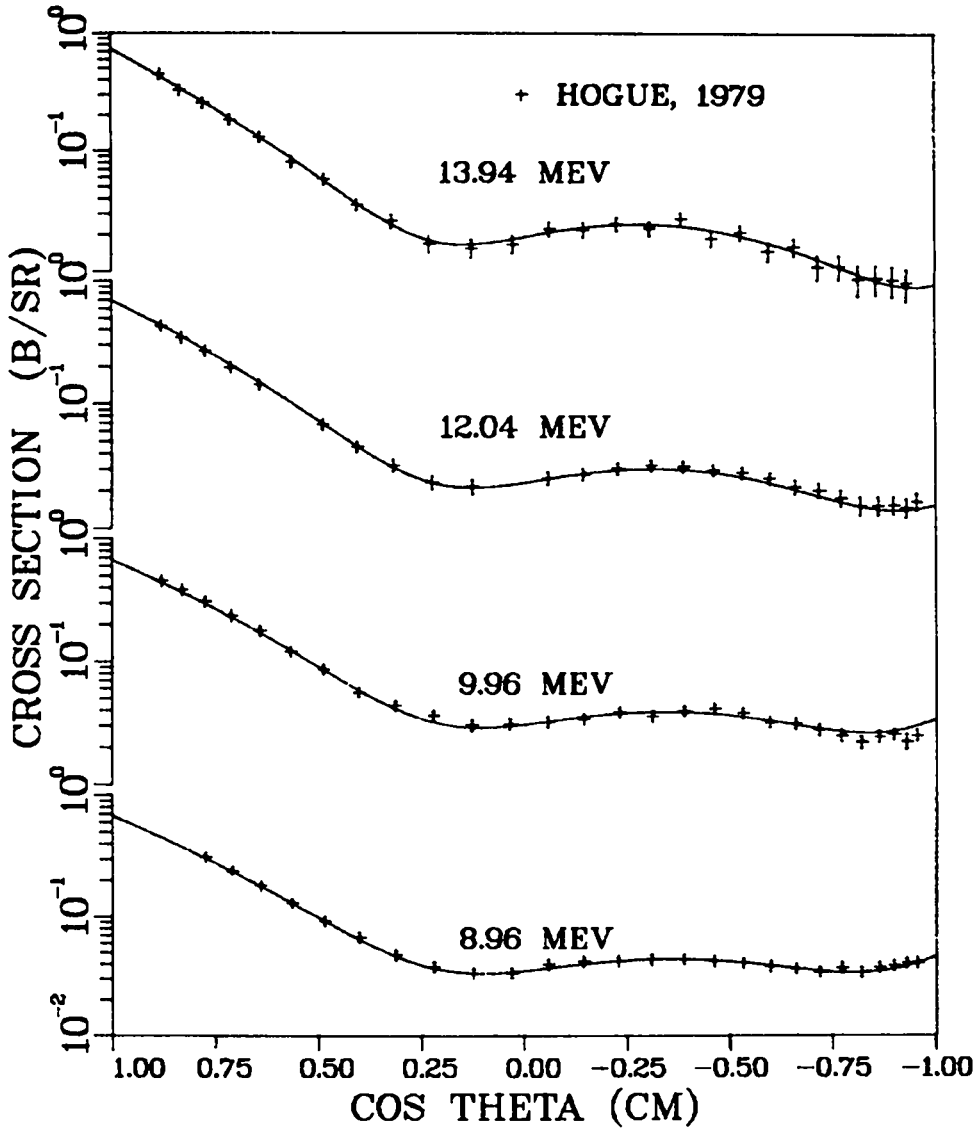

Fig. 3. Comparison of the n+^{7}Li elastic angular distribution measurement by Hogue et al.[13] to the present evaluation. Both measurement and evaluation include the ^{7}Li(n,n') reaction to the first excited state of ^{7}Li.

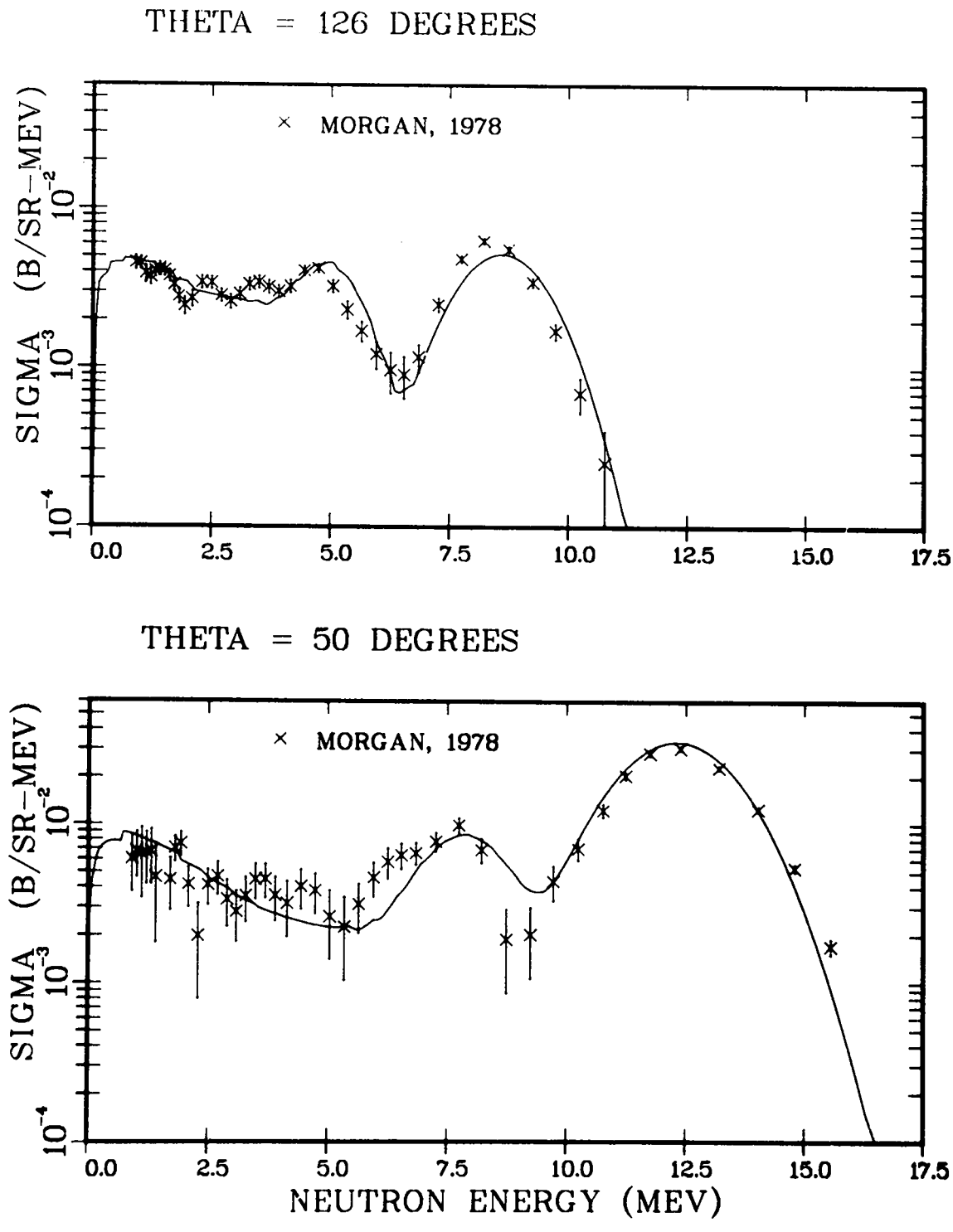

Fig. 4. Measured and evaluated neutron emission spectra from n+^{7}Li reactions with 13.7-MeV incident neutrons.

E. Calculation of Proton Emission Spectra from p+^{91}Zr and p+^{87}Sr Reactions (E. D. Arthur)

Recently, experimental measurements have begun at the Los Alamos Tandem Van de Graaff of the proton emission spectra from p+^{91}Zr and p+^{87}Sr reactions for proton energies between 12 and 18 MeV. Reactions on these nuclei produce compound systems having large "proton windows" resulting from proton binding energies that are appreciably less than those for neutrons. Such measurements, particularly for the p+^{87}Sr system, can provide information relevant to our theoretical analysis of n+^{87}Y reactions, especially for those reactions involving low-energy proton emission.

Because of target contaminent problems for ^{87}Sr, it is not possible to measure directly the low-energy protons from (p,np) and (p, pn) reactions that are of interest for our nuclear model calculations. Instead, these protons must be detected in coincidence with a neutron, which introduces complications in the analysis of such data resulting from neutron detector threshold and efficiency effects. In order to compare directly to such data, we have modified the code[16] that disentangles particle emission spectra produced in our nuclear model calculations using the GNASH preequilibrium Hauser-Feshbach code. We are now able to calculate the proton emission spectrum in "coincidence" with neutron emission, while including a mockup of the neutron detector characteristics in the formulation of the "coincidence" requirement. Figure 5 illustrates our calculated emission spectrum for low-energy protons resulting from (p,np) and (p,pn) reactions induced by 16-MeV protons on ^{91}Zr. The solid curve includes no neutron detector effects, while the dashed curve includes a threshold and efficiency similar to that used in the experimental measurements. Such detector effects prevent the detection of higher energy protons associated with the emission of a low-energy neutron. They also distort significantly the proton emission spectrum resulting from the (p,pn) reaction. Overall inclusion of these effects produces a qualitative shape agreement to preliminary proton emission spectra from this experiment that would be lacking otherwise.

F. Thulium Cross-Section Calculations (E. D. Arthur)

We have noted that the low-energy reaction cross sections obtained from our coupled-channel calculations[17] on ^{169}Tm do not agree with results obtained from optical model calculations using the Moldauer[18] optical model set. Even though the Moldauer parameters are spherical ones, they were obtained from fits to low-energy neutron data and generally reproduce quite successfully

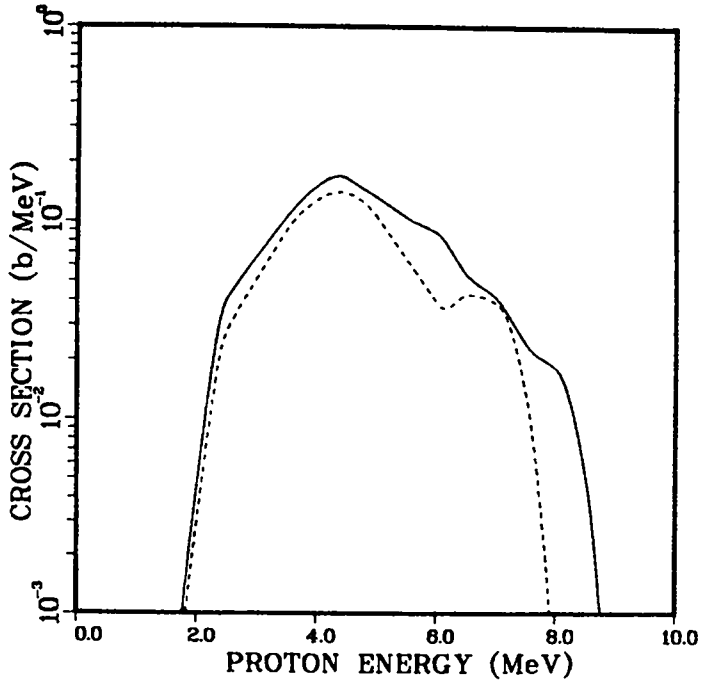

Fig. 5. Comparison of calculated proton emission spectra resulting from 16-MeV proton reactions on ^{91}Zr. The comparison is restricted to protons associated with neutron emission [sum of (p,np) and (p,pn) contributions]. The dashed and solid curves illustrate spectra calculated with and without inclusion of neutron detector effects.

total cross sections, s- and p-wave strengths, and potential scattering radii for energies below a few MeV. In Fig. 6 we compare nonelastic cross sections obtained from these two parameter sets. Similar comparisons are made in Fig. 7 for the ^{165}Ho total cross section, where the coupled-channel parameters used in our n+ ^{169}Tm calculations[17] produce much better agreement to the experimental data. Comparisons to s- and p-wave strength data for ^{165}Ho and ^{169}Tm yield similar results. Our conclusions are that, even though the Moldauer optical parameters produce good agreement to data for nuclei up to A = 140, they are not adequate for use with permanently deformed nuclei in this region of the periodic table.

To further test the nuclear models and their parameters, experimental measurements[19] have been made recently of the 14-MeV (n,2n) cross section on the unstable ^{168}Tm isotope. Our calculations are compared to preliminary results from this experiment in Fig.8. The good agreement indicates that our parameters work well for this nucleus and show, indirectly, that the total direct-reaction component of the inelastic scattering cross section is comparable to that for ^{169}Tm, even though a well-defined rotational structure does not exist for ^{168}Tm.

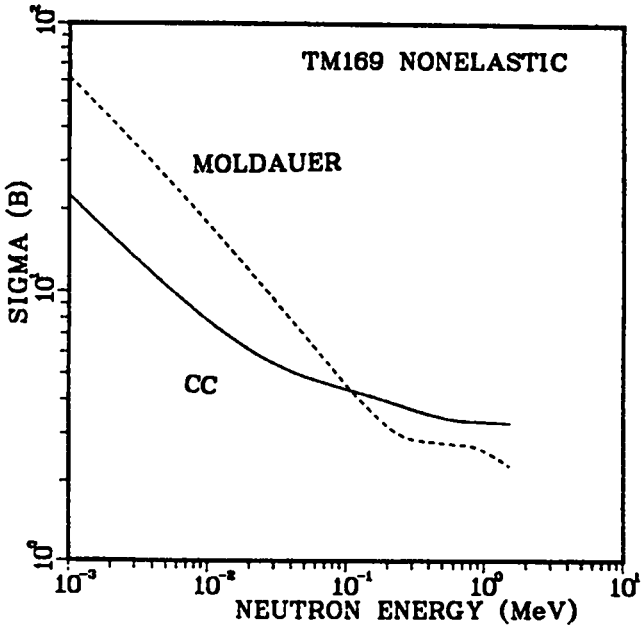

Fig. 6. A comparison of n+^{169}Tm non-elastic cross sections obtained using the coupled-channel optical parameters of Ref. 18 (solid curve) and the Moldauer optical model set.

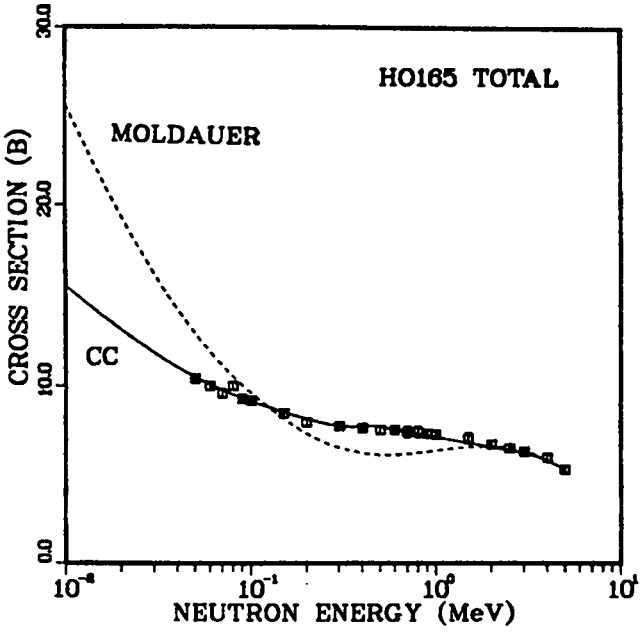

Fig. 7. A similar comparison as that for Fig. 6 to total cross-section data available for ^{165}Ho.

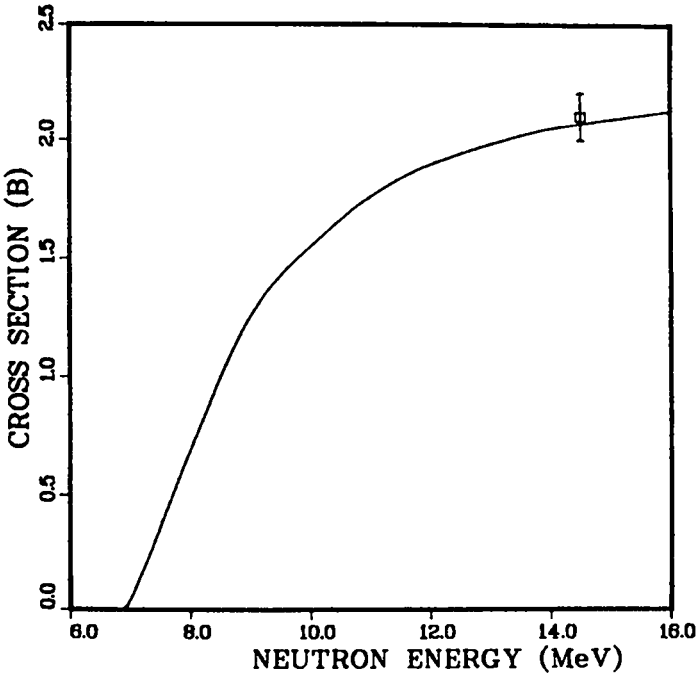

Fig. 8. The calculated ^{168}Tm(n,2n) cross section is compared to preliminary experimental data for this reaction at 14 MeV.

G. Production of a New Evaluation for Natural Tungsten between 0.1 and 20 MeV (E. D. Arthur and P. G. Young)

An evaluated data file for neutron reactions on natural tungsten between 0.1 and 20 MeV has been made through combination of new evaluations for the $^{182,183,184,186}W$ isotopes completed recently.[20,21] The resultant file has been checked through numerous comparisons to experimental data and through use of ENDF checking codes available from Brookhaven National Laboratory.

Since the elemental tungsten evaluated data file was constructed through use of the isotopic evaluations, which were in turn based on extensive model calculations, a direct link may not always exist between this new natural evaluation and data measured for natural tungsten. We have instead relied on the quality and consistency of the isotopic experimental data along with constraints introduced through our application of the relevant nuclear models. The success of this technique is illustrated through comparison of the evaluation to experimental data available for the major reaction channels of natural tungsten.

Figure 9 compares our evaluated total cross section (solid curve) to experimental data and to the ENDF-B/V evaluation (dashed curve). A similar comparison is shown in Fig. 10 for the elastic cross section. Numerous experimental measurements have been made of neutrons elastically scattered from natural tungsten, but some of the more recent and complete sets of such measurements are those of Kinney.[22] We compare to these angular distributions in Fig. 11. Within these comparisons there is general agreement between our evaluation and experimental total and elastic cross-section data. Such agreement, along with isotopic data, implies realistic values for the total reaction cross section. Since (n,xn) cross sections are a major constitutent of the total reaction cross section, we compare the evaluated cross sections in Fig. 12 to recent data available for (n,2n) and (n,3n) reactions from threshold to 20 MeV. Again, reasonable agreement is obtained.

A major deficiency of the ENDF/B-V evaluation was the significant underprediction of portions of the neutron emission spectrum caused by failure to consider the influence of preequilibrium processes at incident energies above 10 MeV. In the present evaluation this deficiency has been rectified as shown in Fig. 13, where the evaluated spectrum is compared to several neutron emission measurements performed around 14 MeV. The agreement is good particularly with the precise data recently measured by Vonach.[23]

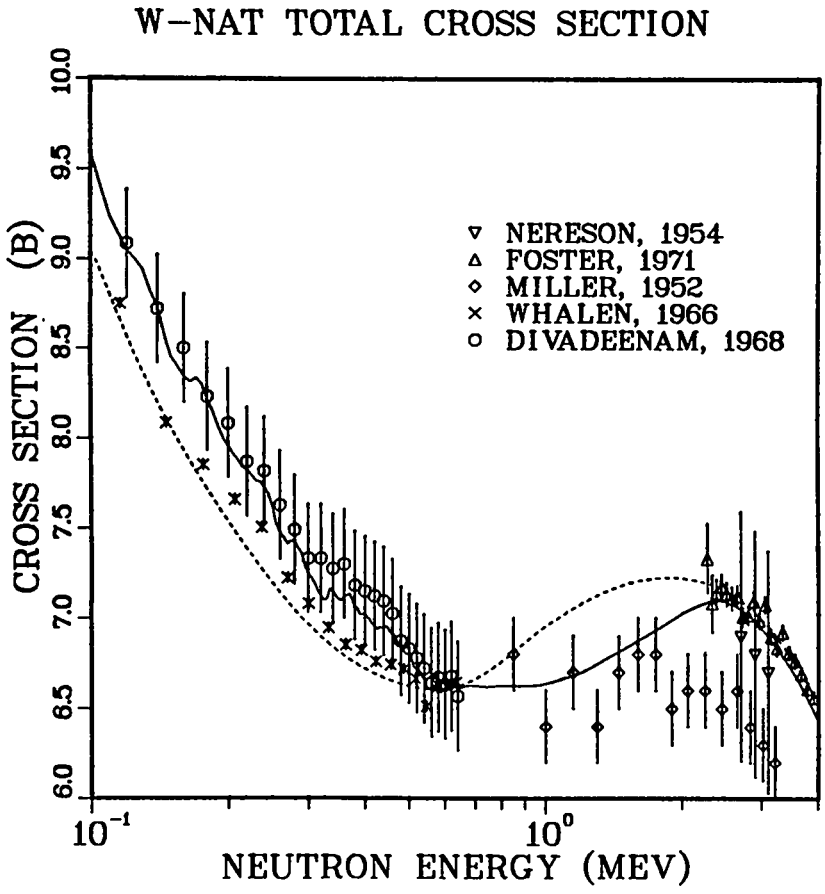

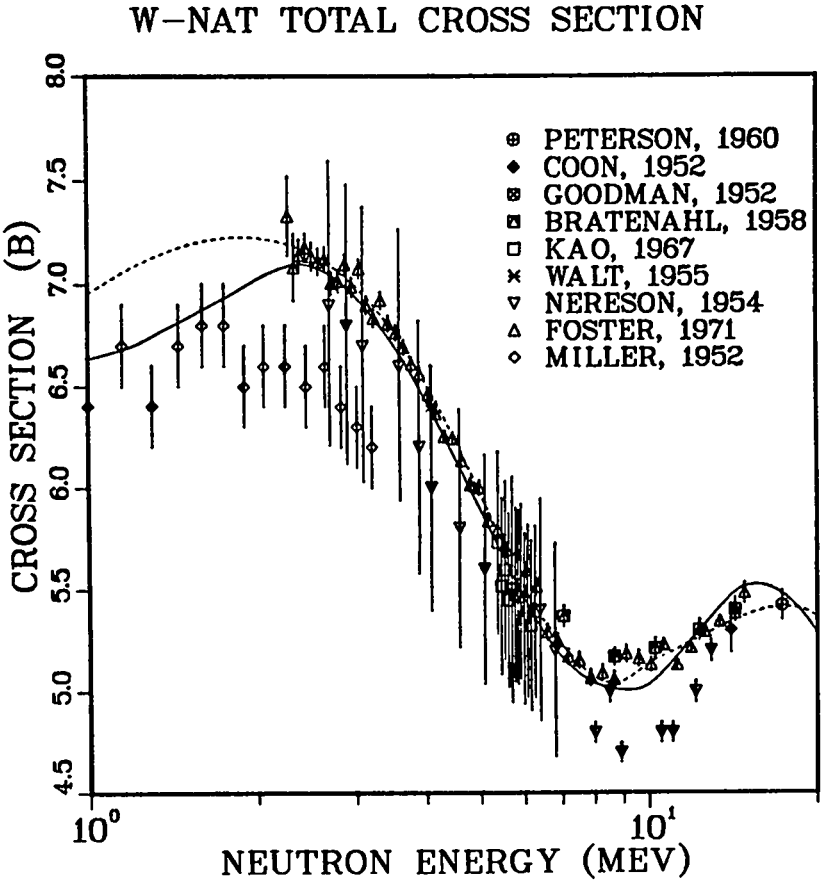

Fig. 9. Evaluated total cross sections for natural tungsten. The dashed curve is ENDF/B-V.

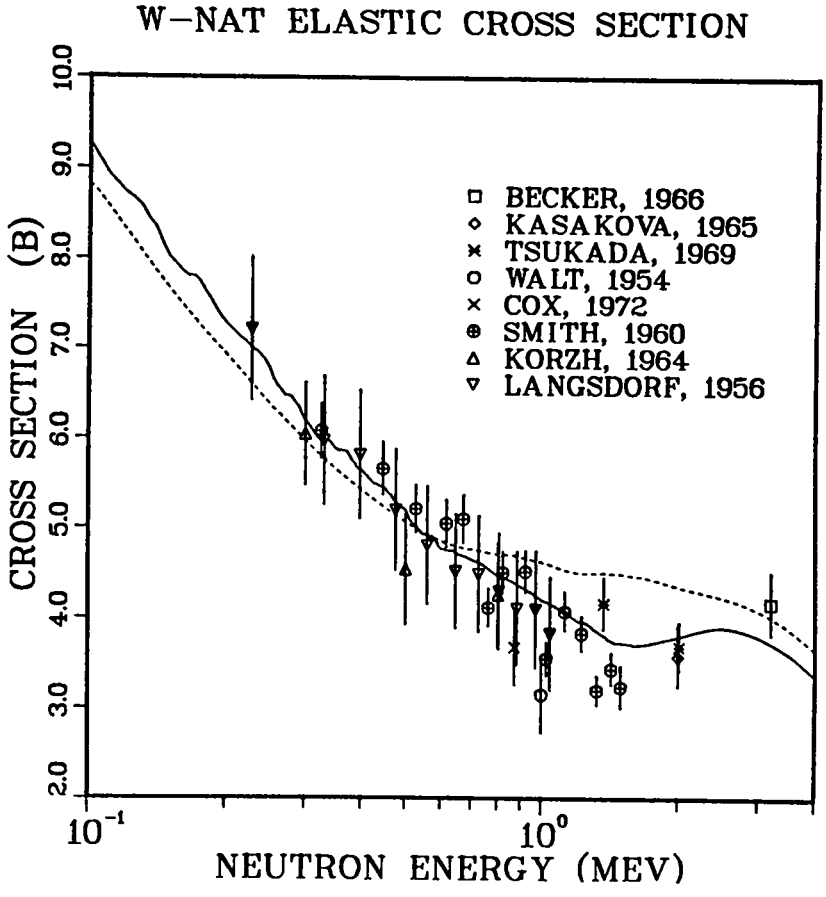

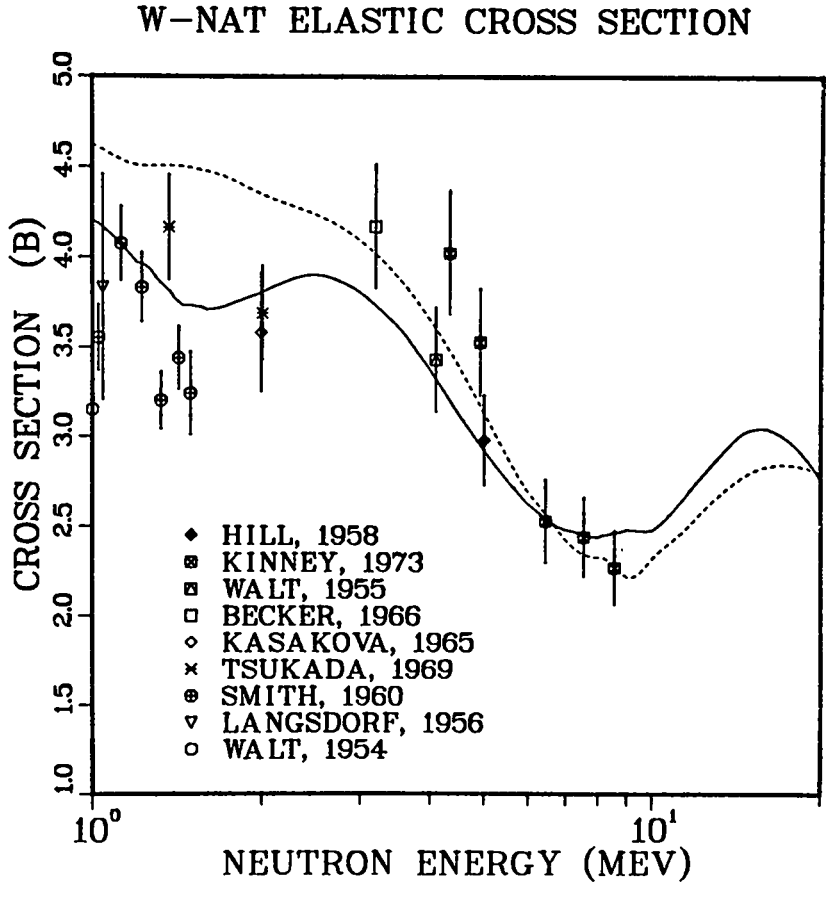

Fig. 10. Evaluated elastic cross sections for natural tungsten. The dashed curve is ENDF/B-V.

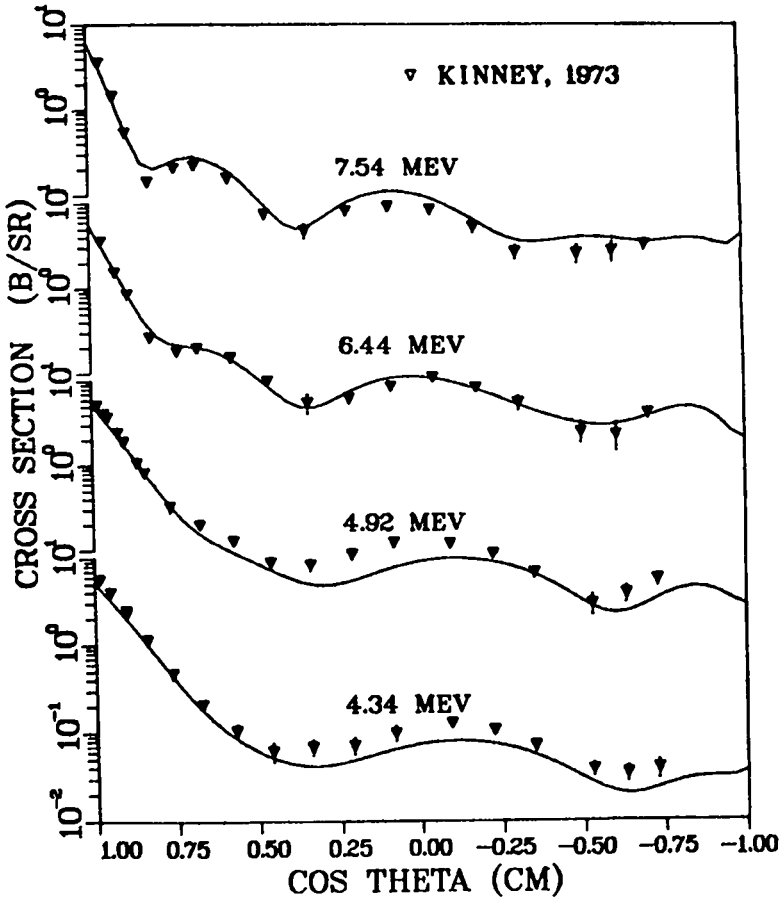

Fig. 11. Comparison of the evaluated angular distributions for elastic scattering (and inelastic scattering producing excitations < 0.1 MeV), and the Kinney measurements.

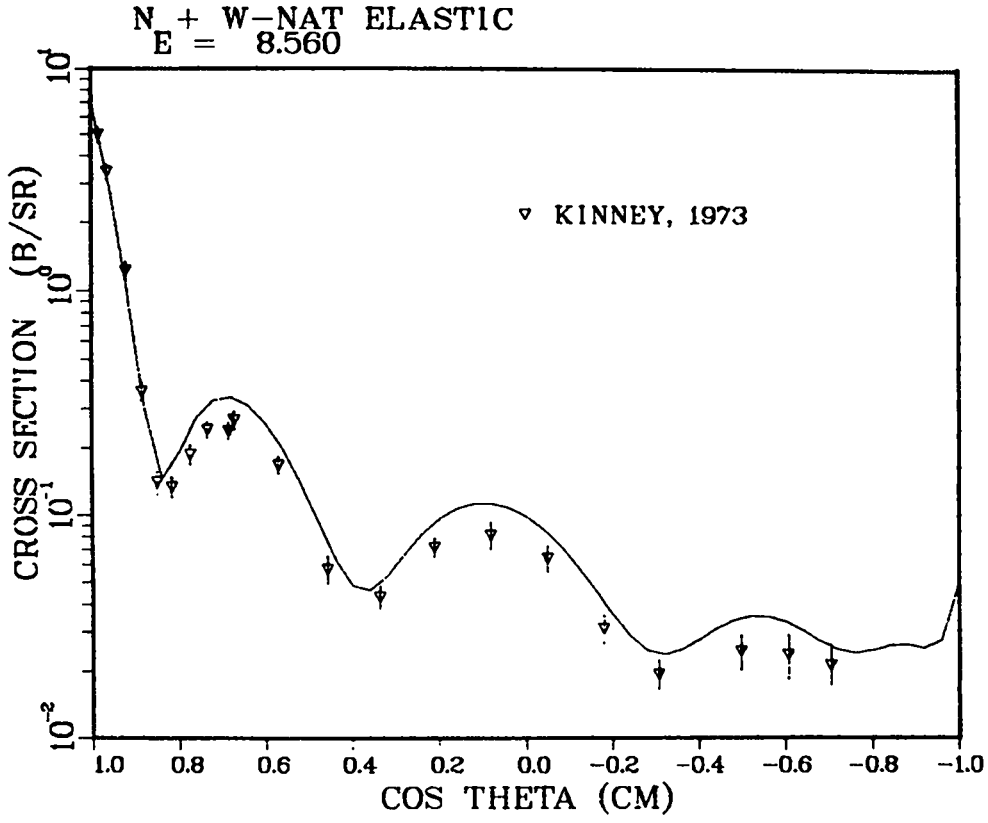

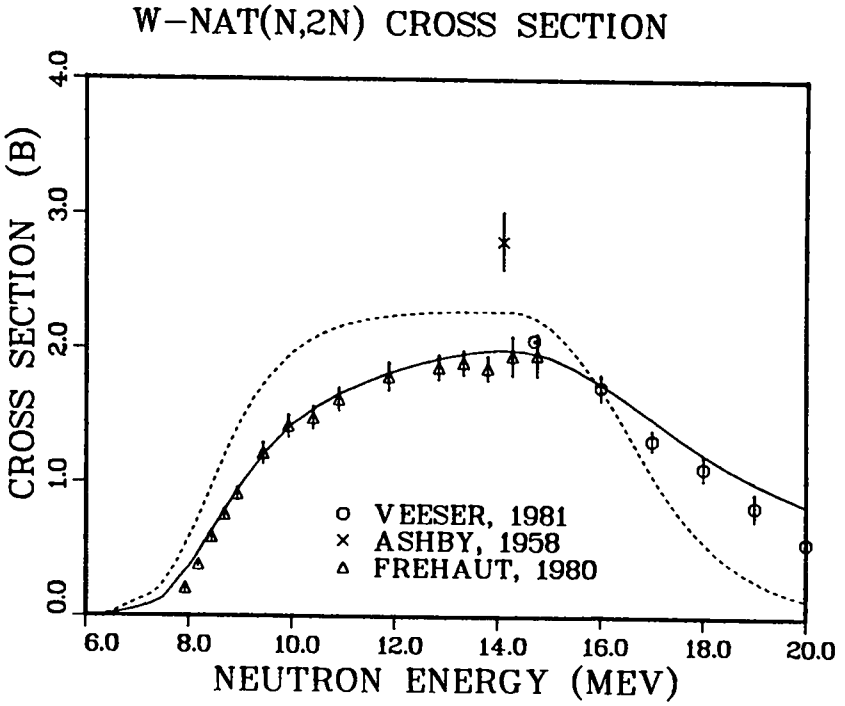

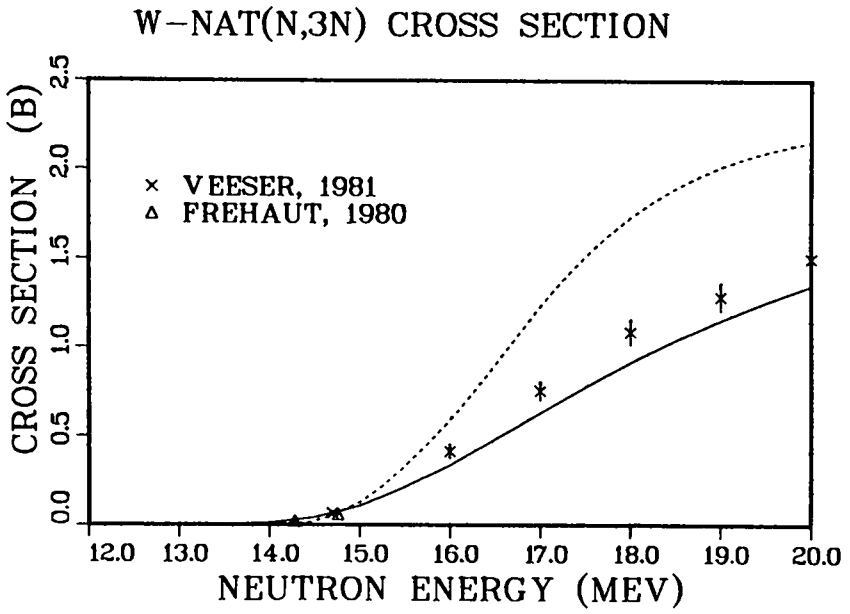

Fig. 12. Evaluated (n,2n) and (n,3n) cross sections are compared to recent experimental data. Again, the solid curve is the present effort; the dashed curve is ENDF/B-V.

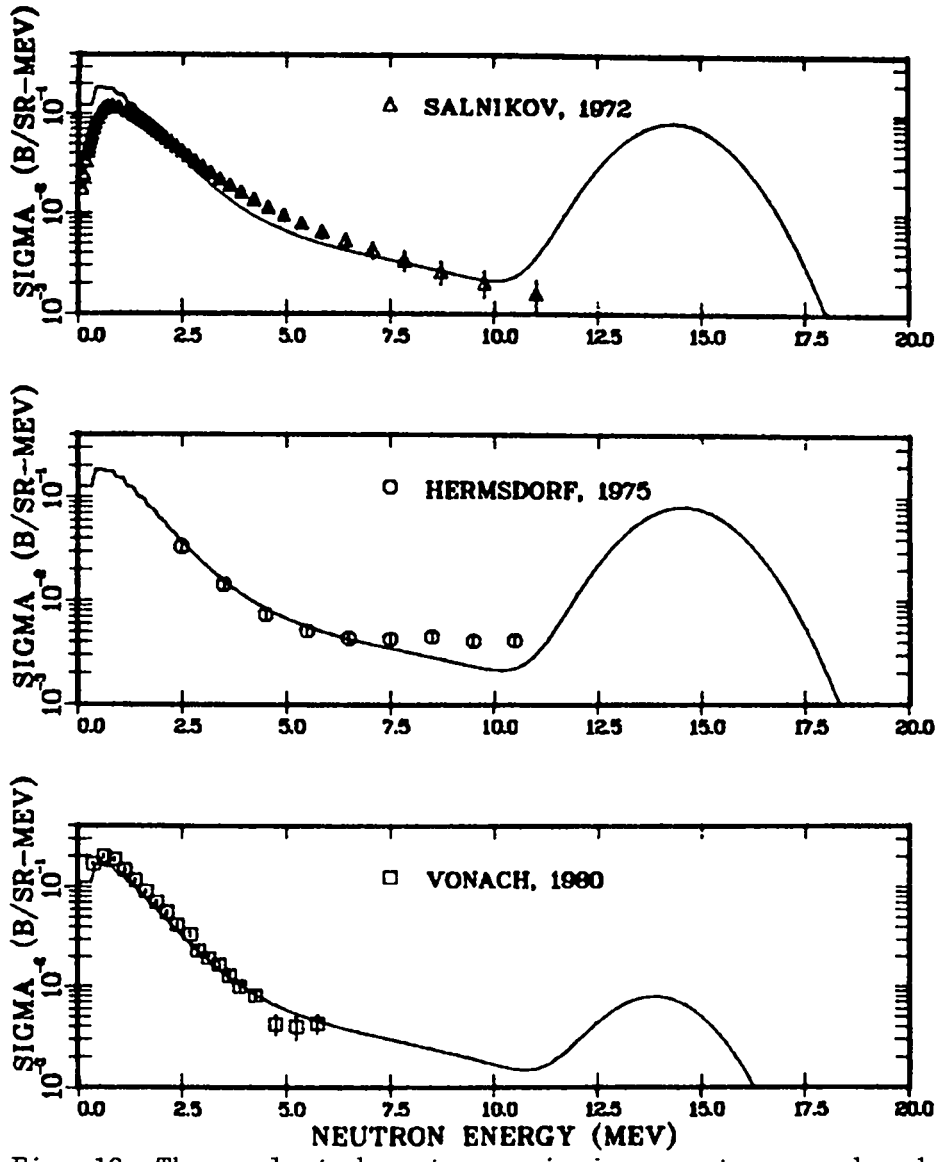

Fig. 13. The evaluated neutron emission spectrum produced by 14-MeV neutrons is compared to experimental results.

Comparisons to the gamma-ray production data of Dickens[24] are shown in Figs. 14-16 for selected incident neutron energy groups. The evaluated gamma-ray production cross sections were obtained from nuclear model calculations to ensure overall energy conservation in the evaluated data files. There are some disagreements to the measurements particularly for gamma rays resulting from continuum inelastic scattering. To some extent this disagreement represents an inconsistency with available neutron cross-section data and is discussed in detail in Ref. 10. We achieve better agreement with the more recent gamma-ray production measurements of Savin,[25] as shown in Figs. 17 and 18, as well as with data measured by Drake.[26]

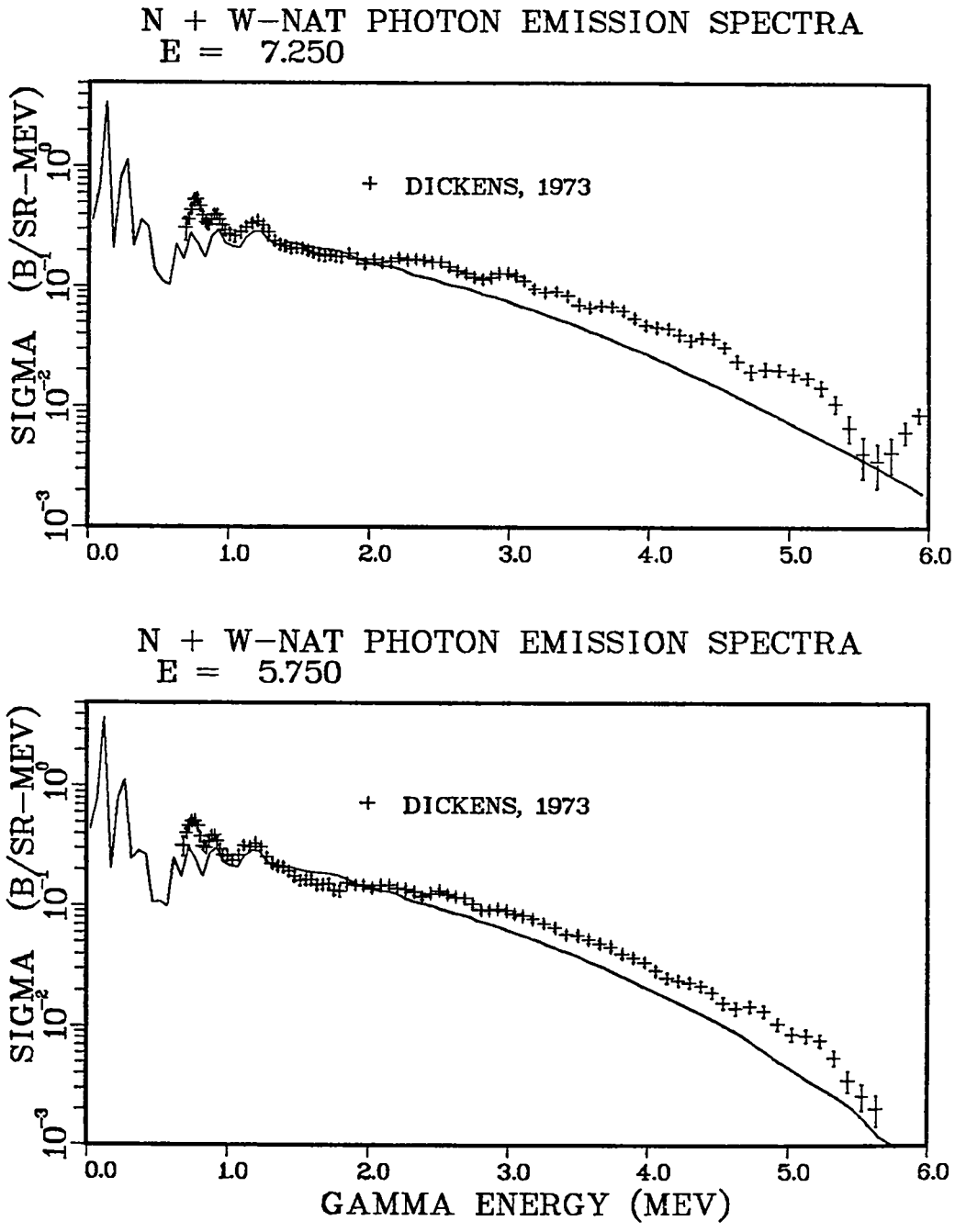

Fig. 14. The evaluated gamma-ray production spectrum obtained in the present effort is compared to Dickens' experimental results.

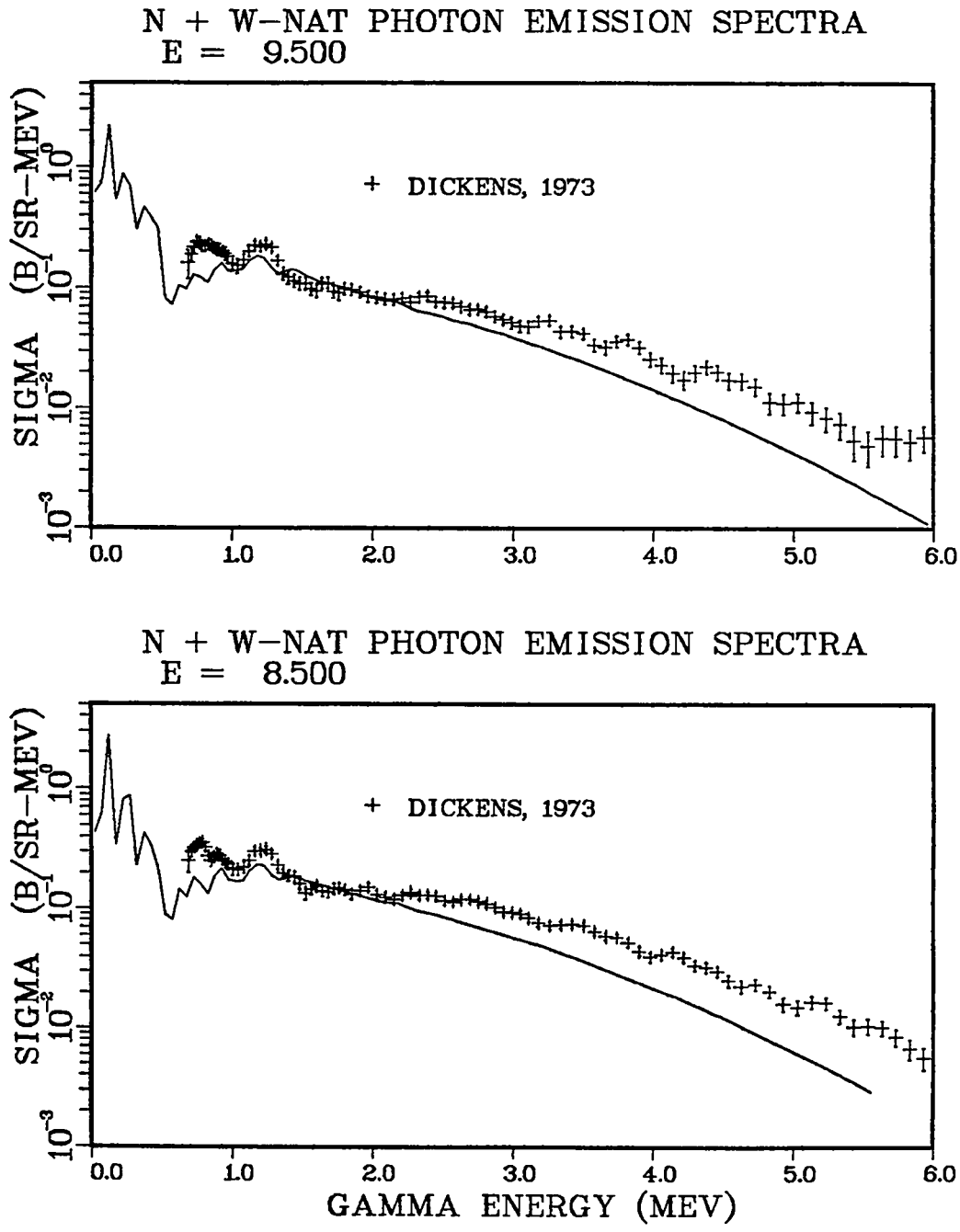

Fig. 15. The evaluated gamma-ray production spectrum obtained in the present effort is compared to Dickens' experimental results.

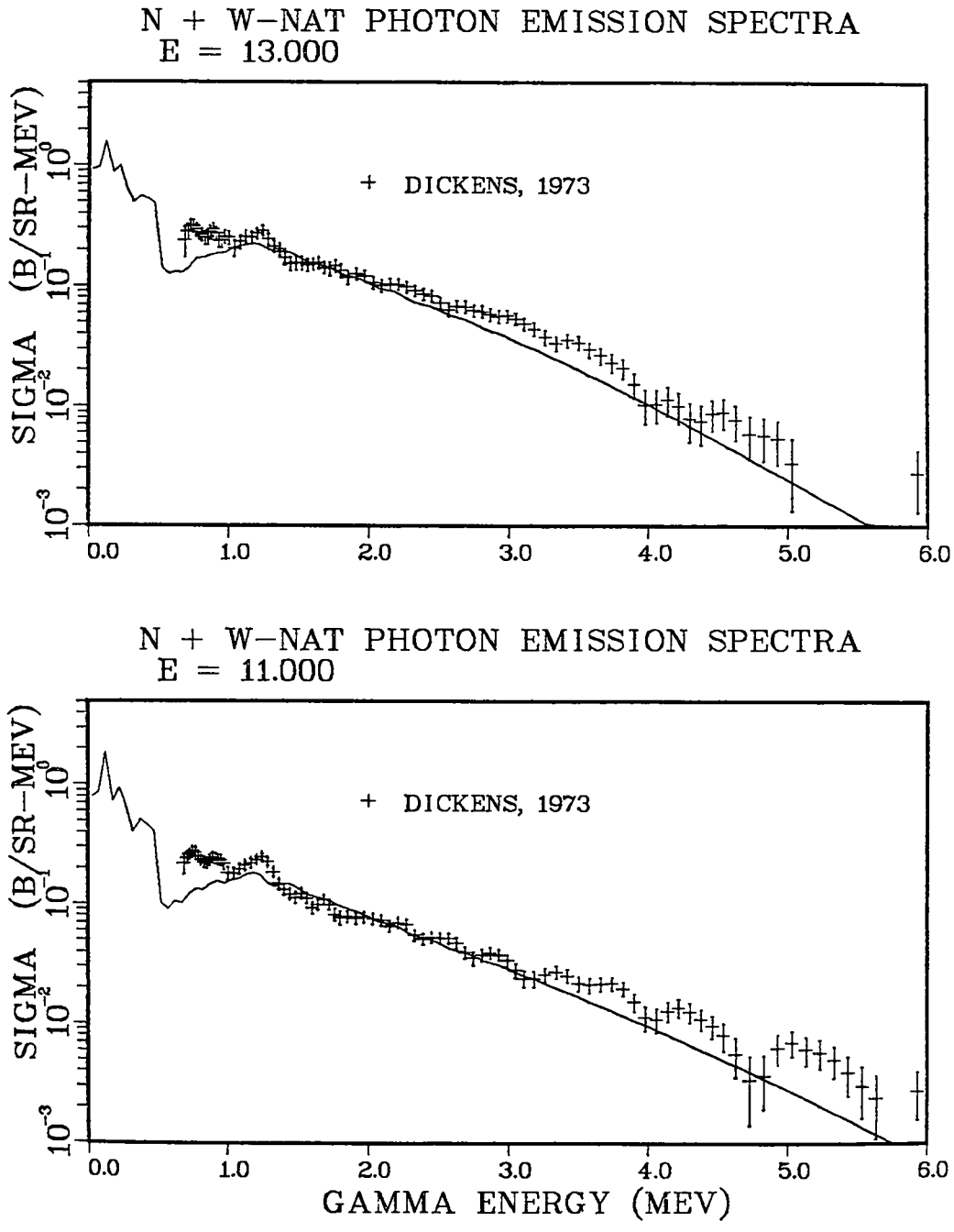

Fig. 16. The evaluated gamma-ray production spectrum obtained in the present effort is compared to Dickens' experimental results.

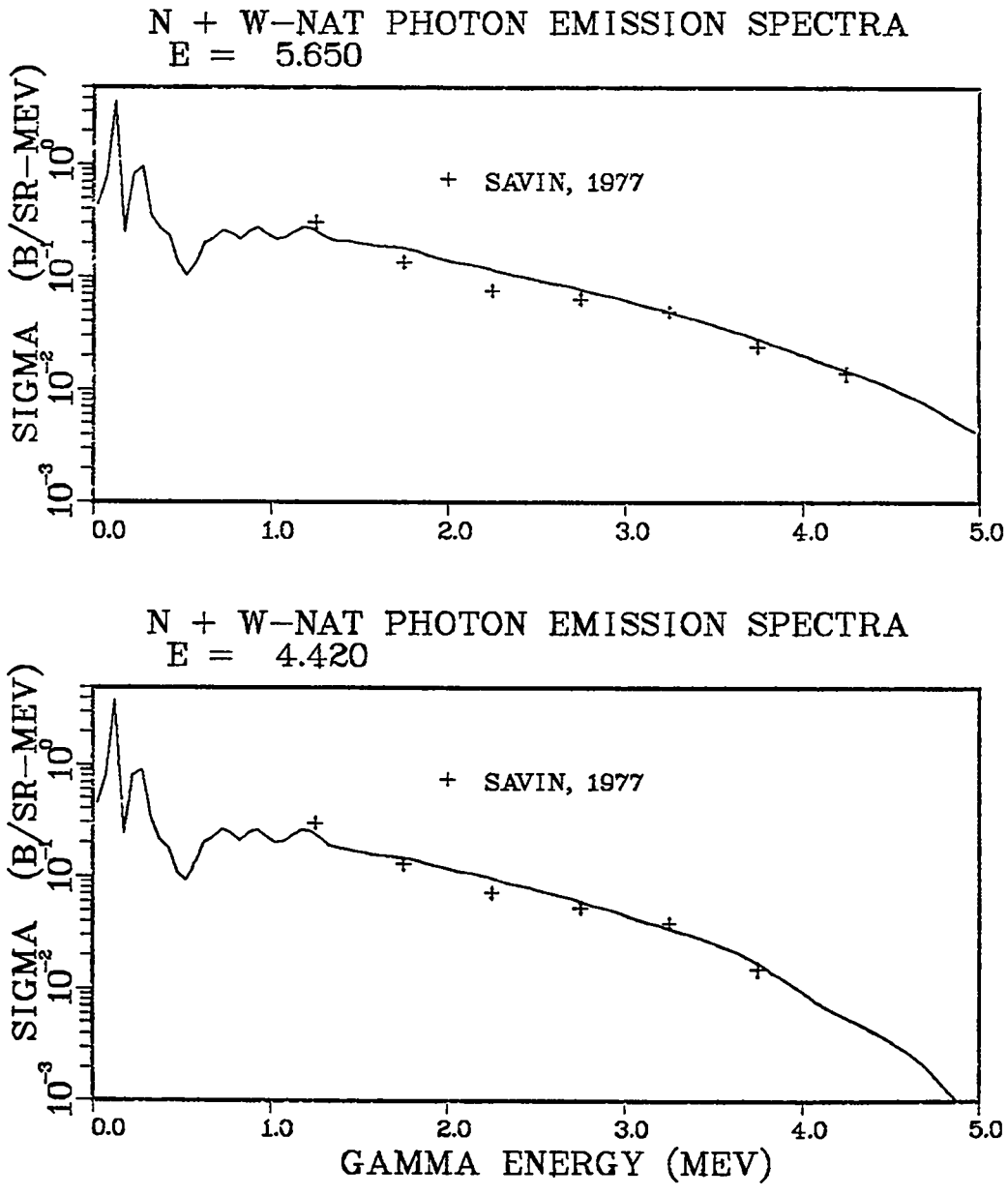

Fig. 17(a). A comparison of the present evaluation to recent gamma production spectra measured by Savin.

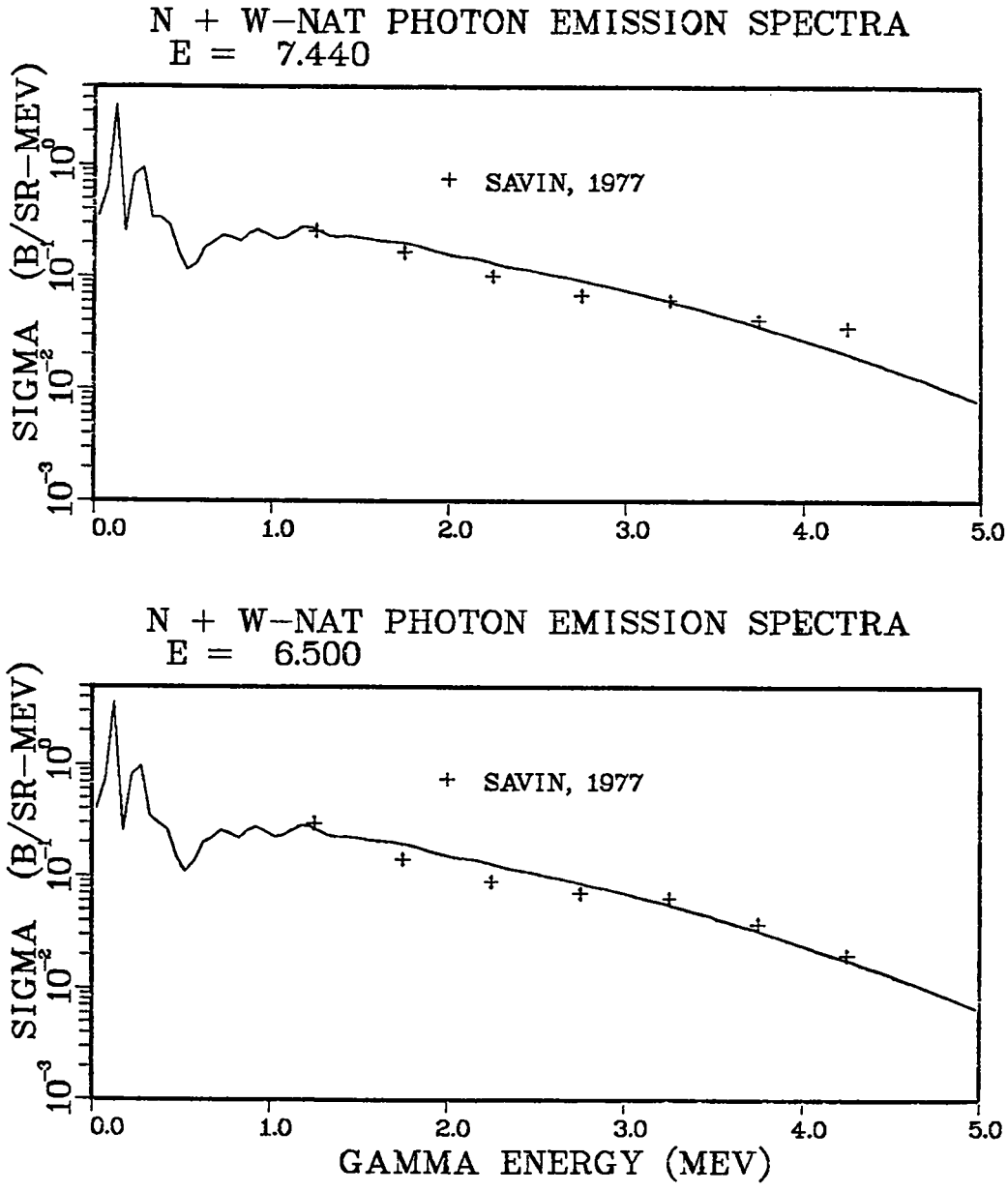

Fig. 17(b). A comparison of the present evaluation to recent gamma production spectra measured by Savin.

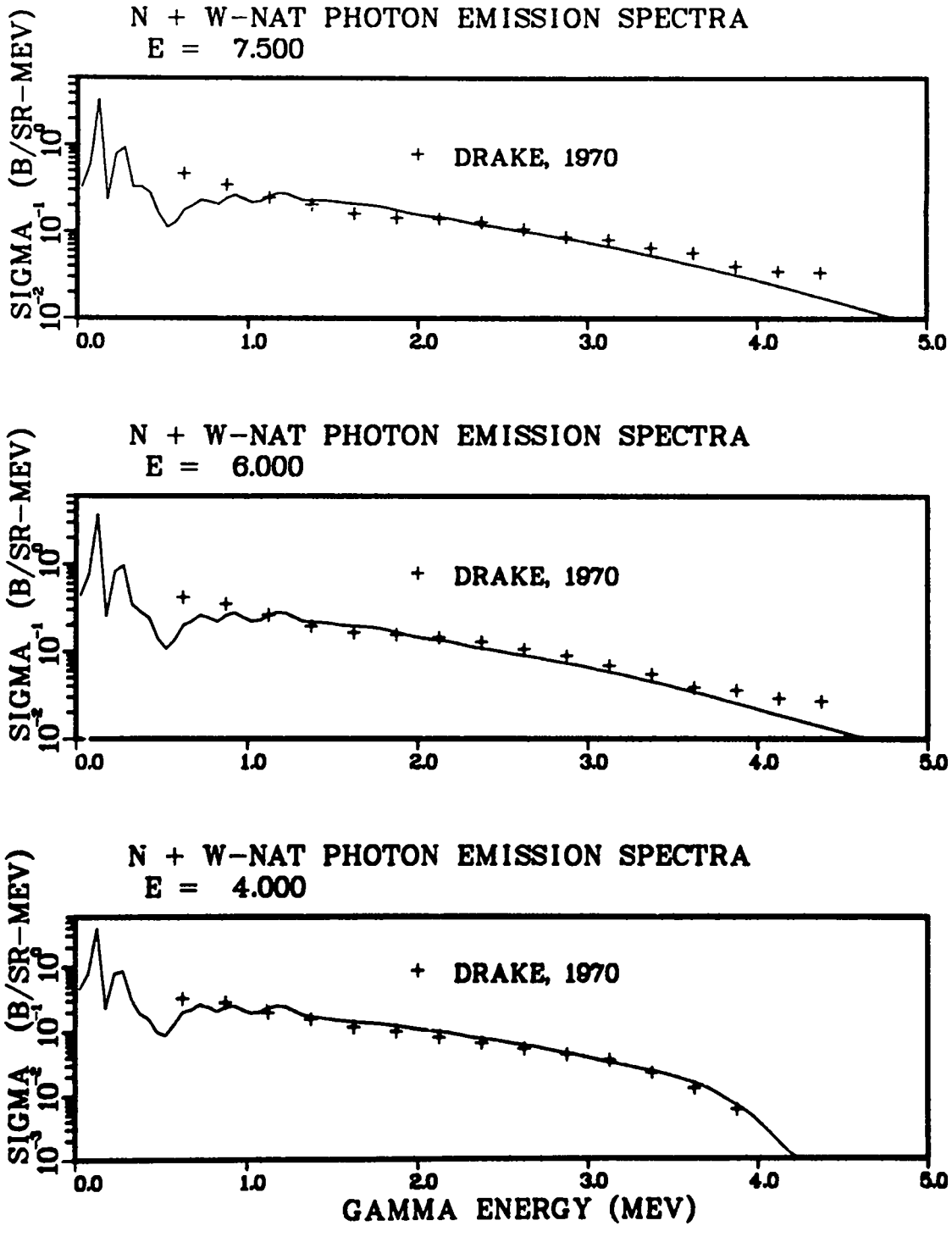

Fig. 18. The present evaluation is compared to the gamma-ray production spectra measured by Drake et al.[27]

H. Application and Further Development of the Improved COMNUC Fission Model (E. D. Arthur)

In our previous progress report,[27] we described implementation of an improved fission model in our Hauser-Feshbach statistical model code, COMNUC.[28] We have used this model to calculate neutron-induced fission cross sections on $^{235,238}U$ and $^{239,242}Pu$ between 0.001 and 5 MeV. A more detailed description of these calculations appears in an invited presentation[29] at the Specialists' Meeting on Fast Neutron Scattering from Actinide Nuclei, Paris, 1981.

As previously described, penetration through the fission barrier is calculated within the code through the use of a three-coupled or two-uncoupled oscillator representation. Furthermore, a spectrum of fission transition states or a continuum of such states must be specified at each barrier to determine the total fission transmission coefficient. To evaluate the continuum of transition states, we use a phenomenological-level density model[30] to which we apply directly an enhancement factor that accounts for symmetry conditions (actually, departures from nuclear symmetry due to deformation effects) existing at each barrier. The enhancements needed at each barrier to reproduce (n,f) data for the nuclei listed above appear in Table II. Also shown in parentheses are results from analyses[31,32] employing transition state densities obtained from microscopic calculations. The agreement is good especially when uncertainties from other barrier parameters are considered. Figure 19 compares our calculated $^{235}U(n,f)$ cross section to data available between 0.1 and 5 MeV.

In such calculations corrections must be applied to account for correlations and fluctuations occurring for partial widths used in the Hauser-Feshbach expression for average cross sections. These include width-fluctuation corrections and, in the case of the fission channels, corrections that account for Class II states occurring in the second well. (See Ref. 29 for more details). The effects of such corrections are shown in Fig. 20 for calculated $^{239}Pu(n,f)$ cross sections between 0.001 and 5 MeV. For actinide nuclei where fission may not dominate the reaction cross section, these corrections can be equally important. The effects of width fluctuation corrections on the calculated compound elastic and the inelastic scattering cross section to the first excited states in ^{238}U are illustrated in Fig. 21.

A final segment of our present effort to upgrade the COMNUC fission channel involves addition of a third barrier parallel to the present outer barrier. Such complexity in the fission barrier description has been shown necessary in

order to fit certain fission probabilities obtained from direct-reaction measurements.[33] Additionally, we have modified our method for description of fission transition states so that bandhead information can be supplied at each barrier. This permits the automated construction of the spectrum of such states. These modifications provide more overlap with models used to analyze fission probability measurements so that the extracted barrier parameters can be used with increased confidence in the production of (n,f) cross sections for short-lived target nuclei.

TABLE II

BARRIER ENHANCEMENTS USED FOR (n,f) CALCULATIONS

Compound Nucleus	Barrier A	Barrier B
^{236}U	2. (1.)	2. (2.)
^{239}U	3. (5.)	5. (10.)
^{240}Pu	16. (20.)	2. (2.)
^{243}Pu	18. (20.)	2. (2.)

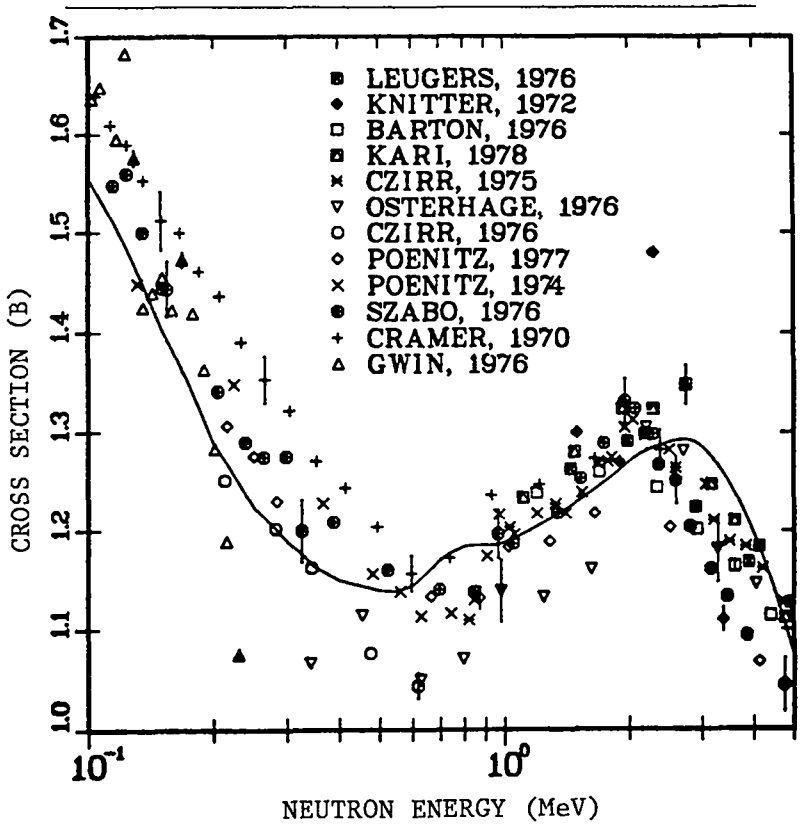

Fig. 19. The calculated $^{235}U(n,f)$ cross section is compared to data between 0.1 and 5 MeV.

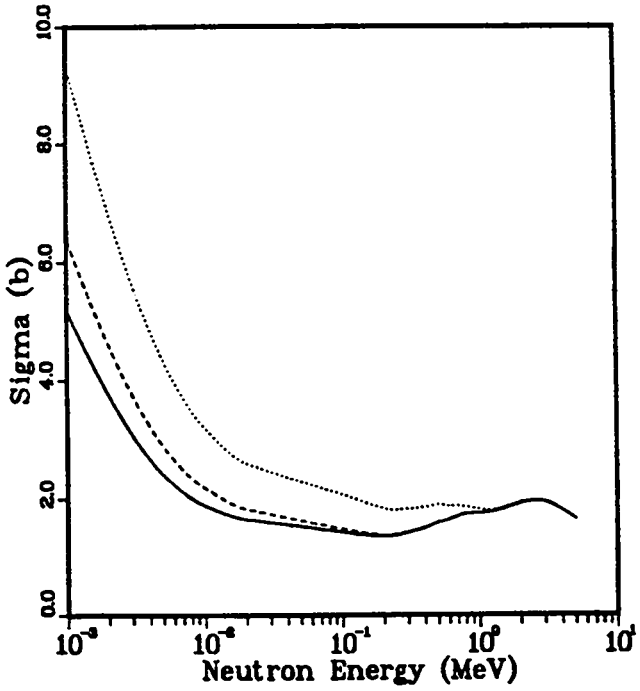

Fig. 20. The effects of fluctuation corrections on calculated $^{239}Pu(n,f)$ cross sections are shown. The solid curve includes both width-fluctuation and Class II-fluctuation corrections. The dotted curve ignores both these effects. The dashed curve includes width fluctuations but excludes Class II fluctuations.

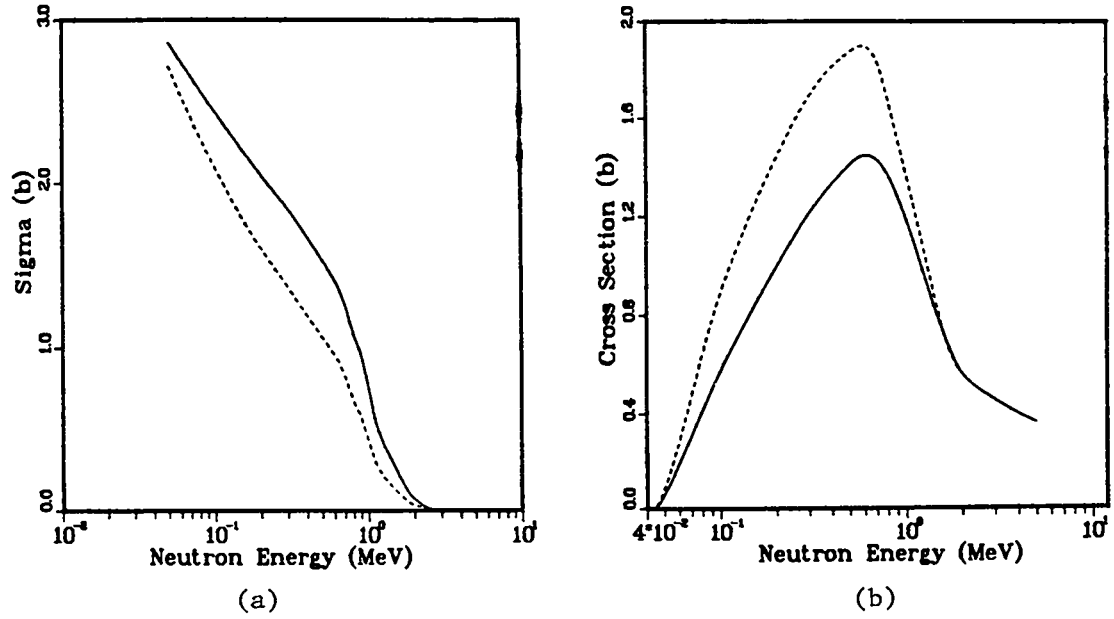

Fig. 21. The effects of width-fluctuation corrections on the calculated (a) compound elastic and (b) inelastic scattering cross section to the 0.045-MeV state in ^{238}U.

I. Inelastic Cross Section Calculations on ^{239}Pu (E. D. Arthur)

In order to improve evaluated neutron inelastic scattering cross sections on ^{239}Pu, we performed coupled-channel direct reaction and Hauser-Feshbach statistical model calculations for neutron energies between 0.01 and 5 MeV. The deformed optical model parameters were described previously,[34] while the statistical model calculations were made with the modified COMNUC code. Cross sections obtained from coupled-channel and compound-nucleus calculations were combined incoherently to produce the desired results. Relevant experimental data for ^{239}Pu are meager, but our earlier comparisons to recent measurements[35] of 0.7-MeV neutron elastic and inelastic scattering to low-lying levels show good agreement.

Figures 22 and 23 compare our calculated inelastic cross sections for scattering from two low-lying levels in ^{239}Pu to evaluated data appearing in ENDF/B-V. The large difference between the results for the 0.057-MeV state arises principally because direct-reaction contributions were included in our calculations but not in the ENDF/B-V work. The shape of our calculated excitation function for the 0.164-MeV state occurs because of its relatively high spin (9/2) and because of direct-reaction components. The ENDF/B-V evaluation, on the other hand, probably employs a shape similar to those assumed for scattering from states with lower spin.

Measurements[36] have recently been made at Argonne National Laboratory whereby the total inelastic cross section to levels lying higher than some excitation energy in the target nucleus can be inferred. The threshold for such inelastic excitations varies between 0.08 and 0.3 MeV and occurs because of experimental resolution effects. For our calculations of inelastic scattering on ^{239}Pu, comparison to such data provides a test of scattering to higher-lying levels that are not members of the ground state rotational band and for which only compound-nucleus contributions were assumed. The solid curve in Fig. 24 compares our calculated values to such data, while the dashed curve represents ENDF/B-V. Our results agree reasonably with the Argonne data but are significantly lower than ENDF/B-V.

Our initial calculations have included direct-reaction contributions only for members of the ground-state rotational band. However, charged-particle experiments[37] show excitation of levels occupying higher-lying bands through direct reaction processes. This is especially true for those levels occurring in the $K^{\pi} = 1/2^{-}$ octupole vibrational band having excitation energies of 0.5-0.6 MeV. As an initial step in determination of direct-reaction components

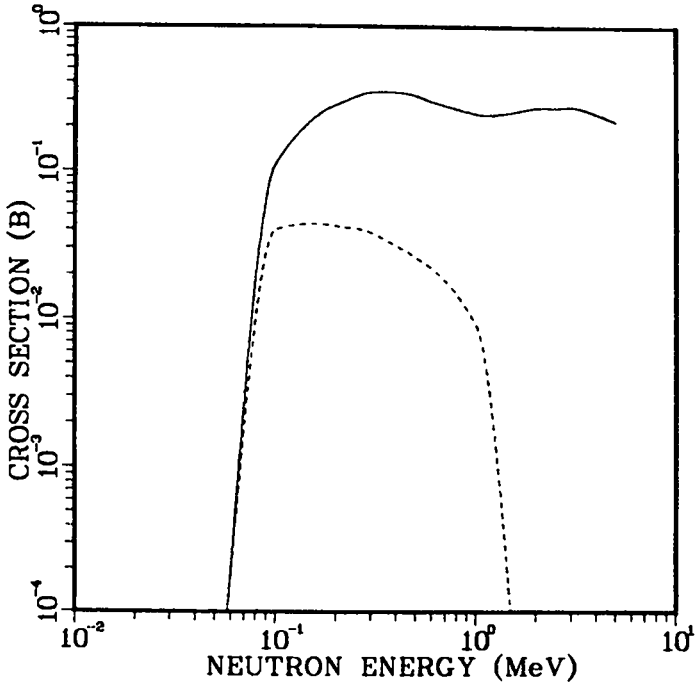

Fig. 22. A comparison of our calculated cross section (solid curve) and that from ENDF/B-V (dashed curve) for excitation of the 0.057-MeV $5/2^+$ state in ^{239}Pu through neutron inelastic scattering.

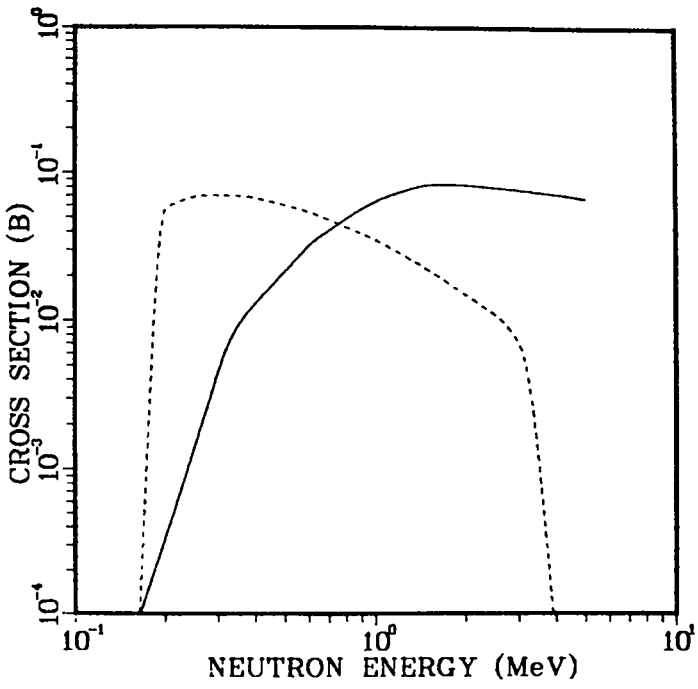

Fig. 23. A comparison of our calculated cross section (solid curve) and that from ENDF/B-V (dashed curve) for excitation of the 0.164-MeV $9/2^+$ state in ^{239}Pu through neutron inelastic scattering.

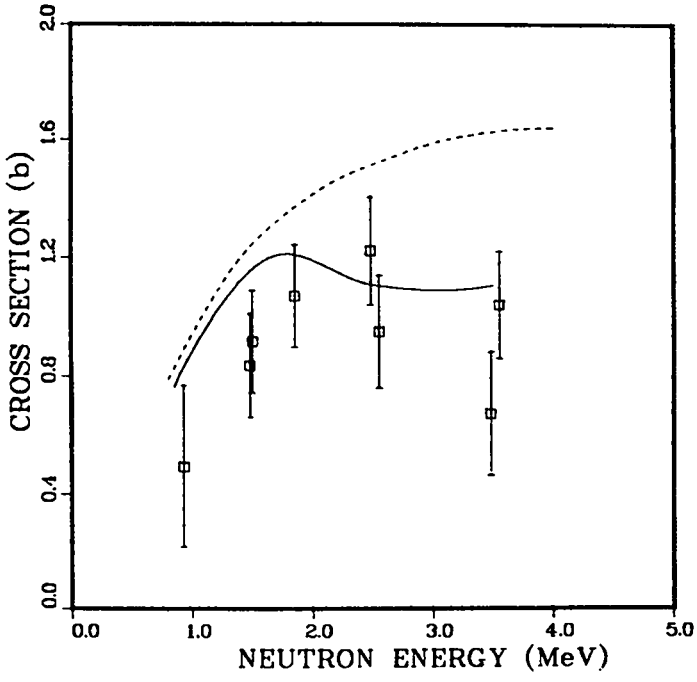

Fig. 24. Comparison of the present calculated "total inelastic" (solid curve) to new measurements by A. Smith, ANL, and to ENDF/B-V (dashed curve).

in neutron inelastic scattering from such states, we performed Distorted Wave Born Approximation (DWBA) calculations for scattering from the 0.555-MeV $7/2^-$ state assuming an $\ell = 3$ angular momentum transfer. The Madland-Young optical model parameters[38] were used, while the normalization for the calculated results was obtained from β_3 values based on measured B(E3) results for octupole states in nearby nuclei.[39] Our direct-reaction cross sections obtained in this manner were only approximately of 5-10 mb for $E_n = 3$ MeV. These results are in apparent disagreement to (n,n') cross sections for scattering from octupole states in ^{238}U and ^{232}Th, as deduced from (n, n'γ) measurements[40,41] on these nuclei.

To further test our calculations, we analyzed charged-particle data for (d,d') and (p,p') measurements of scattering from the 0.731-MeV 3^- octupole state in ^{238}U. We obtained an overall normalization which was then applied to our $\ell = 3$ DWBA calculations. Our β_3 values obtained in this manner again agreed with B(E3) results and produced neutron inelastic scattering cross sections significantly smaller than those deduced using the (n,n'γ) measurements. Figure 25 compares our calculated results for scattering from the 0.731-MeV state in ^{238}U to the data of Olsen[41] obtained via the (n,n'γ) technique.

The disagreement between our calculations and these experimental results indicate a possible inconsistency between the neutron data and charged-particle B(E3) values. An experiment is now planned to help resolve this discrepancy through measurement of (p,p') angular distributions from these levels in ^{238}U and ^{239}Pu.

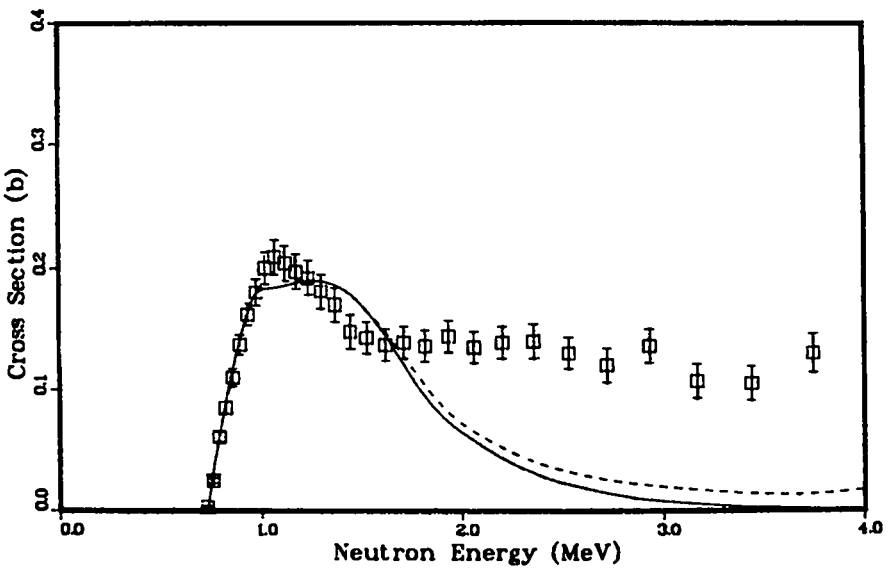

Fig. 25. Comparison of the calculated (n,n') cross section for excitation of the 0.731-MeV 3^- octupole state in ^{238}U. Both compound nucleus and direct-reaction (DWBA) components are included in the dashed curve; the solid curve is the compound nucleus contribution alone. The data are those of Olsen[41] deduced from (n,n'γ) measurements.

J. New Calculation of Prompt Fission Neutron Spectrum N(E) and Average Prompt Neutron Multiplicity $\bar{\nu}_p$ [D. G. Madland and J. R. Nix (T-9)]

An extensive manuscript summarizing this work has been accepted for publication in Nuclear Science and Engineering.[42] The manuscript marks the completion of our presentation of the new theory of N(E) and $\bar{\nu}_p$ that we have developed.

K. New Fission Neutron Spectrum Representation for ENDF (D. G. Madland)

A new representation of the prompt fission neutron spectrum has been proposed for use in the Evaluated Nuclear Data File (ENDF). The proposal has been made because a new theory exists[42] by which the spectrum can be accurately predicted as a function of the fissioning nucleus and its excitation energy. Thus, prompt fission neutron spectra can be calculated for cases where no measurements exist or where measurements are not possible.

The simplest form of the new theory is used, namely, the constant compound-nucleus cross-section approximation.[42] This is done because the resulting expressions for the spectrum and its integral over arbitrary energy range are of closed form, with only slight compromises in accuracy. The proposal document[43] presents the mathematical formalism necessary for application of the theory within the ENDF structure and treats neutron-induced fission and spontaneous fission. In the case of neutron-induced fission, expressions are given for the first-chance, second-chance, third-chance, and fourth-chance fission components of the spectrum together with that for the total spectrum. An ENDF format is provided for the new fission spectrum representation, and an example of the use of the format is given.

L. Calculation of the Prompt Neutron Spectrum and Average Prompt Neutron Multiplicity for the Spontaneous Fission of ^{252}Cf [D. G. Madland and J. R. Nix (T-9)]

On the basis of a new theory[42] of the prompt fission neutron spectrum N(E) and average prompt neutron multiplicity $\bar{\nu}_p$, we are calculating these quantities for the spontaneous fission of ^{252}Cf. We are studying this particular reaction because it is used as a standard in many measurements and applications of neutron physics.

In order to calculate N(E) and $\bar{\nu}_p$ with high accuracy, we require highly accurate values of the average fission energy release $\langle E_r \rangle$, the total average fission-fragment kinetic energy $\langle E_f^{tot} \rangle$, the nuclear level-density parameter a,

the total average prompt gamma energy $\langle E_\gamma^{tot} \rangle$, and the average fission-fragment neutron separation energy $\langle S_n \rangle$. Whereas for ^{252}Cf, $\langle E_f^{tot} \rangle$ and $\langle E_\gamma^{tot} \rangle$ are measured quantities and a is inferred from measurements, the average energy release $\langle E_r \rangle$ and the average fission-fragment neutron separation energy $\langle S_n \rangle$ must be calculated. In our previous work[42,44] we have calculated $\langle E_r \rangle$ and $\langle S_n \rangle$ by use of a seven-point approximation to their integrals over the fission-fragment mass and charge distributions, using measured or systematic masses of Wapstra and Bos[45] when they exist, and otherwise the droplet-model mass formula of Myers.[46] In this work, because of the increased accuracy requirements, we are performing the required integrations without approximation and are using the mass formula of Möller and Nix[47] for determining unmeasured masses. The subroutine QVAL has been constructed for the latter purpose. A call to QVAL results in a search for the desired mass first from the Wapstra and Bos[45] mass table and, if not found, second from the Möller and Nix[47] mass table. With these improvements we calculate N(E), $\bar{\nu}_p$, and the decomposition of $\bar{\nu}_p$ into $\bar{\nu}_p(A)$, where A is the mass number of either the light or the heavy fragment.

Two results have been obtained thus far, but these are preliminary because (a) the fission-fragment mass and charge distributions used in the integrations have yet to be finalized, and (b) the experimental values used for $E_f^{tot}(A)$ and $E_\gamma^{tot}(A)$, that is, the decomposition of $\langle E_f^{tot} \rangle$ and $\langle E_\gamma^{tot} \rangle$, have to be understood more completely. Keeping these points in mind, our preliminary results are

1. $\bar{\nu}_p[^{252}Cf(sf)] = 3.770$, to be compared with the current accepted value of 3.757 ± 0.009, and
2. agreement to within approximately 5% with the $\bar{\nu}_p(A_H)$ experimental data of Boldeman and Walsh,[48] where $126 \leqq A_H \leqq 164$.

M. Calculation of Excited-State Cross Sections for Actinide Nuclei (D. G. Madland)

Further improvements and studies of the coupled-channel excited-state target code JUPXST have been made in preparation of calculating excited-state transmission coefficients for three- and four-state coupling. These are

1. A direct test of the unitarity of the full coupled-channel S matrix in the limit of no absorptive potential with the results that the calculated off-diagonal elements of S are zero to within a few parts in 10^7 and that

the corresponding transmission coefficients are zero to a precision approaching a few parts in 10^{13}.

2. A test of reciprocity between $0^+ \rightarrow 2^+$ and $2^+ \rightarrow 0^+$ coupling with the result, after certain numerical improvements, that reciprocity is satisfied to within a few parts in 10^7.
3. Additional convergence tests for incident neutron energies that are below the excitation energy of the highest coupled target state. Here we have results that are not yet understood, namely, matching radius dependencies of the calculated sub-threshold cross sections and the behavior of the S matrix in the sub-threshold region. We are presently continuing our studies in the sub-threshold region, which is an important one for certain excited-state target calculations.

II. NUCLEAR CROSS-SECTION PROCESSING AND TESTING

A. NJOY Code Development (R. E. MacFarlane, D. W. Muir, and R. M. Boicourt)

A new version of the NJOY nuclear data processing system called NJOY (10/81) has been released to the national code centers and interested individual users. This code is widely used for preparing neutron and photon cross sections from evaluated data in ENDF/B format. The new version corrects a number of errors and adds several new capabilities.

The resonance reconstruction module (RECONR) now supports analytic psi-chi Doppler broadening for the Adler-Adler resonance representations as well as the single-level Breit-Wigner form, control of significant digits has been improved, and an extended resonance reconstruction algorithm[49] has been introduced. In the Doppler broadening module (BROADR), an error that affected low-energy cross sections at high temperatures was repaired, and more control over the energy range for broadening was added to avoid pathological results for cross sections containing sharp steps or resonances represented as triangles (for example, ENDF/B-V lead).

The UNRESR unresolved-resonance calculation was changed to guarantee compatibility between the smooth cross sections in File 3 and the self-shielded numbers in File 2. In the HEATR module, an option to compute radiation-damage energy production[50] was added. In addition, the existing heat production calculation was modified to use momentum balance to compute the recoil for radiative capture.[50] This gives better results for capture heating at low energies, which is difficult to compute well as the difference between two large numbers.

It also gives reasonable results for elements, which cannot be handled by energy balance because the available energy is not given in the ENDF/B files. Unfortunately, total energy is no longer explicitly conserved.

The thermal treatment (THERMR) is now based on the use of discrete angles rather than Legendre coefficients. A representation using eight equally probable angles can be converted to multigroup Legendre data as good as the results of the old P_3 method when the angular variation is modest, and it gives much better results when the scattering is concentrated into a small angular range (which is common in practice). For coherent elastic scatter (for example, graphite), the discrete angles and their weights can be determined directly from the positions and magnitudes of the Bragg edges in the cross section; therefore, the higher moments are no longer calculated. Similar methods are used for incoherent elastic scattering. For the convenience of the user, default effective temperatures for the short-collision-time approximation have been added for use in extending the ENDF/B data to higher energy and momentum transfers.

In the multigroup module (GROUPR), the background cross sections list can now be different from the list in UNRESR. The flux calculator has been improved at the cost of requiring extended memory, and it now includes the capability for representing intermediate-resonance effects due to admixed oxygen and external hydrogen and oxygen using a two-region approximation.[51] More group structures and weight functions have been added, and several improvements have been made to the calculation of fission spectra. The photon interaction module (GAMINR) has a new group structure. The recommended weight funtion has been changed to 1/E with high- and low-energy roll offs.

The (10/81) version of the ERRORR module for processing the ENDF/B covariance files includes several new capabilities, including the treatment of cross-material covariances, fission $\bar{\nu}$ uncertainties, and resonance-parameter covariances. The new COVR module is also included in this version. It makes high-quality plots of uncertainties and correlations.[52] Some more recent developments in ERRORR and COVR (to be included in a later version of NJOY) are described elsewhere in this report.

The CCCCR output module has been updated to the CCCC-IV specifications.[53] Fission matrices are now available, and fission vectors can be computed for an input flux if desired. The self-shielding factor file now includes sub-blocking and elastic removal shielding factors. The MATXS output modules have been updated to include some new reaction names for ENDF/B-V.

Because the input for NJOY(10/81) and certain aspects of the code operation are different from the earlier versions, a new users' manual has been issued. The new manual is available as Volume I of Los Alamos National Laboratory report LA-9303-M.[4,54] Volume I is intended to replace the previous manual, LA-7584-M. Volume II of the new report, which is also complete, provides detailed descriptions of the NJOY module (containing the executive program and utility subroutines used by other modules), and it discusses the theory and computational methods of four of the modules used for producing pointwise cross sections: RECONR, BROADR, HEATR, and THERMR. Future volumes describing the groupwise and covariance modules are also planned.

A more formal procedure has been adopted for communicating changes to the expanding NJOY user community. A mailing list has been established for a series of "NJOY Notes." Notes 1 and 2 have already been issued. They provide corrections to a number of errors found in testing and a group of changes that improves IBM compatibility. Persons interested in being placed on the mailing list to receive these and future Notes should contact the code authors. As a result of IBM testing carried out by C. Stenberg at the Argonne National Laboratory, an IBM version of NJOY has been released to the code centers.

B. New 80-Group Fast Reactor Cross-Section Library (R. B. Kidman, R. E. MacFarlane , R. M. Boicourt)

A new multigroup cross-section library has been prepared using ENDF/B-V evaluated data and the NJOY processing system. The library is intended to be used for fast reactor analysis and benchmark calculations; but, with due care, it is also useful for many fusion and shielding problems.

The weight function and 80-group structure for the library are shown in Figs. 26-26b. The weight function is based on the smoothed core spectrum for a typical large LMFBR benchmark with a fusion peak added at high energies and a 1/E plus thermal tail added at low energies. This tail is intended to improve the results of calculations in the outer regions of the reactor without requiring an unreasonable shape through the keV region important in the core. The group structure is similar to our previous 70-group set, with more low-energy groups, more fusion groups, and one more boundary in the region of the 27-keV iron resonance.

The library contains neutron scattering, photon production, and photon interaction data, including Legendre coefficients to order 5. Self-shielding is

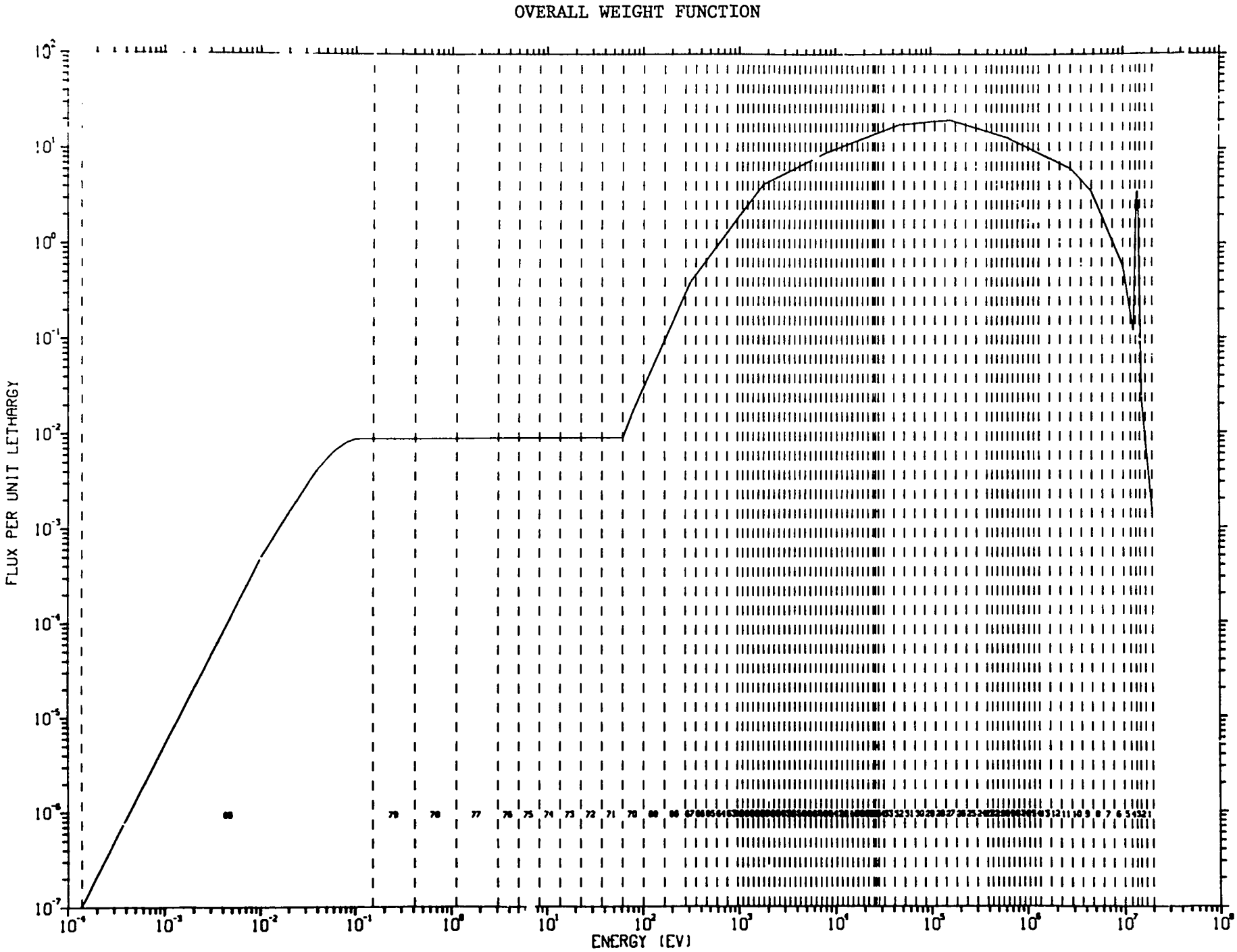

Fig. 26. Weight function and 80-group structure for the new fast reactor cross-section library.

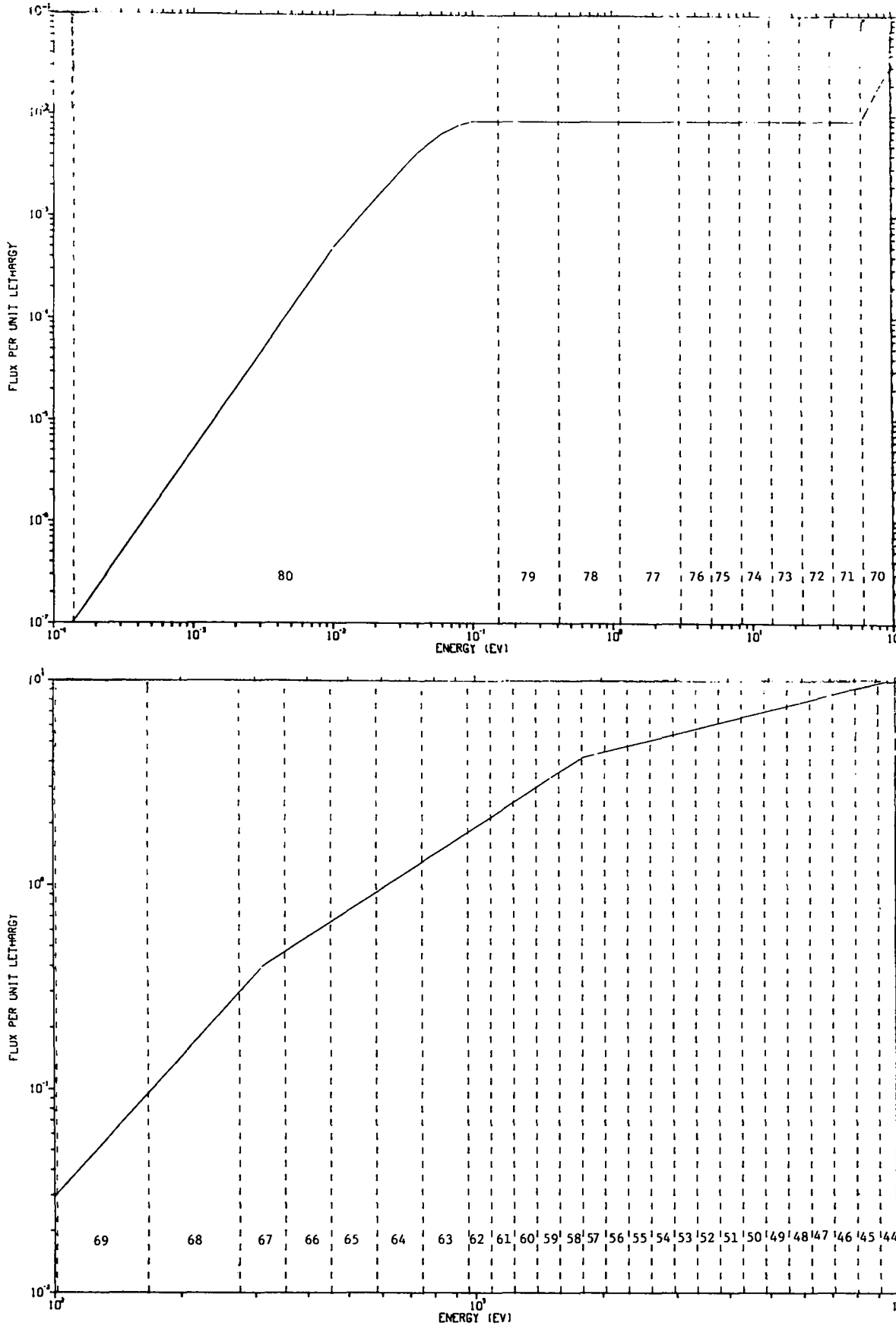

Fig. 26a. Enlargements of the first two sections of the weight function and 80-group structure for the new fast reactor cross-section library (Fig. 26).

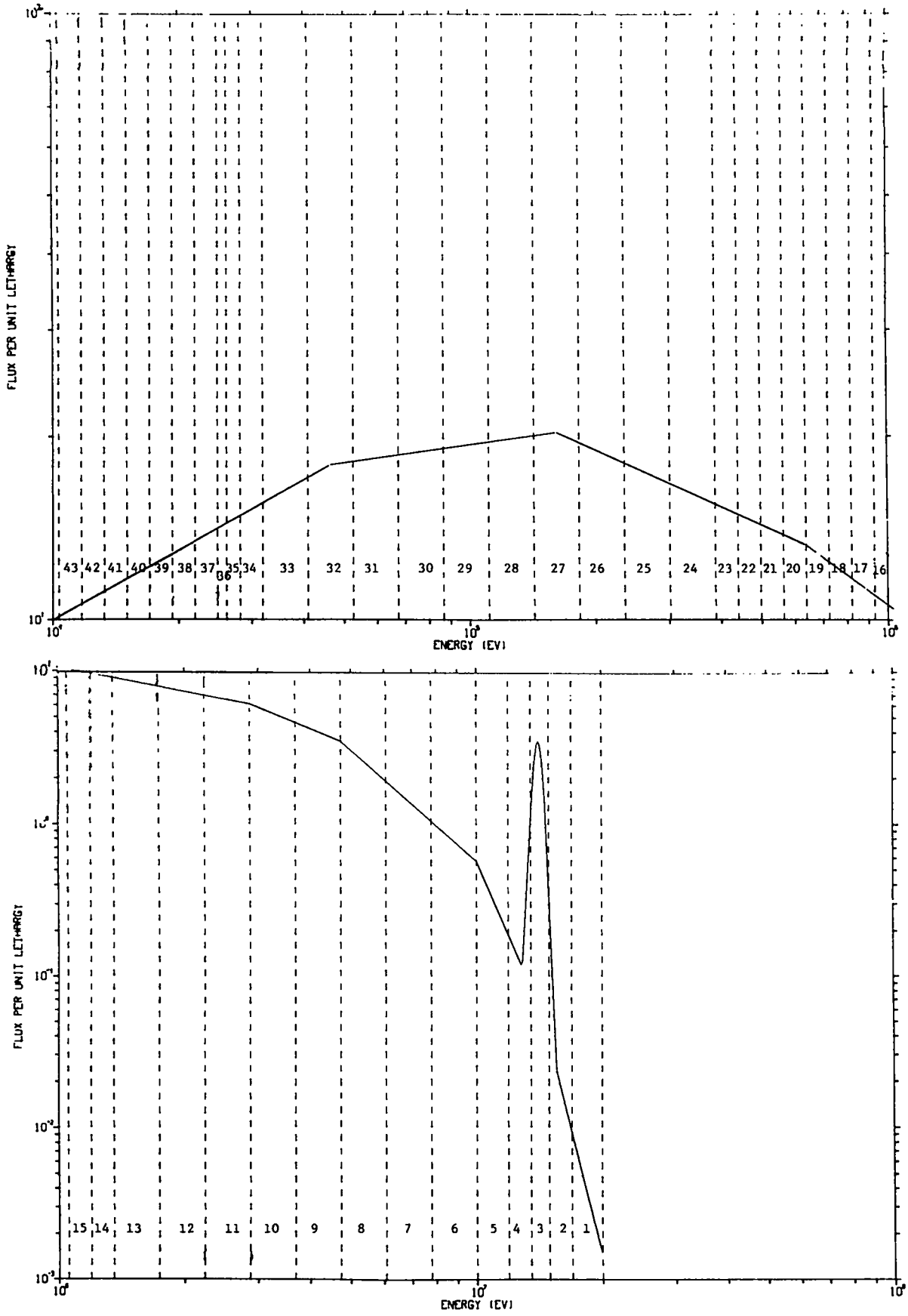

Fig. 26b. Enlargements of the last two sections of the weight function and 80-group structure for the new fast reactor cross-section library (Fig. 26).

given, in some cases for temperatures as high as 8000° K. Heating and radiation damage cross sections are also available. Fission matrices and delayed neutron parameters are included.

The library is available in the CCCC-IV interface format[55] files ISOTXS, BRKOXS, and DLAYXS, and in the new MATXS format. The CCCC files do not include the photon, heating, and radiation damage data. The MATXS file does not include the delayed neutron data.

C. NJOY Covariance Modules, ERRORR and COVR (D. W. Muir, R. M. Boicourt, and R. E. MacFarlane)

The ERRORR module of the NJOY system produces processed multigroup variance-covariance matrices, as well as processed multigroup cross sections, from ENDF/B input. The COVR module of NJOY reads the multigroup data output by ERRORR and produces standard plots of relative standard deviation and gray-shaded graphic representations of the correlation matrices. At least for some cases, this representation is more helpful than the products of alternative plotting packages. However, COVR does require the availability of the DISSPLA proprietary plotting software package. The new NJOY User's Manual[4] includes code description, operating instructions, etc., for both the ERRORR and COVR modules.

ERRORR is a flexible program that allows the user several choices in the particular method used to calculate covariances. The first method, the "pointwise" approach, is used when one has access to a data set containing resonance-reconstructed and linearized cross sections in the NJOY "point-ENDF," or PENDF format. The user can produce such a data set using the RECONR and BROADR modules of NJOY. For example, a PENDF tape containing all of the reactions on the ENDF/B-V dosimetry file, with all resonances reconstructed and Doppler broadened to 300 K, has been produced recently at Los Alamos and is available from the Los Alamos Nuclear Data Group. In order to keep the size of this data file down to a manageable size (56 000 card images), a relatively coarse accuracy criterion (1% for non-fissile nuclides, 5% for fissiles) was employed in the resonance-reconstruction calculation.

In this mode of operation, the user can specify a group structure with complete flexibility (up to 620 user groups are allowed). The ERRORR module will determine the union of the user's energy grid and the ENDF/B evaluator's grid for the material of interest. The relationship between these three grids is illustrated in Fig. 27.

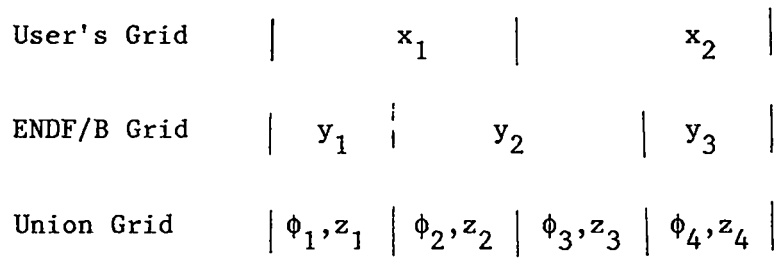

Fig. 27. Illustration of energy grid relations.

After forming the union grid, ERRORR integrates $\sigma(E)$ and the user-supplied weight function $\phi(E)$ to obtain the cross sections z_k and "fluxes" ϕ_k, multigrouped on the union grid. These, in turn, are used to calculate multigroup cross sections x_i on the user's grid according to

$$x_i = \frac{\sum_{k\varepsilon i} \phi_k z_k}{\sum_{k\varepsilon i} \phi_k} . \tag{1}$$

In order to calculate the covariances of x_i, the methodology of ERRORR assumes that the $\phi(E)$ is free of uncertainty, so that the "propagation-of-errors" formula can be used,

$$\mathrm{cov}(x_i,x_j) = \sum_{\substack{k\varepsilon i \\ \ell\varepsilon j}} a_{ik}\, a_{j\ell}\ \mathrm{cov}(z_k,z_\ell) , \tag{2}$$

where the "sensitivity coefficients" a_{ik} are the normalized group fluxes,

$$a_{ik} = \frac{\phi_k}{\sum_{k\varepsilon i} \phi_k} . \tag{3}$$

The union-grid covariances $\mathrm{cov}(z_k,z_\ell)$ in Eq. (2) are formed from the numerical data in the ENDF/B covariance files by combining them, in the ENDF/B prescribed manner,[56,57] with the union-grid cross sections z_k.

The final step, if the user requests it, is to convert the absolute covariances, Eq. (2), to relative covariances,

$$\text{relcov}(x_i,x_j) = \frac{\text{cov}(x_i,x_j)}{x_i\, x_j} \quad . \tag{4}$$

A slightly different calculational path is followed if one wishes to start from a multigroup cross-section library rather than pointwise data. ERRORR will accept such multigroup cross-section input, but only in the format produced by the NJOY group-averaging module GROUPR. Such a library contains both multigroup cross sections and group integrals of the weight function used to produce the cross sections.

In the multigroup input mode, the required union-grid cross sections and fluxes are obtained by collapsing (or expanding) the cross sections and fluxes on the input library. At present, no provision is made for replacing the library group fluxes with a set more appropriate for a given application. If a "library" group is subdivided by a union-group boundary, ERRORR assumes the cross section and weighting function are both energy-independent, in order to estimate ϕ_k and z_k above and below the point of subdivision. The remainder of the calculation proceeds as with pointwise input.

A 620-group (SAND-II) GROUPR output library has been produced recently for the ENDF/B-V dosimetry materials, using a constant weight function. This library is also available on request, either in the GROUPR output format, or as a PENDF tape. With the latter, the ERRORR calculations can be performed in the "pointwise" mode, thus avoiding the library-group-flux problem mentioned above.

In some materials, and in certain energy regions, the cross-section uncertainty is dominated by the uncertainty in resolved resonance parameters. One noteworthy example is ^{63}Cu(n,γ)^{64}Cu (ENDF/B-V Material 6435) in the energy range from 10 eV to 15.9 keV, where the entire cross-section uncertainty is represented by means of resonance-parameter uncertainties. The same is true of ^{237}Np(n,f) (ENDF/B-V Material 6337) from 0 to 10 eV.

Beginning with the (10/81) version of ERRORR, the resonance-parameter contribution to the uncertainty in infinite-dilution fission and capture cross sections is included automatically when cross-section covariances are processed.

This contribution is obtained from the Breit-Wigner formula for the fission and capture areas of a resonance, A_f and A_γ, respectively. By differentiating this formula with respect to the resonance parameters, one obtains a set of sensitivities. With these sensitivities and the covariance matrix of the parameters from ENDF/B, one can apply a propagation-of-errors formula, similar to Eq. (2), to obtain the covariances $cov(A_\gamma,A_\gamma)$, $cov(A_\gamma,A_f)$, and $cov(A_f,A_f)$. These results then are added to the ENDF-specified "long-range" cross-section covariances.

The resonance contribution is properly weighted with the isotopic abundance and the ratio of the weight function at the resonance to the average weight in the group. It is assumed, however, that the area of a resonance lies entirely within the group that contains the resonance energy E_r. Because of this assumption, and because ENDF/B provides no correlations between parameters of different resonances, the calculated resonance-parameter contribution affects only the diagonal elements of the affected matrices.

With the implementation of this feature, the uncertainty in the capture cross section of ^{63}Cu, for example, computed for a group that contains the large 577-eV resonance is 3.0%, rather than zero, as in earlier ERRORR versions.

The (10/81) version of ERRORR also handles <u>explicit</u> cross-material covariances. The only explicit cross-material covariances appearing in ENDF/B-V pertain to fission $\bar{\nu}$ values, but there is a clear need for more information of this type in future versions of ENDF/B.

A third, more recent, extension of the program allows the processing of covariances in cases when one cross section is measured relative to a well-known "standard" cross section. In such a case, the evaluator may represent the uncertainty in the first cross section as being the sum of two components. The first component is described by an explicit statement of the uncertainty in the measured ratio, whereas the second component, due to uncertainty in the standard, is represented implicitly, with the details provided only in the ENDF/B evaluation for the standard reaction.

In the ENDF/B-V dosimetry file, this situation occurs for the $^{238}U(n,\gamma)$ reaction (ENDF/B Material 6398), which was measured relative to $^{10}B(n,\alpha)$ from 4 keV to 20 keV, and the $^{239}Pu(n,f)$ reaction (ENDF/B Material 6399), which was measured relative to $^{235}U(n,f)$ from 0.2 to 15 MeV. When ERRORR was modified to include the uncertainty in the standard, there was little effect for $^{238}U(n,\gamma)$,

but there was a noticeable increase in the uncertainty of $^{239}Pu(n,f)$, from about 2% to 4-5% in the MeV region. The energy-to-energy correlation matrix is also affected, as can be seen by comparing Fig. 28 with Fig. 29. This ratio-to-standard capability is not implemented in the (10/81) version of ERRORR, but a set of code changes to accomplish this is available from the authors on request.

Another recent extension [also not included in the (10/81) version] allows the processing of the "lumped-partial" covariance format approved by the Cross-Section Evaluation Working Group in May 1981. This format allows the evaluator to specify a group of nuclear reactions and to give the uncertainty only in the sum of the cross sections for those reactions. One can, for example, replace 30 or 40 discrete-level inelastic cross sections with 5 or 6 "lumped" cross sections when constructing the covariance files. Since the volume of the covariance data varies, in general, as the square of the number of reactions, this lumping can greatly reduce the size of the files.

The first ENDF/B evaluation to employ the lumped-partial format is P. G. Young's evaluation[58] for ^{7}Li (ENDF/B-V, Rev. 2). All covariance data for this evaluation have been successfully processed into multigroup form using ERRORR. The covariances for MT 854 (a single "real" level with an excitation energy of 4.63 MeV) with MT 855 (5 lumped pseudo-levels,[59] with excitation energies ranging from 4.75 MeV to 6.75 MeV) have been plotted using COVR in Fig. 30. The large negative correlations along the diagonal result from the fact that, below 10 MeV, these inelastic reactions are the major contributors to the fairly well-known tritium-production cross section. An upward variation in one reaction at a given energy must be accompanied by a downward change in the other. As shown in the plot, the magnitude of this negative correlation diminishes at higher energies, as other reactions begin to contribute significantly to the tritium-production cross section. Plots of this type, prepared using ERRORR and COVR, have proven to be useful tools in the validation of the covariance files of new evaluations.

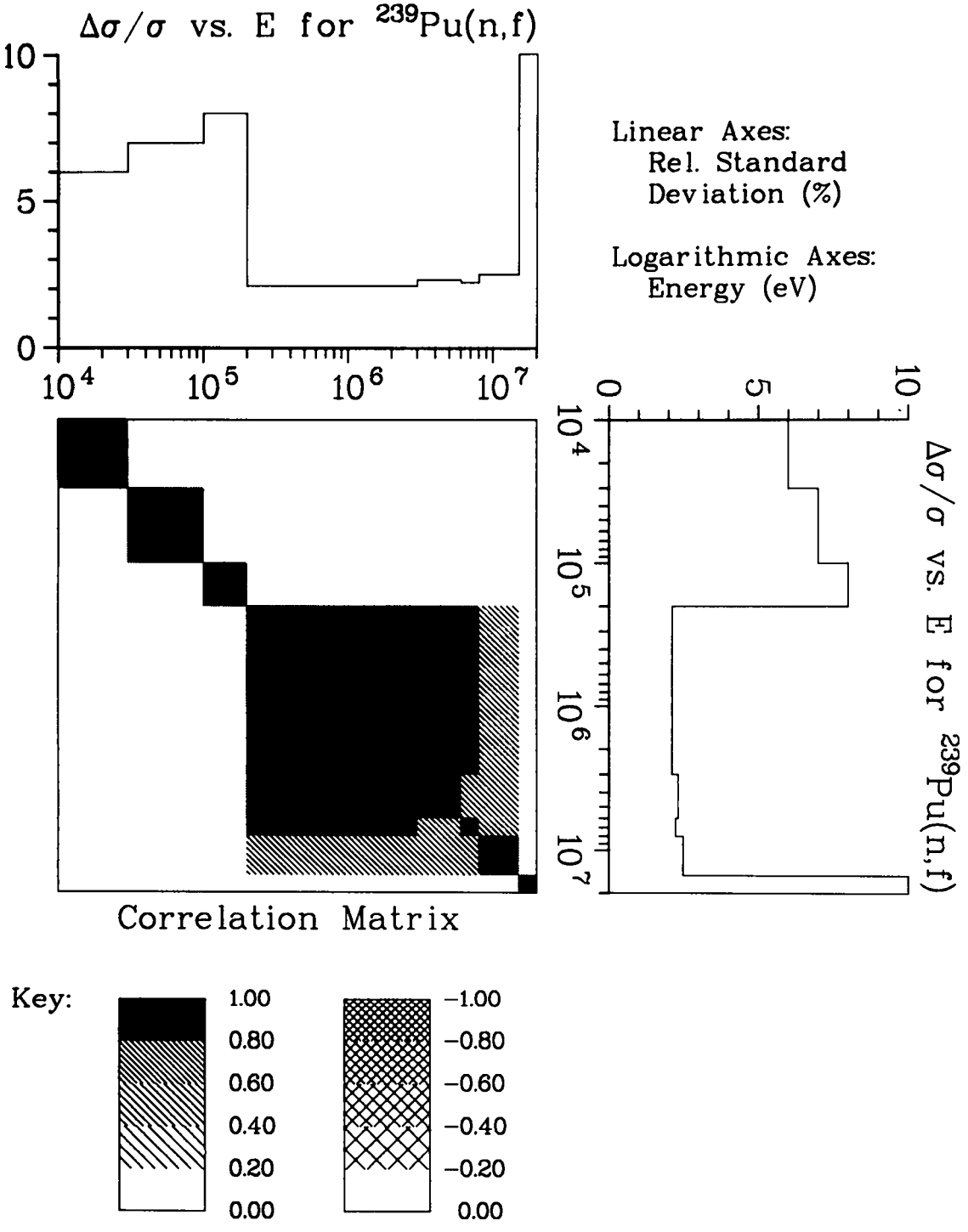

Fig. 28. Covariance data for ^{239}Pu(n,f), neglecting uncertainty in standard.

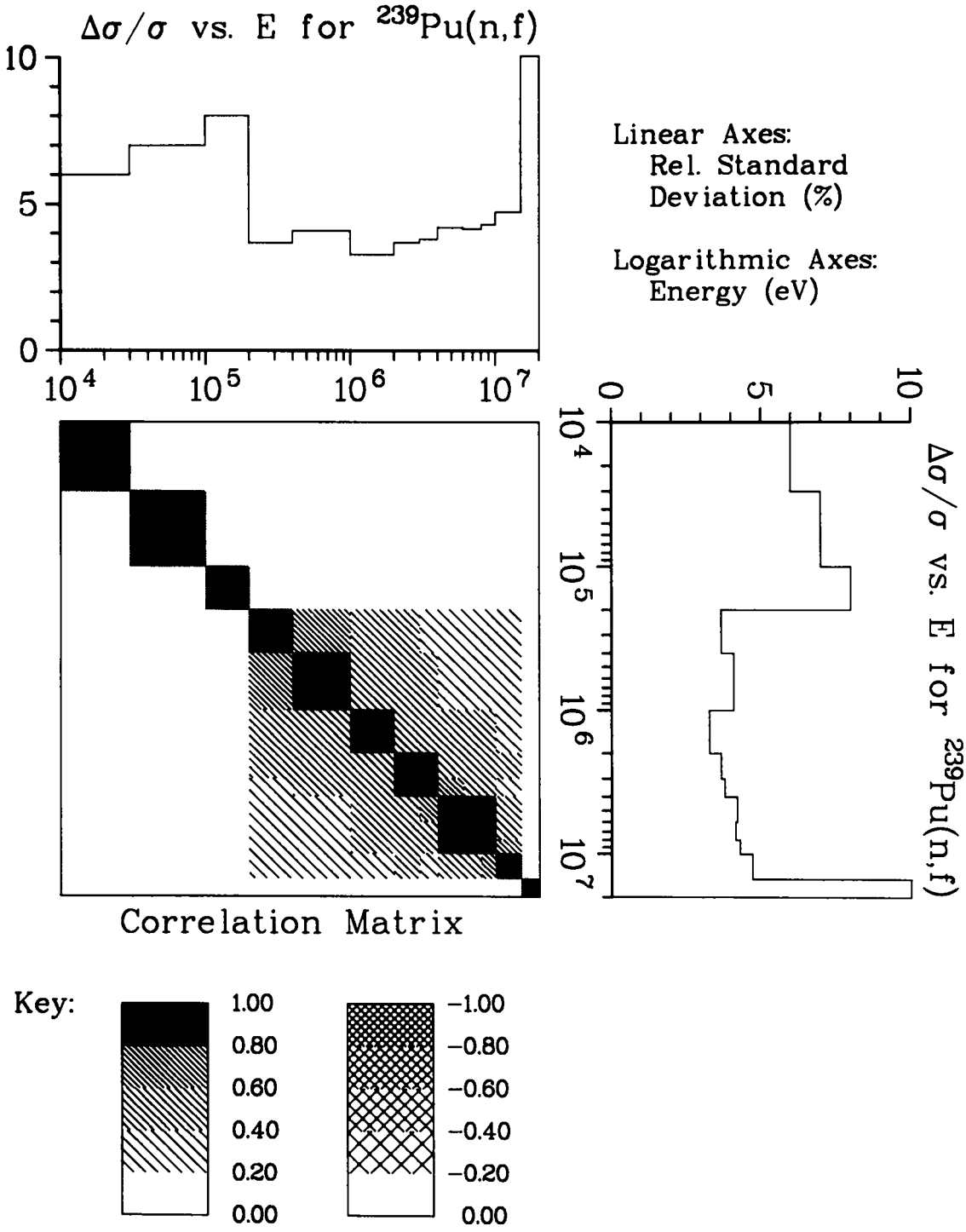

Fig. 29. Covariance data for ^{239}Pu(n,f), including uncertainty in standard.

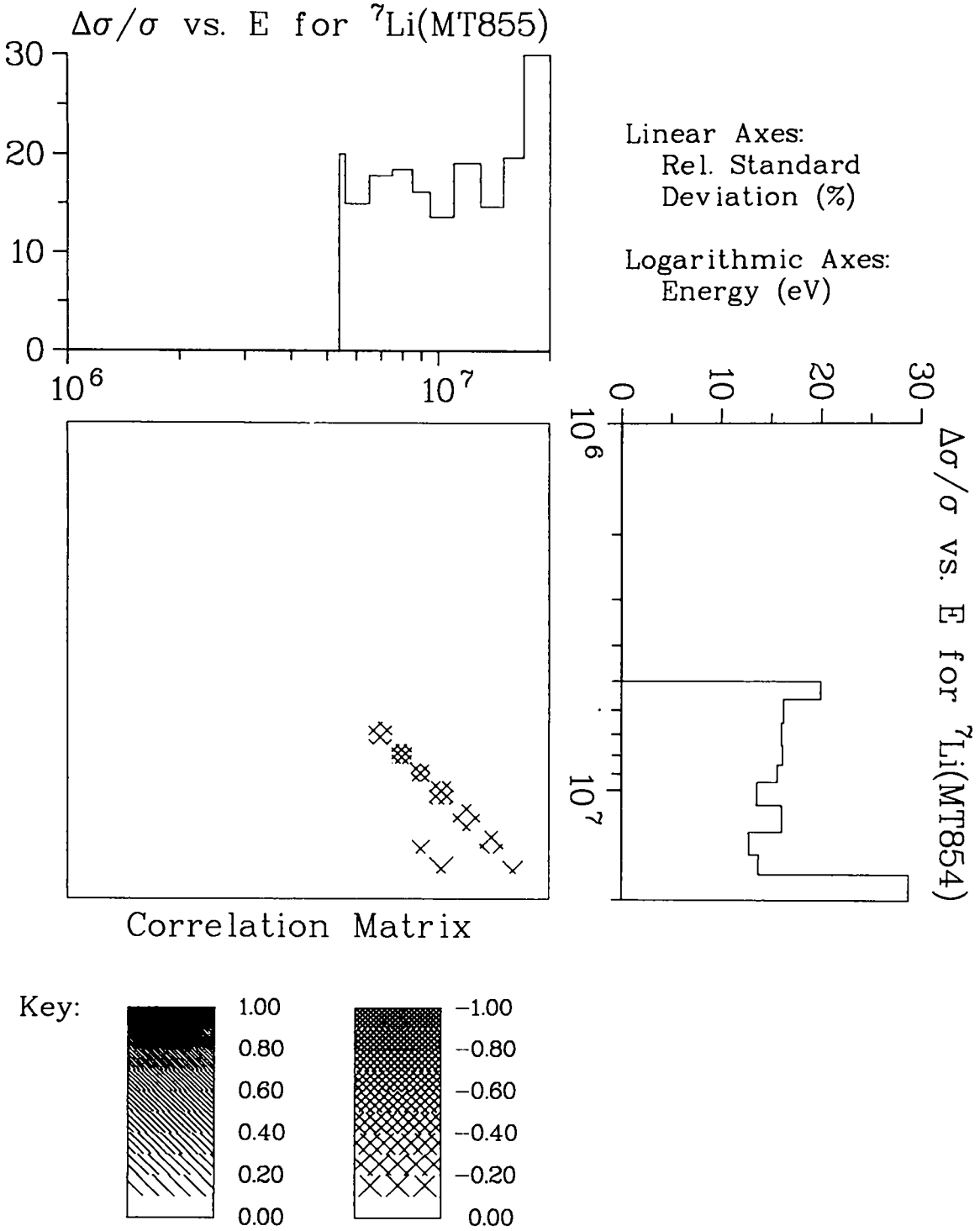

Fig. 30. Covariance data for ^{7}Li(MT854) with ^{7}Li(MT855).

D. Integral Data Testing of Representations of ^{235}U and ^{239}Pu Thermal Fission Spectra (R. J. LaBauve and D. G. Madland)

In previous reports [59-63] we have described comparisons of integral cross sections averaged over a number of representations of ^{235}U thermal and ^{252}Cf spontaneous fission spectra with experiment. In this report, an additional integral experiment,[64] performed by J. A. Grundl, was selected so that representations of the ^{239}Pu thermal fission spectrum could also be included in the comparisons.

In the Grundl experiment, the energy spectra of neutrons from the thermal neutron induced fission of ^{235}U, ^{233}U, and ^{239}Pu were compared by means of observations with eight activation detectors. Results from seven of these detectors, namely, $^{238}U(n,f)$, $^{237}Np(n,f)$, P(n,p), Al(n,p), $^{56}Fe(n,p)$, Al(n,α), and $^{63}Cu(n,2n)$, in the ^{235}U and ^{239}Pu thermal fission spectra, were used in this report. In particular, we used the detector ratios shown in Grundl's Tables V and VII and the multigroup spectrum ratios shown in Table VII in our comparisons.

The integral reaction cross section $\bar{\sigma}_R$ for a particular reaction cross section $\sigma_R(E)$ is given by

$$\bar{\sigma}_R = \frac{\int_{E_1}^{E_2} \sigma_R(E)N(E)dE}{\int_{E_1}^{E_2} N(E)dE},$$

where $\sigma_R(E)$ is the pointwise reaction cross section, which, in this study, is taken from ENDF/B-V[65] for each of the above reactions. E1 and E2 specify the incident neutron energy range (1×10^{-5} eV to 20 MeV for ENDF/B-V) and N(E) is one of six thermal-neutron-induced fission spectra for ^{235}U and ^{239}Pu, as follows.

(a) ^{235}U ENDF/B-V Watt representation with A = 0.988 MeV and B = 2.249/MeV,

(b) ^{239}Pu ENDF/B-V Watt representation with A = 0.966 MeV and B = 2.842/MeV,

(c) ^{235}U Los Alamos approximate representation of Madland-Nix Theory,[42]

(d) ^{239}Pu Los Alamos approximate representation of Madland-Nix Theory,[42]
(e) ^{235}U Los Alamos exact representation of Madland-Nix Theory,[42] and
(f) ^{239}Pu Los Alamos exact representation of Madland-Nix Theory.[42]

As a first step in this study, integral cross sections were calculated for each reaction in each of the above spectra. This was done with the NJOY code (Ref. 4) in which the integrals in the above equation are computed in an essentially pointwise manner. Next, in accordance with the Grundl report, "detector ratios" were calculated by taking the ratios of the $^{238}U(n,f)$ integral cross sections to the integrals of the threshold cross sections and also the integral Np(n,f) cross sections to the integral $^{238}U(n,f)$ cross sections. Finally, "detector ratios" obtained for the reactions calculated in the ^{239}Pu thermal spectral representations were ratioed to those obtained for the ^{235}U representations.

Results are shown in Table III in which we give the calculated values and their deviations from the experiment. Experimental data shown in this table are from Table V in the Grundl report. Note that, as compared to experiment, the ENDF/B-V results tend to be higher than the experiment, whereas those for both Los Alamos represention tend to be low.

TABLE III

RATIO OF SPECTRA INDICES ($^{239}Pu/^{235}U$)

	Measured*		ENDF/B-V		Madland-approx.		Madland-exact	
Detector Ratio	Ratio	1-σ	Ratio	Dev.	Ratio	Dev.	Ratio	Dev.
$Np(n,f)/^{238}U(n,f)$	0.971	0.006	0.975	+0.004	0.970	-0.001	0.970	-0.001
$^{238}U(n,f)/P(n,p)$	0.979	0.009	0.978	-0.001	0.968	-0.011	0.966	-0.013
$^{238}U(n,f)/Al(n,p)$	0.914	0.009	0.943	+0.029	0.882	-0.032	0.876	-0.038
$^{238}U(n,f)/^{56}Fe(n,p)$	0.880	0.010	0.922	+0.040	0.812	-0.068	0.805	-0.075
$^{238}U(n,f)/Al(n,\alpha)$	0.850	0.010	0.912	+0.060	0.773	-0.077	0.765	-0.085
$^{238}U(n,f)/^{63}Cu(n,2n)$	0.746	0.016	0.889	+0.143	0.595	-0.151	0.590	-0.156

*Taken from Table V of Ref. 64.

These results can be illustrated graphically by estimating an "effective" threshold energy for each of the threshold reactions used in this study. Figure 31 shows plots of these reactions, and our estimates of the "effective" threshold energy for each reaction are indicated in the figure. Note that these "effective" threshold energies are used only for illustrative purposes and are not used in any of our calculations.

A plot of the experimental and calculated threshold reaction ratios in Table III against the "effective" threshold energies is shown in Fig. 32. Also shown in this figure are curves that are the ratios of the integrals of the ^{239}Pu spectral representations to those for ^{235}U in which the lower limits of the integrals are taken at increasing incident neutron energy, thus simulating the threshold energies of fictitious reactions. The close agreement of these curves with the calculated points in the figure demonstrates that the Grundl experiment is highly spectrum dependent, but appears to be independent of the evaluated cross-section data used in the analysis.

The question arises as to the interpretation of the results shown in Table III and Fig. 32, because these are for $^{239}Pu/^{235}U$. We maintain that the discrepancies between calculation and experiment are due to deficient representations of the ^{239}Pu thermal fission spectrum, because our previous work, as well as comparisons with the Grundl work, show that the ^{235}U spectral representations are all more or less valid, as shown in Table IV. This table compares calculated detector ratios in the ^{235}U thermal fission spectral representations with experimental results. The experimental results shown in this table are from Table VII of the Grundl report. Note that, except for the $^{63}Cu(n,2n)$ ratio, essentially all calculated results are within 2-sigma of the experiment. Also note that the $^{63}Cu(n,2n)$ cross section we used is probably deficient due to its being obtained from ENDF/B-V by subtracting the sum of the partials given in the file from the total cross section. For an indeterminate reason, the ^{63}Cu (n,2n) cross section is not given explicity in ENDF/B-V.

Assuming the ^{235}U representations to be valid, we thus conclude from the results in Table III and Fig.32 that the ENDF/B-V ^{239}Pu thermal fission spectrum is somewhat too soft, and that both of the Los Alamos representations are too hard. This is further indicated by plotting the direct ratios of the spectra (rather than the integrals) and comparing them with the multigroup data from Table VIII of the Grundl report. These are shown in Fig. 33.

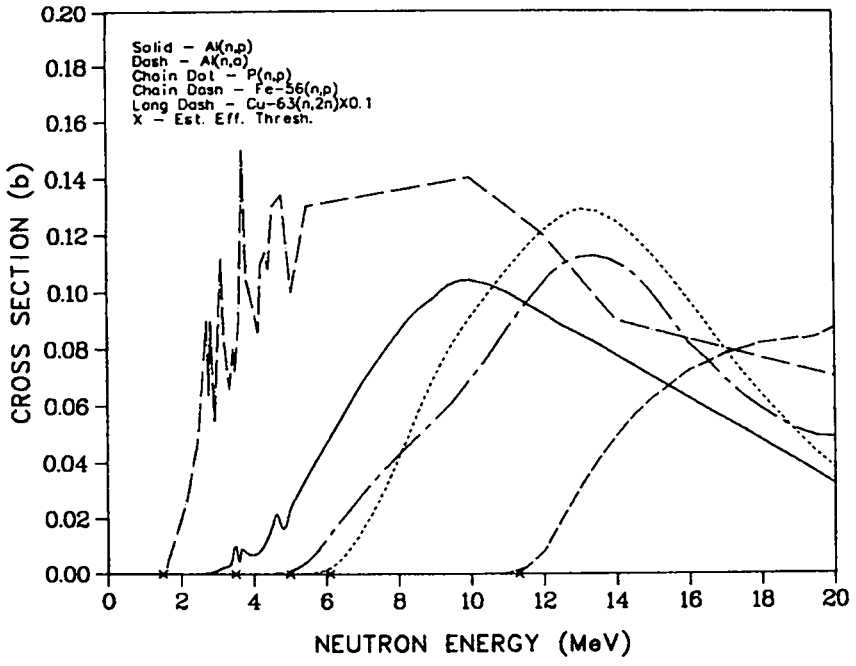

Fig. 31. Cross sections of five threshold reactions.

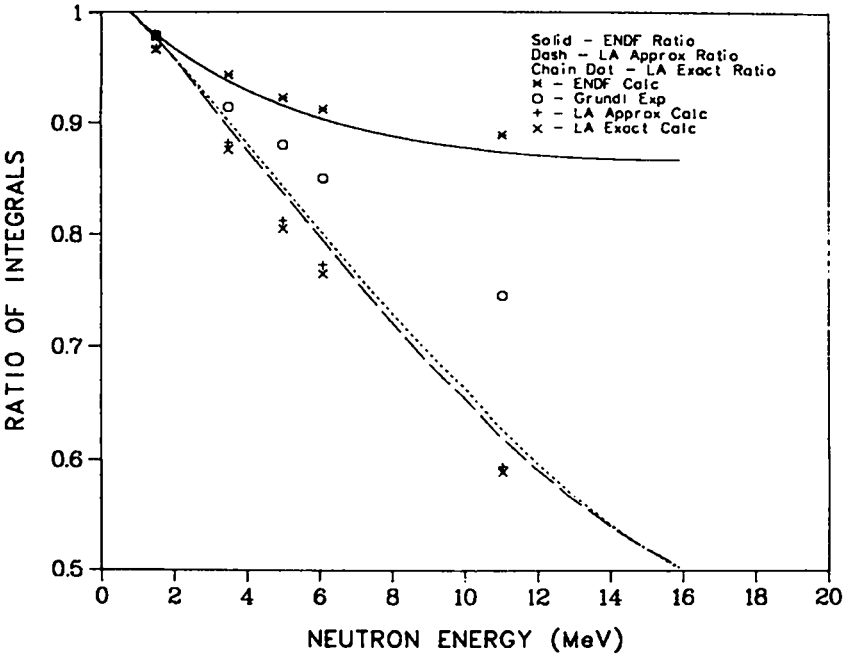

Fig. 32. Ratio of ^{239}Pu spectral integrals to ^{235}U spectral integrals.

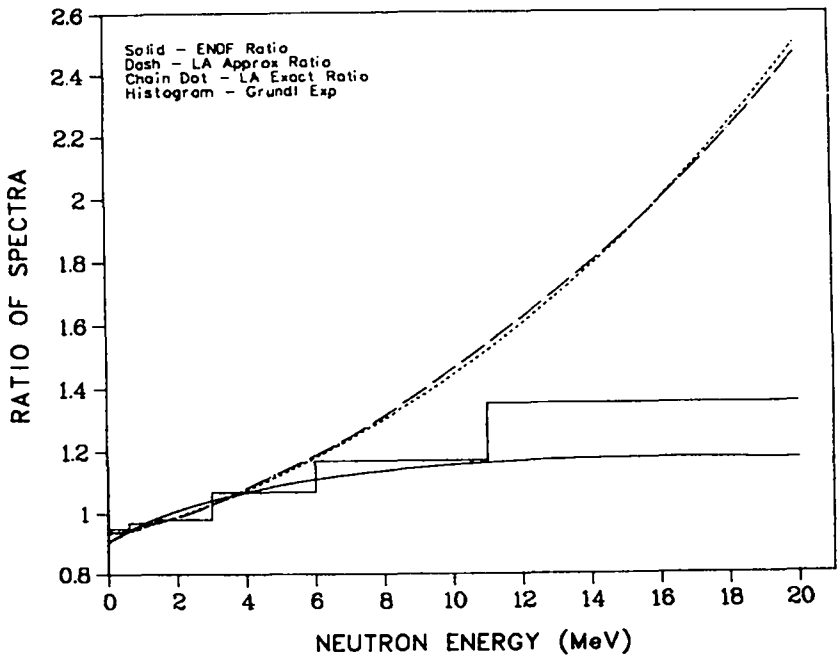

Fig. 33. Ratio of ^{239}Pu spectral representations to ^{235}U spectral representations.

TABLE IV

SPECTRAL INDICES FOR ^{235}U THERMAL FISSION NEUTRONS

Detector Ratio	Meas.+	2-σ	ENDF/B-V	Dev.	LA-Approx.	Dev.	LA-Exact	Dev.
NP(N,F)/^{238}U(N,F)	4.20	0.29	4.42	.22	4.37	.15	4.42	.22
^{238}U(N,F)/P(N,P)	8.40	0.76	9.05	.65	9.05	.65	9.16	.76
^{238}U(N,F)/Al(N,P)	69.1	6.3	71.6	2.5	72.4	3.3	73.3	4.2
^{238}U(N,F)^{56}Fe(N,P)	274.0	24.7	294.5	20.5	300.2	26.2*	298.5	24.5
^{238}U(N,F)/Al(N,A)	432.0	30.2	424.6	-8.4	433.3	1.3	427.1	-5.9
^{238}U(N,F)/^{63}Cu(N,2N)	2640.0	316.8	3286.7	646.7*	3306.5	666.5*	2968.1	328.1*

+ - Taken from Table VII of Ref. 64.

* - Calculation outside 2-σ

Average energies of all the representations used are compared with the Grundl results in Table V. Note again from this table that the Los Alamos representations seem too hard.

TABLE V

COMPARISON OF AVERAGE ENERGIES FOR DIFFERENT SPECTRAL REPRESENTATIONS

Quantity	Exper.	2-σ	ENDF/B-V	LA-Approx.	LA-Exact
<E> (^{235}U)	—	—	2.031	2.060	2.030
<E> (^{239}Pu)	—	—	2.112	2.168	2.140
Ratio	1.039	.004	1.040	1.052	1.054

As explained in Ref. [42], the Los Alamos theoretical spectra representations can be adjusted to fit experiment by changing the level density parameter "a", which would be valid for all incident neutron energies. This, however, would be done on the basis of microscopic experimental data rather than integral data. Such microscopic comparisons are shown in Fig. 34 for ^{235}U and in Fig. 35 for ^{239}Pu. The experimental data [66] are from Studsvik, and the measurements were made for an incident neutron energy of 0.53 MeV. The curves in the two figures were calculated using the Madland-Nix theory, of course at the proper incident neutron energy. Although these microscopic results are for a different incident energy, the conclusions that can be drawn from them are the same as those drawn from the Grundl comparison, namely that (a) the Los Alamos representations of the ^{235}U fission spectrum are in agreement with experiment, but (b) the ^{239}Pu representations are too hard and must be adjusted in the direction of a softer spectrum.

Reference 66 also gives measurements from Cadarache taken at lower incident neutron energies (.01-.05 MeV), but these data are, unfortunately, not as consistent as the Studsvik data. Even so, as can be seen in Figs. 36 and 37, the Cadarache measurements indicate that the Los Alamos ^{235}U representations agree with experiment, whereas the Los Alamos ^{239}Pu representations are too hard.

Both the integral and microscopic experiments described in this report should be useful in making adjustments to the ^{239}Pu fission spectrum. To illustrate this utility, consider the progress we have made to date in adjusting the level density parameter for the exact Madland-Nix ^{239}Pu spectrum representation. The value of the level density parameter "a" for all the preceding exact theoretical calculations was set as: a = A/11 MeV, in which A is the mass number of the fissioning nuclide. As a first pass in adjusting "a", we ran the following cases.

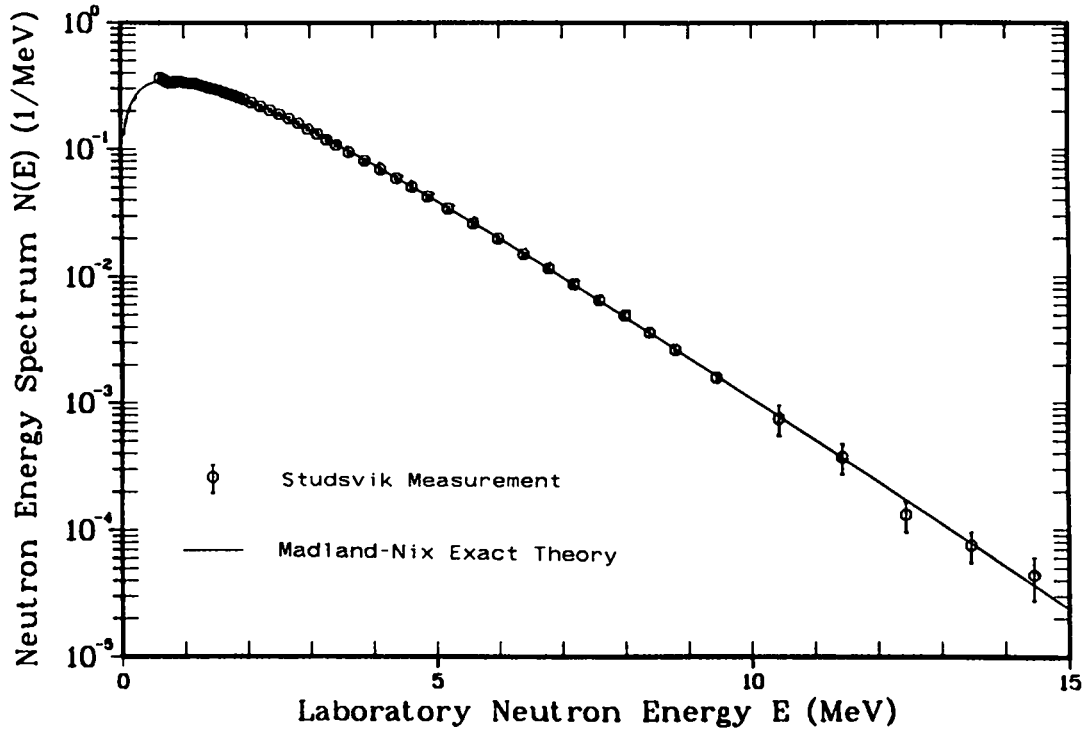

Fig. 34. ^{235}U + n(0.53 MeV) spectrum compared to Studsvik measurement.

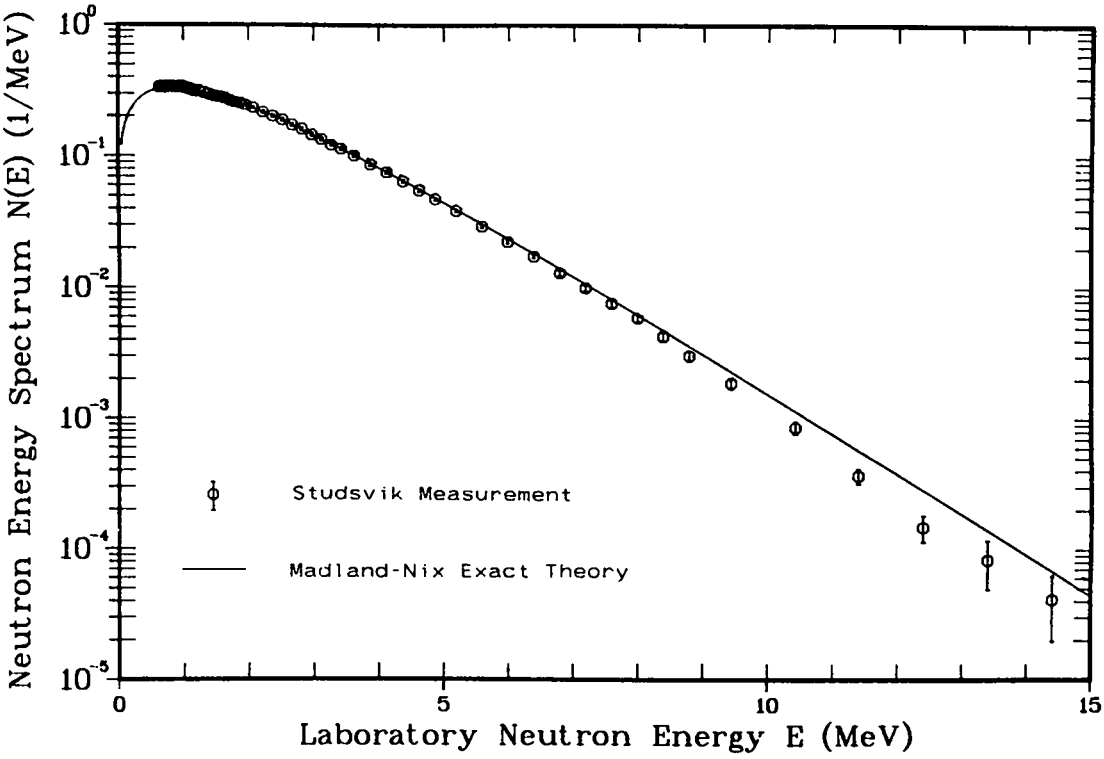

Fig. 35. ^{239}Pu + n(0.53 MeV) spectrum compared to Studsvik measurement.

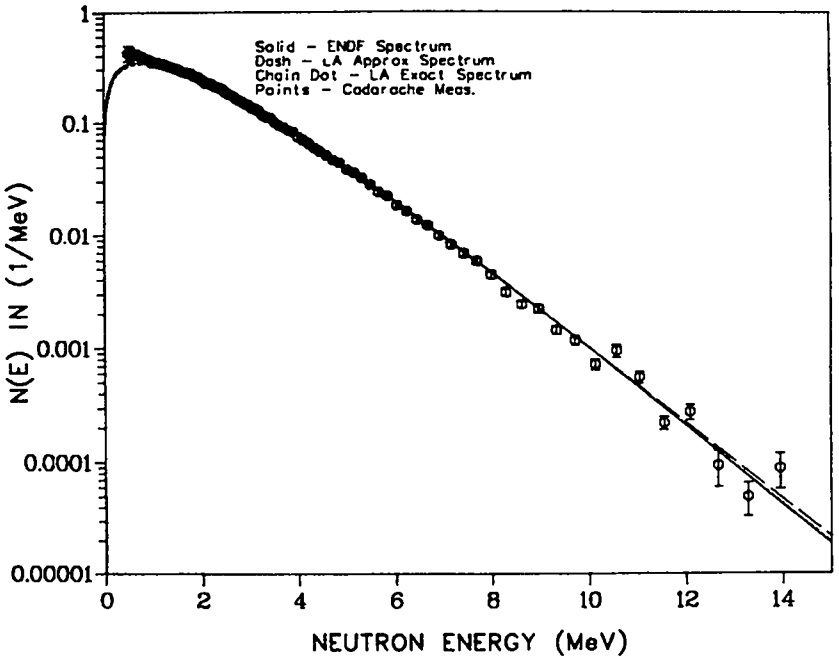

Fig. 36. Comparison of three representations of the ^{235}U thermal fission spectrum with experiment.

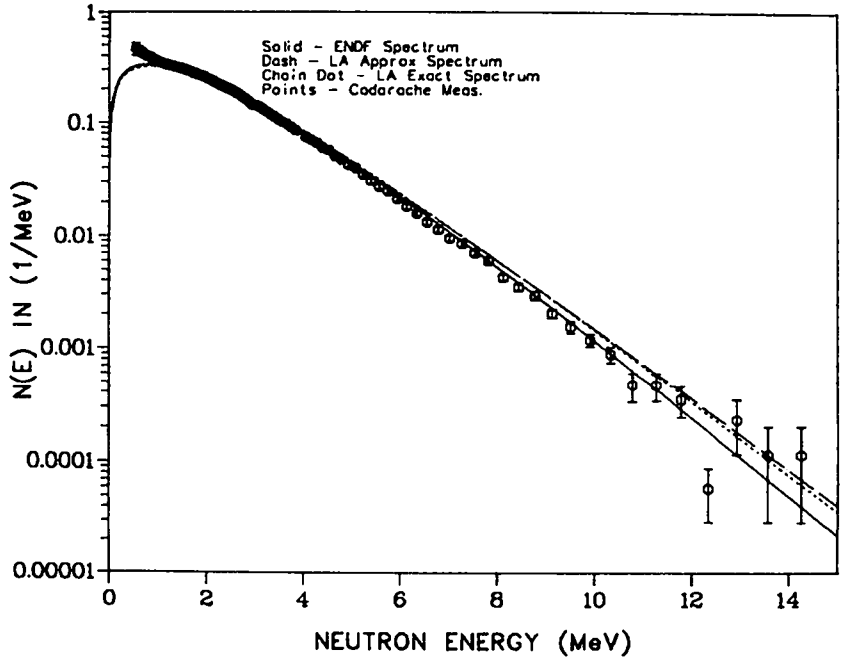

Fig. 37. Comparison of three representations of the ^{239}Pu thermal fission spectrum with experiment.

Case 1 - a = A/(10.50), yielding <E> (Thermal) = 2.1086 MeV

Case 2 - a = A/(10.25), yielding <E> (Thermal) = 2.0925 MeV

Case 3 - a = A/(10.00), yielding <E> (Thermal) = 2.0762 MeV.

The results from these runs are compared with those above in Figs. 38, 39, and 40. In Fig. 38, note that Cases 1 and 2 lie much closer to the Grundl experiment than any of the previous calculations shown in Fig. 32. Of course, it will be necessary to actually calculate the integral cross-section ratios to obtain a final comparison.

Figure 39 indicates that Case 2 seems to lie closest to the results of the Grundl experiment; but, when one considers the ratios of the average energies for the three cases to the average energy for the exact ^{235}U thermal fission representation, namely, 1.039, 1.031, and 1.023, respectively, Case 1 is favored. Results of the comparisons with the Cadarache measurement (Fig. 40) are, unfortunately, inconclusive due to the large experimental error at high energy. Other comparisons, for example, the Studsvik measurements with measurements of $\bar{\nu}$, are in progress.

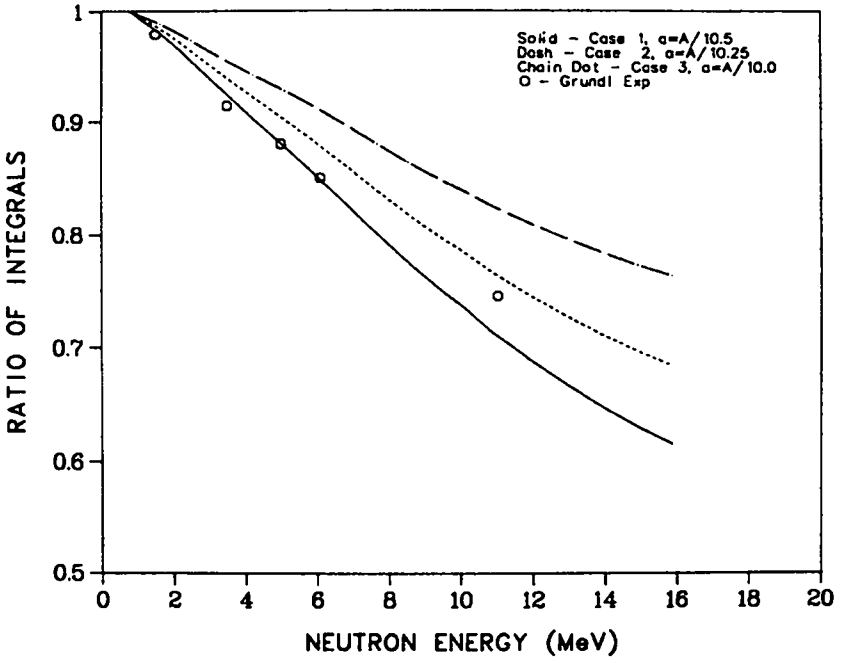

Fig. 38. Ratio of ^{239}Pu spectral integrals to ^{235}U spectral integrals.

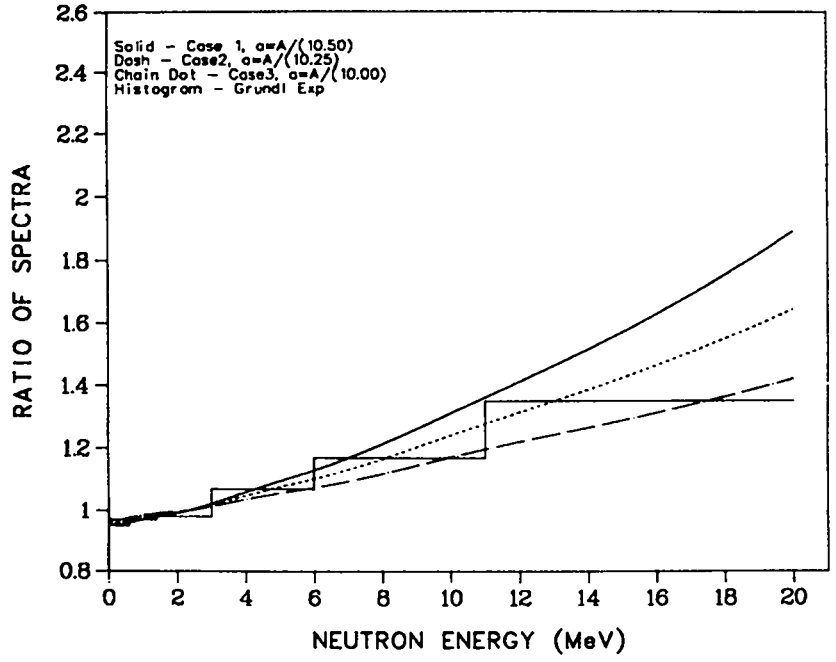

Fig. 39. Ratio of ^{239}Pu spectral representations to ^{235}U spectral representations.

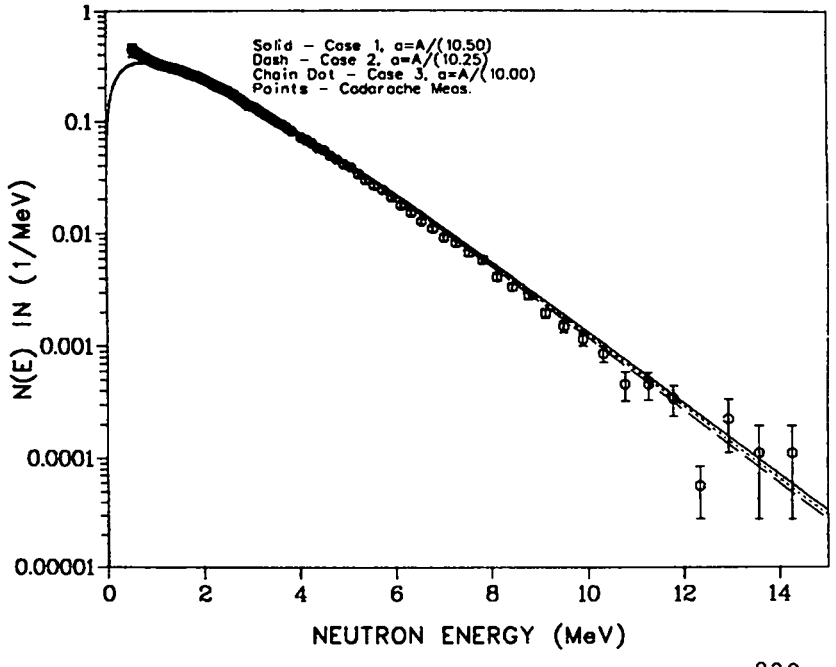

Fig. 40. Comparison of three representations of ^{239}Pu thermal spectrum with experiment.

III. FISSION PRODUCTS AND ACTINIDES: YIELDS, DECAY DATA, DEPLETION, AND BUILDUP

A. ENDF/B-VI Yields [T. R. England and B. F. Rider (G.E.)]

Preliminary yield evaluations for 50-yield sets, all codes, and experimental data files collected by B. F. Rider (General Electric Co.) are now stored for possible continued work at Los Alamos. The evaluated data represent a 2½ factor increase over the amount of data in ENDF/B-V and a 20-fold increase over ENDF/B-IV. Table VI lists the fissionable nuclides and incident fission energies for which there is a preliminary evaluation. The data sets are complete, but recent work on delayed neutron yields (described in the following section) show that some experimental precursor yields are not included in the evaluations.

B. Delayed Neutron Data [T. R. England, W. B. Wilson, R. E. Schenter, and F. M. Mann (Hanford Engineering Development Laboratory)]

An invited talk and paper reviewing the status of delayed neutron precursor data for aggregate time-group values and spectral data was presented in March 1982, at the American Chemical Society Symposium on Beta-Delayed Neutron Emission.[67] The basis of the talk was an extensive review effort done largely to examine the current adequacy of ENDF/B-V evaluations (summarized in Table VII).

We find that the ENDF/B-V evaluations, largely unchanged from ENDF/B-IV,[68] can now be improved and extended to other fissionable nuclides and incident fission energies, particularly the aggregate spectra, using individual precursor fission yields, emission probabilities (Pn),[69] and spectra. Currently we are using 105 precursors, as summarized in Table VIII. The column labeled "spectra source" lists either GR or MOD; this refers to the G. Rudstam experimental spectra[70] or model estimates using a recent Hanford Engineering Development Laboratory code, BETA,[71] which is still being tested here and at HEDL. While only 29 precursor daughters have measured spectra, these account for 70-87% of the total number of delayed neutrons, as can be seen from Table IX. This table also summarizes the results of calculated $\bar{\nu}_d$ in the conventional 6 time-groups; Table X compares calculations with ENDF/B-V and with Tuttle;[72] Tables XI and XII provide individual values and average energies; and Figs. 41-47 show the plotted spectra for one of the 20 fissionable nuclide/incident

neutron energies examined. All results to date are based on the evaluated ENDF/B-V precursor yields, Pn's, and combined measured and model calculated spectra. We have found that the Pn data require an updating, particularly their uncertainties. This is now in progress. In addition, preliminary fission yields, evaluated for ENDF/B-VI, will be used to further improve the calculated $\bar{\nu}_d$ and spectra.

TABLE VI

ENDF/B FISSION-PRODUCT YIELD SETS[a]

Fissionable Nuclide	Average Energy			
	Thermal	Fast	High Energy	Spontaneous
^{227}Th	6			
^{229}Th	6			
^{232}Th		4,5,6	5,6	
^{231}Pa		6		
^{232}U		6		
^{233}U	4,5,6	5,6	5,6	
^{234}U		6	6	
^{235}U	4,5,6	4,5,6	4,5,6	
^{236}U		5,6	6	
^{237}U		6		
^{238}U		4,5,6	4,5,6	6
^{237}Np		5,6	6	
^{238}Np		6		
^{238}Pu		6		
^{239}Pu	4,5,6	4,5,6	5,6	
^{240}Pu		5,6	6	
^{241}Pu	4,5,6	5,6		
^{242}Pu		5,6		
^{241}Am	6	6	6	
^{242m}Am	6			
^{243}Am		6		
^{242}Cm		6		
^{244}Cm				6
^{245}Cm	6			
^{248}Cm				6
^{249}Cf	6			
^{250}Cf				6
^{251}Cf	6			
^{252}Cf				5,6
^{253}Es				6
^{254}Es	6			
^{254}Fm				6
^{255}Fm	6			
^{256}Fm				6

[a]The numbers 4,5, and 6 refer to availability in ENDF/B Versions IV, V, and preliminary VI. ENDF/B-IV contains only independent yields and does not include uncertainties.

TABLE VII

SUMMARY OF ENDF/B-V EVALUATION
FOR
DELAYED NEUTRONS

FISSIONABLE NUCLIDE	NU (100 FISSIONS)	ENERGY RANGE	SPECTRA
TH232	5.27	CONST. TO 4 MEV	SAME AS U235
	5.27-3.00	LIN-LIN 4-7 MEV	
	3.00	CONST. 7-20 MEV	
U233	0.740	CONST. TO 4.5 MEV	SAME AS U235
	0.740-0.470	LIN-LIN 4.5-6 MEV	
	0.470	CONST. 6-14 MEV	
	0.470-0.420	LIN-LIN 14-15 MEV	
	0.420	CONST 15-20 MEV	
U235	1.67	CONST. TO 4 MEV	GROUP 4 SPECTRA USED FOR 5,6
	1.67-0.900	LIN-LIN 4-7 MEV	
	0.900	CONST. 7-20 MEV	
U238	4.40	CONST. TO 4 MEV	GROUP 4 SPECTRA USED FOR 5,6
	4.40-2.60	LIN-LIN 4-9 MEV	
	2.60	CONST. TO 20 MEV	
PU239	0.645	CONST. TO 4 MEV	GROUP 4 SPECTRA USED FOR 5,6
	0.645-0.430	LIN-LIN 4-7 MEV	
	0.430	CONST. 7-20 MEV	
PU240	0.900	CONST. TO 4 MEV	SAME AS PU239
	0.900-0.615	LIN-LIN 4-7 MEV	
	0.615	CONST. 7-20 MEV	
PU241	1.62	CONST.TO 4 MEV	SAME AS PU239
	1.62-0.840	LIN-LIN 4-7 MEV	
	0.840	CONST. 7-20 MEV	

TABLE VIII

DELAYED NEUTRON PRECURSOR DATA

NUCLIDE	HALFLIFE	PN (%)	AVE E (KEV)	GP	SPECTRA SOURCE	%U235 THERM	%PU239 THERM
30-ZN- 79	0.313	1.100+/- 0.000	298.	5	MOD	<.01%	<.01%
31-GA- 79	3.000	0.102+/- 0.015	354.	4	GR	<.01%	<.01%
31-GA- 80	1.660	0.870+/- 0.050	363.	4	GR	<.01%	.01
31-GA- 81	1.230	12.200+/- 0.900	370.	4	GR	.05	.05
31-GA- 82	0.600	21.000+/- 1.400	125.	5	MOD	.08	.01
31-GA- 83	0.310	56.000+/- 0.000	125.	5	MOD	.01	.01
32-GE- 83	1.900	0.170+/- 0.000	1377.	4	MOD	<.01%	<.01%
32-GE- 84	1.200	10.000+/- 0.000	209.	4	MOD	.18	.04
32-GE- 85	0.250	20.000+/- 0.000	125.	6	MOD	.05	.01
32-GE- 86	0.247	22.000+/- 0.000	125.	6	MOD	.01	<.01%
33-AS- 84	5.300	0.130+/- 0.060	328.	3	MOD	.02	.01
33-AS- 85	2.030	22.000+/- 8.000	704.	4	GR	1.93	.66
33-AS- 86	0.900	10.500+/- 2.200	125.	4	MOD	.53	.15
33-AS- 87	0.300	44.000+/-14.000	693.	6	MOD	1.72	.10
34-SE- 87	5.600	0.190+/- 0.030	328.	3	MOD	.08	.04
34-SE- 88	1.500	0.500+/- 0.300	209.	4	MOD	.10	.03
34-SE- 89	0.427	5.000+/- 1.500	125.	5	MOD	.34	.07
34-SE- 90	0.555	11.000+/- 0.000	125.	5	MOD	.15	.02
34-SE- 91	0.270	21.000+/- 8.000	125.	6	MOD	.02	<.01%
35-BR- 87	55.700	2.540+/- 0.100	201.	1	GR	2.88	2.29
35-BR- 88	16.000	6.900+/- 0.300	252.	2	GR	7.96	4.81
35-BR- 89	4.380	13.900+/- 1.000	433.	3	GR	10.38	6.41
35-BR- 90	1.800	21.200+/- 2.400	481.	4	GR	8.18	6.39
35-BR- 91	0.600	10.900+/- 1.800	301.	5	GR	1.51	.24
35-BR- 92	0.360	22.000+/- 6.000	1388.	5	MOD	.45	.08
35-BR- 93	0.176	41.000+/- 0.000	1437.	6	MOD	.07	.38
36-KR- 92	0.360	0.033+/- 0.003	226.	5	MOD	.03	.01
36-KR- 93	1.290	1.950+/- 0.110	499.	4	MOD	.58	.17
36-KR- 94	0.210	5.700+/- 2.200	384.	6	MOD	.71	.16
36-KR- 95	0.780	9.500+/- 0.000	1377.	5	MOD	.04	.01
37-RB- 92	4.530	0.012+/- 0.001	205.	3	GR	.03	.03
37-RB- 93	5.860	1.370+/- 0.080	361.	3	GR	2.79	3.24
37-RB- 94	2.760	10.300+/- 0.500	385.	4	GR	10.41	10.84
37-RB- 95	0.380	8.800+/- 0.400	356.	5	GR	4.07	4.28
37-RB- 96	0.204	13.900+/- 0.700	451.	6	GR	1.62	.89
37-RB- 97	0.170	27.800+/- 2.500	503.	6	GR	1.23	.25
37-RB- 98	0.110	16.000+/- 1.000	482.	6	GR	.02	.01
37-RB- 99	0.145	15.000+/- 3.000	1694.	6	MOD	<.01%	<.01%
38-SR- 97	0.400	0.270+/- 0.090	125.	5	MOD	.31	.27
38-SR- 98	0.650	0.360+/- 0.110	248.	5	MOD	.14	.11
38-SR- 99	0.600	3.400+/- 2.400	280.	5	MOD	.68	.16
38-SR-100	0.618	5.000+/- 0.000	209.	5	MOD	.04	.04
39-Y - 97M	1.110	0.060+/- 0.020	209.	4	MOD	.05	.12
39-Y - 97	3.700	0.330+/- 0.000	671.	3	MOD	.97	1.61
39-Y - 98M	0.650	3.440+/- 0.950	391.	5	MOD	2.16	4.90
39-Y - 98	2.000	0.540+/- 0.000	552.	4	MOD	1.10	1.70
39-Y - 99	1.400	1.200+/- 0.800	383.	4	MOD	1.60	1.85
39-Y -100	0.800	5.500+/- 0.000	500.	5	MOD	1.67	2.99
40-ZR-104	2.573	0.110+/- 0.000	298.	4	MOD	.01	.01
40-ZR-105	0.493	1.400+/- 0.000	125.	5	MOD	.07	.02
41-NB-103	1.500	0.130+/- 0.000	392.	4	MOD	.16	.61
41-NB-104	4.800	0.710+/- 0.000	224.	3	MOD	.30	1.40
41-NB-105	2.800	2.900+/- 0.000	453.	4	MOD	.42	2.03
41-NB-106	1.000	5.500+/- 0.000	125.	4	MOD	.05	.61
42-MO-109	1.409	0.530+/- 0.000	209.	4	MOD	<.01%	<.01%
42-MO-110	2.772	1.300+/- 0.000	209.	4	MOD	<.01%	<.01%
43-TC-109	1.400	1.700+/- 0.000	209.	4	MOD	.01	.58
43-TC-110	0.830	3.100+/- 0.000	125.	4	MOD	.01	.11
47-AG-122	1.500	1.400+/- 0.000	735.	4	MOD	<.01%	.01

TABLE VIII (Cont)

47-AG-123	0.390	4.600+/- 0.000	125.	5	MOD	<.01%	.01
48-CD-128	1.053	0.110+/- 0.000	125.	4	MOD	<.01%	<.01%
49-IN-127M	1.300	0.720+/- 0.040	298.	4	MOD	.01	.08
49-IN-127	3.760	0.720+/- 0.040	522.	3	MOD	.01	.08
49-IN-128	0.840	0.063+/- 0.008	125.	4	MOD	<.01%	.01
49-IN-129	0.990	3.500+/- 0.500	542.	4	GR	.18	.33
49-IN-129M	2.500	3.500+/- 0.500	125.	4	GR	.09	.16
49-IN-130	0.580	1.390+/- 0.080	509.	5	GR	.07	.05
49-IN-131	0.280	1.660+/- 0.190	840.	6	MOD	.03	.01
49-IN-132	0.120	4.100+/- 0.800	125.	6	MOD	.02	.01
50-SN-133	1.470	0.020+/- 0.000	209.	4	MOD	<.01%	<.01%
50-SN-134	1.040	17.000+/- 7.000	528.	4	GR	.11	.04
50-SN-135	0.418	8.600+/- 0.000	125.	5	MOD	<.01%	<.01%
51-SB-134M	0.850	0.086+/- 0.012	392.	4	MOD	.01	.01
51-SB-135	1.820	14.000+/- 2.000	676.	4	GR	1.16	.98
51-SB-136	0.820	23.000+/- 8.000	125.	4	MOD	.20	.08
51-SB-137	0.478	20.000+/- 0.000	125.	5	MOD	.59	.01
52-TE-136	19.000	0.900+/- 0.400	280.	2	GR	.78	.63
52-TE-137	3.500	2.200+/- 0.500	298.	3	MOD	.53	.38
52-TE-138	1.600	5.600+/- 1.600	209.	4	MOD	.21	.08
52-TE-139	0.580	6.300+/- 0.000	125.	5	MOD	.02	.01
53-I -137	24.500	7.200+/- 0.700	540.	2	GR	13.11	22.83
53-I -138	6.500	2.600+/- 0.300	376.	3	GR	2.34	3.94
53-I -139	2.380	10.200+/- 0.900	404.	4	GR	5.65	4.12
53-I -140	0.860	22.000+/- 6.000	396.	4	GR	2.71	1.70
53-I -141	0.460	39.000+/-13.000	261.	5	GR	.32	.35
53-I -142	0.200	16.000+/- 0.000	1101.	6	MOD	.06	.01
53-I -143	0.401	18.000+/- 0.000	561.	5	MOD	<.01%	<.01%
54-XE-141	1.720	0.043+/- 0.003	36.	4	MOD	.03	.03
54-XE-142	1.220	0.410+/- 0.030	209.	4	MOD	.10	.07
54-XE-143	0.960	1.200+/- 0.000	218.	4	MOD	.04	.01
54-XE-144	1.100	0.730+/- 0.000	320.	4	MOD	<.01%	<.01%
55-CS-141	24.900	0.053+/- 0.004	78.	2	MOD	.13	.23
55-CS-142	1.690	0.190+/- 0.100	253.	4	GR	.29	.37
55-CS-143	1.780	1.600+/- 0.200	223.	4	GR	1.34	1.13
55-CS-144	1.001	2.800+/- 0.700	294.	4	GR	.56	.49
55-CS-145	0.590	14.000+/- 2.000	405.	5	MOD	.46	.39
55-CS-146	0.340	13.400+/- 0.700	589.	5	MOD	.13	.03
55-CS-147	0.546	25.000+/- 3.000	754.	5	MOD	<.01%	<.01%
56-BA-147	1.755	5.200+/- 0.500	298.	4	MOD	.27	.14
56-BA-148	3.325	23.900+/- 2.100	298.	3	MOD	.14	.06
56-BA-149	0.695	0.030+/- 0.000	125.	5	MOD	<.01%	<.01%
56-BA-150	0.962	0.240+/- 0.000	209.	4	MOD	<.01%	<.01%
57-LA-147	5.000	0.500+/- 0.170	69.	3	MOD	.26	.32
57-LA-149	2.408	0.810+/- 0.000	117.	4	MOD	.03	.02
57-LA-150	0.608	0.940+/- 0.000	253.	5	MOD	<.01%	<.01%

[a] GR DENOTES SPECTRA SUPPLIED BY G. RUDSTAM AND MOD DENOTES MODEL GENERATED SPECTRA. THE LAST TWO COLUMNS ARE CALCULATED CONTRIBUTIONS TO THE TOTAL NUMBER OF DELAYED NEUTRONS.

TABLE IX

CALCULATED FRACTIONS OF TOTAL DELAYED NEUTRONS (NU)
FROM THE
29 PRECURSORS HAVING SPECTRA AND FROM THE 105 HAVING PN VALUES

DECAY GROUP	THERMAL FISSION 29	THERMAL FISSION 105	FAST FISSION 29	FAST FISSION 105	HIGH-E FISSION 29	HIGH-E FISSION 105
	********** TH232 **********					
1	-----	-----	0.0354	0.0354	0.0351	0.0351
2	-----	-----	0.1740	0.1748	0.1442	0.1451
3	-----	-----	0.1615	0.1880	0.1594	0.1726
4	-----	-----	0.3336	0.4125	0.4079	0.4637
5	-----	-----	0.0621	0.1281	0.0535	0.1007
6	-----	-----	0.0184	0.0611	0.0184	0.0828
TOTAL	-----	-----	0.7850	1.0 (NU=.0476)	0.8184	1.0 (NU=.0303)
	********** U233 **********					
1	0.0645	0.0645	0.0742	0.0742	0.0650	0.0650
2	0.2694	0.2714	0.2756	0.2776	0.2298	0.2314
3	0.1991	0.2222	0.2078	0.2292	0.2147	0.2408
4	0.3062	0.3467	0.2638	0.3061	0.2796	0.3358
5	0.0207	0.0762	0.0384	0.0971	0.0424	0.1098
6	0.0093	0.0190	0.0102	0.0157	0.0129	0.0172
TOTAL	0.8692	1.0 (NU=.00845)	0.8701	1.0 (NU=.00916)	0.8442	1.0 (NU=.00708)
	********** U235 **********					
1	0.0288	0.0288	0.0272	0.0272	0.0414	0.0414
2	0.2185	0.2198	0.2102	0.2113	0.2175	0.2189
3	0.1555	0.1786	0.1740	0.1973	0.1981	0.2246
4	0.3257	0.3838	0.3251	0.3804	0.3013	0.3664
5	0.0598	0.1335	0.0587	0.1432	0.0487	0.1237
6	0.0287	0.0555	0.0271	0.0405	0.0188	0.0250
TOTAL	0.8169	1.0 (NU=.0177)	0.8224	1.0 (NU=.0198)	0.8257	1.0 (NU=.00978)
	********** U236 **********					
1	-----	-----	0.0227	0.0227	-----	-----
2	-----	-----	0.2002	0.2013	-----	-----
3	-----	-----	0.1501	0.1770	-----	-----
4	-----	-----	0.3274	0.3997	-----	-----
5	-----	-----	0.0701	0.1559	-----	-----
6	-----	-----	0.0269	0.0433	-----	-----
TOTAL	-----	-----	0.7974	1.0 (NU=.0226)	-----	-----
	********** U238 **********					
1	-----	-----	0.0106	0.0106	0.0144	0.0144
2	-----	-----	0.1539	0.1547	0.1336	0.1343
3	-----	-----	0.1063	0.1524	0.1116	0.1413
4	-----	-----	0.3230	0.4327	0.3420	0.4390
5	-----	-----	0.0774	0.1897	0.0818	0.1960
6	-----	-----	0.0314	0.0599	0.0551	0.0750
TOTAL	-----	-----	0.7027	1.0 (NU=.0351)	0.7384	1.0 (NU=.0269)

DECAY GROUP	THERMAL FISSION 29	THERMAL FISSION 105	FAST FISSION 29	FAST FISSION 105	HIGH-E FISSION 29	HIGH-E FISSION 105
	********** NP237 **********					
1	-----	-----	0.0283	0.0283	-----	-----
2	-----	-----	0.2327	0.2344	-----	-----
3	-----	-----	0.1386	0.1711	-----	-----
4	-----	-----	0.3019	0.3806	-----	-----
5	-----	-----	0.0561	0.1563	-----	-----
6	-----	-----	0.0221	0.0293	-----	-----
TOTAL	-----	-----	0.7797	1.0 (NU=.0128)	-----	-----
	********** PU239 **********					
1	0.0229	0.0229	0.0264	0.0264	0.0569	0.0569
2	0.2827	0.2850	0.2534	0.2556	0.2115	0.2134
3	0.1362	0.1750	0.1389	0.1870	0.1539	0.2088
4	0.2710	0.3583	0.2404	0.3515	0.2366	0.3416
5	0.0492	0.1405	0.0466	0.1566	0.0375	0.1627
6	0.0115	0.0183	0.0182	0.0228	0.0140	0.0166
TOTAL	0.7734	1.0 (NU=.00769)	0.7238	1.0 (NU=.00724)	0.7103	1.0 (NU=.00387)
	********** PU240 **********					
1	-----	-----	0.0218	0.0218	-----	-----
2	-----	-----	0.2596	0.2615	-----	-----
3	-----	-----	0.1162	0.1615	-----	-----
4	-----	-----	0.2540	0.3727	-----	-----
5	-----	-----	0.0498	0.1517	-----	-----
6	-----	-----	0.0226	0.0309	-----	-----
TOTAL	-----	-----	0.7241	1.0 (NU=.00923)	-----	-----
	********** PU241 **********					
1	0.0105	0.0105	0.0112	0.0112	-----	-----
2	0.2268	0.2282	0.2280	0.2295	-----	-----
3	0.0911	0.1346	0.1009	0.1444	-----	-----
4	0.3071	0.4328	0.2787	0.4132	-----	-----
5	0.0524	0.1493	0.0552	0.1618	-----	-----
6	0.0289	0.0446	0.0299	0.0399	-----	-----
TOTAL	0.7168	1.0 (NU=.0158)	0.7039	1.0 (NU=.0149)	-----	-----
	********** PU242 **********					
1	-----	-----	0.0135	0.0135	-----	-----
2	-----	-----	0.2408	0.2424	-----	-----
3	-----	-----	0.0978	0.1464	-----	-----
4	-----	-----	0.2581	0.3963	-----	-----
5	-----	-----	0.0563	0.1565	-----	-----
6	-----	-----	0.0299	0.0449	-----	-----
TOTAL	-----	-----	0.6965	1.0 (NU=.0141)	-----	-----

TABLE X

COMPARISONS OF TOTAL $\bar{\nu}_d$ PER 100 FISSIONS

Fissionable Nuclide[a]	Calculated	ENDF/B-V	Tuttle[22]
Th232F	4.76 ± 0.34	5.27	5.31 ± 0.23
Th232H	3.03 ± 0.29	3.00	2.85 ± 0.13
U233T	0.845 ± 0.066	0.740	0.667 ± 0.029
U233F	0.916 ± 0.089	0.740	0.731 ± 0.036
U233H	0.708 ± 0.095	0.420	0.422 ± 0.025
U235T	1.77 ± 0.081	1.67	1.62 ± 0.05
U235F	1.98 ± 0.18	1.67	1.67 ± 0.036
U235H	0.978 ± 0.097	0.900	0.927 ± 0.029
U236F	2.26 ± 0.19	- -	2.21 ± 0.24
U238F	3.51 ± 0.27	4.40	4.39 ± 0.10
U238H	2.69 ± 0.21	2.60	2.73 ± 0.08
Np239F	1.28 ± 0.13	- -	- - -
Pu239T	0.769 ± 0.058	0.645	0.628 ± 0.038
Pu239F	0.724 ± 0.009	0.645	0.630 ± 0.016
Pu239H	0.387 ± 0.062	0.430	0.417 ± 0.016
Pu240F	0.923 ± 0.108	0.900	0.95 ± 0.08
Pu241T	1.58 ± 0.13	1.62	1.52 ± 0.11
Pu241F	1.49 ± 0.16	1.62	1.52 ± 0.11
Pu242F	1.41 ± 0.14	- -	2.21 ± 0.26
Cf252S	0.690 ± 0.092	- -	- - -

[a] T, F, H, and S denote thermal, fast, high energy (∿ 14 MeV) and spontaneous fission, respectively.

TABLE XI

SUMMATION CALCULATIONS OF DELAYED NEUTRONS PER 100 FISSIONS

GROUP	NUCLIDE	TH232F	TH232H	U233T	U233F	U233H	U235T	U235F	U235H	U236F	U238F
1	35BR 870	.168E+00	.106E+00	.545E-01	.680E-01	.460E-01	.510E-01	.538E-01	.405E-01	.513E-01	.372E-01
TOTAL GROUP		.168E+00	.106E+00	.545E-01	.680E-01	.460E-01	.510E-01	.538E-01	.405E-01	.513E-01	.372E-01
2	35BR 880	.407E+00	.214E+00	.105E+00	.136E+00	.113E+00	.141E+00	.158E+00	.128E+00	.143E+00	.115E+00
2	52TE1360	.324E-01	.977E-02	.388E-02	.349E-02	.713E-03	.138E-01	.139E-01	.146E-02	.195E-01	.421E-01
2	53I 1370	.388E+00	.213E+00	.119E+00	.113E+00	.491E-01	.232E+00	.243E+00	.831E-01	.289E+00	.383E+00
2	55CS1410	.370E-02	.266E-02	.170E-02	.179E-02	.114E-02	.234E-02	.224E-02	.140E-02	.255E-02	.272E-02
TOTAL GROUP		.831E+00	.439E+00	.229E+00	.254E+00	.164E+00	.389E+00	.418E+00	.214E+00	.454E+00	.543E+00
3	33AS 840	.287E-02	.148E-02	.369E-03	.408E-03	.535E-03	.322E-03	.537E-03	.551E-03	.537E-03	.614E-03
3	34SE 870	.865E-02	.309E-02	.142E-02	.104E-02	.558E-03	.143E-02	.166E-02	.724E-03	.180E-02	.177E-02
3	35BR 890	.606E+00	.380E+00	.122E+00	.139E+00	.112E+00	.184E+00	.253E+00	.145E+00	.231E+00	.239E+00
3	37RB 920	.766E-03	.610E-03	.473E-03	.510E-03	.452E-03	.581E-03	.495E-03	.490E-03	.658E-03	.444E-03
3	37RB 930	.718E-01	.527E-01	.305E-01	.373E-01	.310E-01	.494E-01	.450E-01	.363E-01	.529E-01	.547E-01
3	39Y 970	.139E-01	.971E-02	.119E-01	.122E-01	.111E-01	.172E-01	.172E-01	.136E-01	.150E-01	.174E-01
3	41NB1040	.413E-03	.439E-02	.156E-02	.215E-02	.390E-02	.529E-02	.674E-02	.539E-02	.127E-01	.245E-01
3	49IN1270	.275E-03	.208E-02	.546E-03	.471E-03	.753E-03	.222E-03	.589E-03	.142E-02	.547E-03	.394E-03
3	52TE1370	.480E-01	.717E-02	.165E-02	.135E-02	.228E-03	.936E-02	.962E-02	.722E-03	.156E-01	.520E-01
3	53I 1380	.898E-01	.492E-01	.152E-01	.133E-01	.844E-02	.414E-01	.453E-01	.117E-01	.542E-01	.793E-01
3	56BA1480	.404E-01	.574E-02	.233E-03	.221E-03	.115E-03	.247E-02	.419E-02	.564E-03	.748E-02	.543E-01
3	57LA1470	.115E-01	.622E-02	.177E-02	.184E-02	.130E-02	.460E-02	.565E-02	.291E-02	.693E-02	.106E-01
TOTAL GROUP		.894E+00	.522E+00	.188E+00	.210E+00	.170E+00	.316E+00	.390E+00	.220E+00	.400E+00	.535E+00
4	31GA 790	.538E-04	.560E-03	.305E-04	.245E-04	.525E-04	.191E-04	.467E-04	.519E-04	.535E-04	.228E-04
4	31GA 800	.519E-03	.321E-02	.125E-03	.121E-03	.212E-03	.952E-04	.303E-03	.246E-03	.333E-03	.199E-03
4	31GA 810	.724E-02	.156E-01	.522E-03	.734E-03	.951E-03	.866E-03	.213E-02	.896E-03	.251E-02	.284E-02
4	32GE 830	.149E-02	.498E-03	.861E-04	.744E-04	.726E-04	.850E-04	.158E-03	.101E-03	.178E-03	.225E-03
4	32GE 840	.650E-01	.103E-01	.121E-02	.117E-02	.988E-03	.315E-02	.420E-02	.144E-02	.514E-02	.157E-01
4	33AS 850	.316E+00	.264E+00	.291E-01	.320E-01	.300E-01	.343E-01	.592E-01	.361E-01	.786E-01	.612E-01
4	33AS 860	.690E-01	.448E-01	.319E-02	.353E-02	.313E-02	.944E-02	.107E-01	.541E-02	.113E-01	.154E-01
4	34SE 880	.140E-01	.343E-02	.904E-03	.834E-03	.470E-03	.183E-02	.242E-02	.720E-03	.254E-02	.431E-02
4	35BR 900	.392E+00	.303E+00	.943E-01	.646E-01	.531E-01	.145E+00	.180E+00	.822E-01	.170E+00	.186E+00
4	36KR 930	.407E-01	.143E-01	.298E-02	.395E-02	.258E-02	.103E-01	.557E-02	.406E-02	.160E-01	.279E-01
4	37RB 940	.295E+00	.401E+00	.930E-01	.109E+00	.978E-01	.184E+00	.229E+00	.138E+00	.230E+00	.296E+00
4	39Y 971	.459E-03	.528E-03	.870E-03	.899E-03	.849E-03	.956E-03	.962E-03	.980E-03	.784E-03	.537E-03
4	39Y 980	.158E-01	.109E-01	.922E-02	.105E-01	.973E-02	.195E-01	.206E-01	.120E-01	.214E-01	.260E-01
4	39Y 990	.190E-01	.126E-01	.931E-02	.990E-02	.891E-02	.283E-01	.270E-01	.168E-01	.305E-01	.449E-01
4	40ZR1040	.220E-04	.832E-04	.133E-04	.161E-04	.200E-04	.124E-03	.137E-03	.387E-04	.305E-03	.145E-02
4	41NB1030	.176E-03	.103E-02	.102E-02	.117E-02	.161E-02	.292E-02	.325E-02	.258E-02	.434E-02	.735E-02
4	41NB1050	.535E-03	.989E-02	.114E-02	.236E-02	.435E-02	.747E-02	.783E-02	.570E-02	.203E-01	.494E-01
4	41NB1060	.355E-03	.841E-02	.236E-03	.325E-03	.124E-02	.810E-03	.235E-02	.262E-02	.504E-02	.215E-01
4	42MO1090	.355E-04	.181E-03	.490E-06	.105E-05	.873E-05	.202E-05	.113E-04	.207E-04	.204E-04	.149E-03
4	42MO1100	.308E-04	.831E-04	.954E-07	.330E-06	.174E-05	.808E-06	.420E-05	.458E-05	.783E-05	.592E-04
4	43TC1090	.572E-03	.899E-02	.800E-04	.186E-03	.266E-02	.136E-03	.628E-03	.383E-02	.900E-03	.247E-02
4	43TC1100	.609E-03	.762E-02	.258E-04	.102E-03	.108E-02	.827E-04	.382E-03	.168E-02	.536E-03	.115E-02
4	47AG1220	.207E-03	.358E-02	.121E-04	.595E-04	.313E-03	.305E-04	.112E-03	.646E-03	.177E-03	.211E-03
4	48CD1280	.385E-04	.176E-04	.212E-05	.243E-05	.285E-06	.700E-05	.175E-04	.134E-05	.300E-04	.112E-03
4	49IN1271	.275E-03	.208E-02	.546E-03	.471E-03	.753E-03	.222E-03	.589E-03	.142E-02	.547E-03	.394E-03
4	49IN1280	.710E-04	.281E-03	.481E-04	.724E-04	.422E-04	.558E-04	.140E-03	.997E-04	.160E-03	.187E-03
4	49IN1290	.495E-02	.629E-02	.203E-02	.194E-02	.479E-03	.321E-02	.977E-04	.179E-02	.773E-02	.148E-01
4	49IN1291	.223E-02	.318E-02	.103E-02	.988E-03	.245E-03	.161E-02	.500E-04	.914E-03	.381E-02	.654E-02
4	50SN1330	.129E-03	.108E-04	.356E-05	.243E-05	.121E-06	.292E-04	.311E-04	.792E-06	.617E-04	.264E-03
4	50SN1340	.207E-01	.135E-02	.165E-03	.124E-03	.338E-05	.191E-02	.286E-02	.270E-04	.719E-02	.547E-01
4	51SB1341	.392E-03	.292E-03	.609E-04	.593E-04	.747E-05	.227E-03	.328E-03	.303E-04	.534E-03	.864E-03
4	51SB1350	.895E-01	.158E-01	.282E-02	.265E-02	.251E-03	.205E-01	.257E-01	.117E-02	.380E-01	.122E+00
4	51SB1360	.309E-01	.482E-02	.366E-03	.367E-03	.386E-04	.363E-02	.569E-02	.154E-03	.111E-01	.476E-01
4	52TE1380	.476E-01	.496E-02	.577E-03	.428E-03	.106E-03	.378E-02	.542E-02	.269E-03	.938E-02	.478E-01
4	53I 1390	.196E+00	.931E-01	.213E-01	.130E-01	.627E-02	.100E+00	.664E-01	.127E-01	.902E-01	.189E+00
4	53I 1400	.144E+00	.662E-01	.380E-02	.407E-02	.144E-02	.479E-01	.322E-01	.511E-02	.518E-01	.129E+00
4	54XE1410	.195E-02	.661E-03	.149E-03	.163E-03	.412E-04	.566E-03	.395E-03	.106E-03	.784E-03	.140E-02

TABLE XI (Cont)

4 54XE1420	.968E-02	.257E-02	.358E-03	.284E-03	.107E-03	.183E-02	.189E-02	.341E-03	.296E-02	.794E-02
4 54XE1430	.884E-02	.173E-02	.523E-04	.860E-04	.282E-04	.637E-03	.760E-03	.118E-03	.196E-02	.488E-02
4 54XE1440	.136E-02	.151E-03	.454E-05	.340E-05	.103E-05	.457E-04	.819E-04	.586E-05	.150E-03	.927E-03
4 55CS1420	.950E-02	.680E-02	.269E-02	.286E-02	.191E-02	.509E-02	.572E-02	.303E-02	.685E-02	.743E-02
4 55CS1430	.594E-01	.350E-01	.644E-02	.790E-02	.413E-02	.237E-01	.241E-01	.935E-02	.360E-01	.379E-01
4 55CS1440	.512E-01	.235E-01	.257E-02	.255E-02	.129E-02	.996E-02	.154E-01	.390E-02	.200E-01	.322E-01
4 56BA1470	.426E-01	.990E-02	.699E-03	.671E-03	.337E-03	.474E-02	.689E-02	.139E-02	.111E-01	.435E-01
4 56BA1500	.132E-05	.266E-06	.224E-08	.207E-08	.117E-08	.573E-07	.132E-06	.852E-08	.310E-06	.694E-05
4 57LA1490	.157E-02	.119E-02	.807E-04	.887E-04	.656E-04	.470E-03	.682E-03	.172E-03	.126E-02	.335E-02
TOTAL GROUP	.196E+01	.140E+01	.293E+00	.280E+00	.238E+00	.680E+00	.752E+00	.358E+00	.902E+00	.152E+01
5 30ZN 790	.142E-03	.564E-03	.125E-04	.928E-05	.142E-04	.185E-04	.481E-04	.197E-04	.666E-04	.684E-04
5 31GA 820	.819E-02	.798E-02	.218E-03	.263E-03	.323E-03	.145E-02	.114E-02	.483E-03	.137E-02	.215E-02
5 31GA 830	.105E-01	.297E-02	.985E-04	.980E-04	.101E-03	.209E-03	.622E-03	.203E-03	.835E-03	.188E-02
5 34SE 890	.428E-01	.108E-01	.109E-02	.131E-02	.766E-03	.602E-02	.680E-02	.145E-02	.739E-02	.193E-01
5 34SE 900	.204E-01	.409E-02	.599E-03	.317E-03	.175E-03	.261E-02	.272E-02	.391E-03	.315E-02	.114E-01
5 35BR 910	.837E-01	.467E-01	.591E-02	.736E-02	.573E-02	.268E-01	.204E-01	.907E-02	.366E-01	.513E-01
5 35BR 920	.358E-01	.193E-01	.124E-02	.172E-02	.141E-02	.795E-02	.575E-02	.292E-02	.160E-01	.242E-01
5 36KR 920	.150E-02	.704E-03	.265E-03	.297E-03	.161E-03	.568E-03	.346E-03	.283E-03	.850E-03	.863E-03
5 36KR 950	.101E-01	.267E-02	.300E-04	.238E-03	.172E-03	.662E-03	.233E-02	.388E-03	.328E-02	.137E-01
5 37RB 950	.127E+00	.935E-01	.107E-01	.269E-01	.240E-01	.720E-01	.877E-01	.375E-01	.102E+00	.146E+00
5 38SR 970	.741E-02	.320E-02	.191E-02	.187E-02	.147E-02	.547E-02	.541E-02	.235E-02	.527E-02	.917E-02
5 38SR 980	.498E-02	.146E-02	.577E-03	.592E-03	.423E-03	.247E-02	.283E-02	.714E-03	.343E-02	.891E-02
5 38SR 990	.108E-01	.295E-02	.763E-03	.771E-03	.581E-03	.120E-01	.583E-02	.155E-02	.783E-02	.291E-01
5 38SR1000	.199E-02	.713E-03	.133E-03	.142E-03	.901E-04	.760E-03	.182E-02	.262E-03	.223E-02	.128E-01
5 39Y 981	.269E-01	.277E-01	.266E-01	.305E-01	.290E-01	.382E-01	.521E-01	.348E-01	.520E-01	.408E-01
5 39Y 1000	.195E-01	.237E-01	.117E-01	.139E-01	.120E-01	.295E-01	.598E-01	.236E-01	.600E-01	.107E+00
5 40ZR1050	.323E-04	.215E-03	.841E-05	.161E-04	.203E-04	.124E-02	.155E-03	.392E-04	.497E-03	.332E-02
5 47AG1230	.311E-03	.386E-02	.147E-04	.510E-04	.154E-03	.315E-04	.162E-03	.397E-03	.367E-03	.424E-03
5 49IN1300	.166E-02	.102E-02	.209E-03	.226E-03	.265E-04	.132E-02	.127E-02	.115E-03	.208E-02	.431E-02
5 50SN1350	.159E-02	.339E-04	.269E-05	.206E-05	.519E-07	.545E-04	.858E-04	.482E-06	.196E-03	.260E-02
5 51SB1370	.703E-02	.473E-03	.196E-04	.174E-04	.160E-05	.105E-01	.494E-03	.100E-04	.114E-02	.906E-02
5 52TE1390	.939E-02	.101E-02	.358E-04	.336E-04	.775E-05	.430E-03	.705E-03	.307E-04	.137E-02	.106E-01
5 53I 1410	.829E-01	.207E-01	.678E-03	.723E-03	.250E-03	.567E-02	.666E-02	.959E-03	.180E-01	.700E-01
5 53I 1430	.165E-03	.194E-04	.561E-07	.693E-07	.166E-07	.223E-05	.522E-05	.185E-06	.144E-04	.165E-03
5 55CS1450	.796E-01	.243E-01	.150E-02	.156E-02	.776E-03	.809E-02	.160E-01	.315E-02	.233E-01	.693E-01
5 55CS1460	.141E-01	.404E-02	.763E-04	.844E-04	.489E-04	.226E-02	.163E-02	.264E-03	.295E-02	.150E-01
5 55CS1470	.850E-03	.132E-03	.541E-06	.613E-06	.312E-06	.139E-04	.352E-04	.302E-05	.829E-04	.111E-02
5 56BA1490	.346E-05	.859E-06	.107E-07	.109E-07	.579E-08	.187E-06	.336E-06	.287E-07	.871E-06	.877E-05
5 57LA1500	.200E-03	.170E-03	.704E-05	.748E-05	.649E-05	.578E-04	.113E-03	.246E-04	.184E-03	.875E-03
TOTAL GROUP	.609E+00	.305E+00	.644E-01	.890E-01	.777E-01	.236E+00	.283E+00	.121E+00	.352E+00	.666E+00
6 32GE 850	.274E-01	.750E-02	.304E-03	.309E-03	.204E-03	.883E-03	.171E-02	.353E-03	.281E-02	.625E-02
6 32GE 860	.602E-02	.920E-03	.268E-04	.257E-04	.145E-04	.186E-03	.247E-03	.365E-04	.330E-03	.161E-02
6 33AS 870	.105E+00	.327E-01	.305E-02	.255E-02	.150E-02	.305E-01	.117E-01	.279E-02	.150E-01	.234E-01
6 34SE 910	.432E-02	.777E-03	.321E-04	.382E-04	.221E-04	.339E-03	.332E-03	.508E-04	.727E-03	.318E-02
6 35BR 930	.134E-01	.126E+00	.305E-02	.247E-03	.186E-03	.129E-02	.105E-02	.482E-03	.351E-02	.109E-01
6 36KR 940	.390E-01	.218E-01	.167E-02	.176E-02	.113E-02	.126E-01	.103E-01	.226E-02	.124E-01	.436E-01
6 37RB 960	.502E-01	.398E-01	.621E-02	.747E-02	.721E-02	.287E-01	.374E-01	.141E-01	.423E-01	.808E-01
6 37RB 970	.347E-01	.149E-01	.158E-02	.182E-02	.181E-02	.217E-01	.151E-01	.414E-02	.170E-01	.237E-01
6 37RB 980	.270E-02	.100E-02	.558E-04	.718E-04	.718E-04	.391E-03	.103E-02	.176E-03	.143E-02	.574E-02
6 37RB 990	.589E-04	.134E-04	.336E-06	.450E-06	.433E-06	.593E-05	.143E-04	.191E-05	.233E-04	.202E-03
6 49IN1310	.140E-02	.226E-03	.582E-04	.431E-04	.216E-05	.484E-03	.509E-03	.128E-04	.936E-03	.362E-02
6 49IN1320	.125E-02	.633E-04	.955E-05	.775E-05	.237E-06	.277E-03	.200E-03	.173E-05	.427E-03	.283E-02
6 53I 1420	.460E-02	.468E-02	.138E-04	.149E-04	.565E-05	.974E-03	.404E-03	.344E-04	.839E-03	.450E-02
TOTAL GROUP	.291E+00	.251E+00	.161E-01	.144E-01	.122E-01	.983E-01	.800E-01	.244E-01	.978E-01	.210E+00
TOTAL	.476E+01	.303E+01	.845E+00	.916E+00	.708E+00	.177E+01	.198E+01	.978E+00	.226E+01	.351E+01

TABLE XI (Cont)

GROUP	NUCLIDE	U238H	NP237F	PU239T	PU239F	PU239H	PU240F	PU241T	PU241F	PU242F	CF252S
1	35BR 870	.386E-01	.364E-01	.176E-01	.191E-01	.220E-01	.201E-01	.166E-01	.166E-01	.190E-01	.548E-02
TOTAL	GROUP	.386E-01	.364E-01	.176E-01	.191E-01	.220E-01	.201E-01	.166E-01	.166E-01	.190E-01	.548E-02
2	35BR 880	.105E+00	.824E-01	.370E-01	.416E-01	.478E-01	.433E-01	.415E-01	.410E-01	.478E-01	.144E-01
2	52TE1360	.134E-01	.739E-02	.486E-02	.488E-02	.505E-03	.105E-01	.198E-01	.165E-01	.250E-01	.642E-02
2	53I 1370	.240E+00	.209E+00	.175E+00	.137E+00	.335E-01	.186E+00	.297E+00	.282E+00	.267E+00	.179E+00
2	55CS1410	.211E-02	.213E-02	.174E-02	.163E-02	.739E-03	.174E-02	.218E-02	.221E-02	.226E-02	.239E-02
TOTAL	GROUP	.361E+00	.301E+00	.219E+00	.185E+00	.826E-01	.241E+00	.361E+00	.341E+00	.342E+00	.203E+00
3	33AS 840	.856E-03	.365E-03	.873E-04	.156E-03	.177E-03	.154E-03	.202E-03	.197E-03	.163E-03	.432E-04
3	34SE 870	.152E-02	.723E-03	.282E-03	.346E-03	.211E-03	.561E-03	.447E-03	.567E-03	.824E-03	.117E-03
3	35BR 890	.205E+00	.103E+00	.493E-01	.512E-01	.408E-01	.549E-01	.579E-01	.736E-01	.723E-01	.159E-01
3	37RB 920	.440E-03	.429E-03	.233E-03	.256E-03	.104E-03	.266E-03	.217E-03	.244E-03	.261E-03	.675E-04
3	37RB 930	.461E-01	.414E-01	.249E-01	.221E-01	.158E-01	.273E-01	.259E-01	.276E-01	.277E-01	.706E-02
3	39Y 970	.166E-01	.167E-01	.124E-01	.129E-01	.969E-02	.135E-01	.143E-01	.127E-01	.143E-01	.451E-02
3	41NB1040	.180E-01	.133E-01	.107E-01	.154E-01	.872E-02	.129E-01	.245E-01	.264E-01	.186E-01	.175E-01
3	49IN1270	.348E-02	.647E-03	.597E-03	.664E-03	.605E-03	.656E-03	.517E-03	.668E-03	.621E-03	.195E-03
3	52TE1370	.126E-01	.409E-02	.289E-02	.205E-02	.126E-03	.554E-02	.152E-01	.123E-01	.180E-01	.453E-02
3	53I 1380	.486E-01	.334E-01	.303E-01	.270E-01	.291E-02	.248E-01	.601E-01	.488E-01	.376E-01	.323E-01
3	56BA1480	.184E-01	.124E-02	.427E-03	.531E-03	.970E-04	.206E-02	.707E-02	.571E-02	.968E-02	.269E-02
3	57LA1470	.822E-02	.475E-02	.244E-02	.276E-02	.160E-02	.637E-02	.664E-02	.617E-02	.631E-02	.833E-02
TOTAL	GROUP	.380E+00	.220E+00	.135E+00	.135E+00	.808E-01	.149E+00	.213E+00	.215E+00	.206E+00	.933E-01
4	31GA 790	.112E-03	.229E-04	.651E-05	.172E-04	.160E-04	.171E-04	.738E-05	.178E-04	.164E-04	.245E-05
4	31GA 800	.707E-03	.163E-03	.751E-04	.882E-04	.741E-04	.876E-04	.525E-04	.123E-03	.930E-04	.197E-04
4	31GA 810	.619E-02	.125E-02	.400E-03	.428E-03	.325E-03	.672E-03	.590E-03	.912E-03	.928E-03	.145E-03
4	32GE 830	.287E-03	.585E-04	.256E-04	.329E-04	.188E-04	.599E-04	.717E-04	.604E-04	.105E-03	.849E-05
4	32GE 840	.845E-02	.133E-02	.300E-03	.554E-03	.259E-03	.107E-02	.204E-02	.166E-02	.261E-02	.168E-03
4	33AS 850	.823E-01	.321E-01	.504E-02	.123E-01	.106E-01	.159E-01	.191E-01	.196E-01	.182E-01	.500E-02
4	33AS 860	.206E-01	.484E-02	.113E-02	.153E-02	.891E-03	.225E-02	.391E-02	.378E-02	.329E-02	.587E-03
4	34SE 880	.224E-02	.623E-03	.262E-03	.310E-03	.156E-03	.586E-03	.718E-03	.528E-03	.128E-02	.116E-03
4	35BR 900	.224E+00	.839E-01	.491E-01	.291E-01	.190E-01	.346E-01	.584E-01	.551E-01	.470E-01	.148E-01
4	36KR 930	.149E-01	.586E-02	.129E-02	.282E-02	.103E-02	.589E-02	.377E-02	.757E-02	.114E-01	.101E-02
4	37RB 940	.316E+00	.168E+00	.834E-01	.838E-01	.529E-01	.988E-01	.135E+00	.138E+00	.119E+00	.423E-01
4	39Y 971	.768E-03	.116E-02	.895E-03	.911E-03	.766E-03	.821E-03	.737E-03	.692E-03	.608E-03	.314E-03
4	39Y 980	.249E-01	.196E-01	.131E-01	.138E-01	.102E-01	.146E-01	.182E-01	.182E-01	.176E-01	.655E-02
4	39Y 990	.420E-01	.238E-01	.142E-01	.163E-01	.798E-02	.195E-01	.306E-01	.280E-01	.251E-01	.908E-02
4	40ZR1040	.455E-03	.125E-03	.963E-04	.142E-03	.347E-04	.196E-03	.616E-03	.560E-03	.724E-03	.176E-03
4	41NB1030	.534E-02	.507E-02	.470E-02	.511E-02	.319E-02	.526E-02	.618E-02	.643E-02	.591E-02	.484E-02
4	41NB1050	.401E-01	.171E-01	.156E-01	.193E-01	.819E-02	.215E-01	.464E-01	.503E-01	.400E-01	.317E-01
4	41NB1060	.227E-01	.640E-02	.470E-02	.711E-02	.229E-02	.906E-02	.283E-01	.295E-01	.200E-01	.181E-01
4	42MO1090	.256E-03	.164E-04	.325E-04	.388E-04	.823E-05	.649E-04	.306E-03	.282E-03	.541E-03	.264E-03
4	42MO1100	.127E-03	.322E-05	.339E-05	.416E-05	.117E-05	.180E-04	.796E-04	.762E-04	.187E-03	.117E-03
4	43TC1090	.105E-01	.190E-02	.447E-02	.525E-02	.310E-02	.552E-02	.133E-01	.148E-01	.172E-01	.259E-01
4	43TC1100	.899E-02	.715E-03	.817E-03	.102E-02	.954E-03	.233E-02	.533E-02	.658E-02	.779E-02	.198E-01
4	47AG1220	.307E-02	.132E-03	.473E-04	.779E-04	.217E-03	.124E-03	.689E-04	.254E-03	.202E-03	.153E-03
4	48CD1280	.394E-04	.631E-05	.222E-05	.369E-05	.177E-06	.794E-05	.144E-04	.164E-04	.220E-04	.304E-05
4	49IN1271	.348E-02	.647E-03	.597E-03	.664E-03	.605E-03	.656E-03	.517E-03	.668E-03	.621E-03	.195E-03
4	49IN1280	.417E-03	.117E-03	.453E-04	.856E-04	.327E-04	.806E-04	.807E-04	.128E-03	.876E-04	.393E-04
4	49IN1290	.124E-01	.545E-02	.251E-02	.273E-02	.386E-03	.323E-02	.498E-02	.581E-02	.446E-02	.171E-02
4	49IN1291	.621E-02	.276E-02	.127E-02	.139E-02	.198E-03	.162E-02	.246E-02	.290E-02	.218E-02	.864E-03
4	50SN1330	.294E-04	.117E-04	.630E-05	.497E-05	.850E-07	.150E-04	.548E-04	.378E-04	.557E-04	.933E-05
4	50SN1340	.301E-02	.829E-03	.314E-03	.278E-03	.221E-05	.104E-02	.595E-02	.392E-02	.599E-02	.670E-03
4	51SB1341	.426E-03	.243E-03	.103E-03	.105E-03	.613E-05	.162E-03	.431E-03	.413E-03	.295E-03	.130E-03
4	51SB1350	.323E-01	.144E-01	.752E-02	.570E-02	.178E-03	.130E-01	.406E-01	.331E-01	.328E-01	.110E-01
4	51SB1360	.987E-02	.248E-02	.627E-03	.712E-03	.219E-04	.202E-02	.920E-02	.774E-02	.774E-02	.239E-02
4	52TE1380	.816E-02	.160E-02	.640E-03	.111E-02	.330E-04	.226E-02	.101E-01	.630E-02	.971E-02	.188E-02
4	53I 1390	.920E-01	.374E-01	.317E-01	.190E-01	.283E-02	.330E-01	.874E-01	.778E-01	.690E-01	.418E-01
4	53I 1400	.779E-01	.156E-01	.130E-01	.591E-02	.744E-03	.120E-01	.908E-01	.366E-01	.288E-01	.215E-01
4	54XE1410	.600E-03	.289E-03	.200E-03	.181E-03	.337E-04	.346E-03	.642E-03	.577E-03	.817E-03	.423E-03

TABLE XI (Cont)

4 54XE1420	.208E-02	.559E-03	.557E-03	.338E-03	.469E-04	.906E-03	.236E-02	.181E-02	.284E-02	.769E-03
4 54XE1430	.259E-02	.289E-03	.111E-03	.120E-03	.134E-04	.363E-03	.120E-02	.105E-02	.161E-02	.347E-03
4 54XE1440	.288E-03	.157E-04	.457E-05	.548E-05	.598E-06	.222E-04	.102E-03	.815E-04	.131E-03	.313E-04
4 55CS1420	.588E-02	.395E-02	.282E-02	.277E-02	.105E-02	.344E-02	.549E-02	.513E-02	.451E-02	.523E-02
4 55CS1430	.357E-01	.164E-01	.868E-02	.866E-02	.250E-02	.128E-01	.233E-01	.242E-01	.224E-01	.197E-01
4 55CS1440	.302E-01	.790E-02	.374E-02	.324E-02	.963E-03	.564E-02	.140E-01	.141E-01	.108E-01	.151E-01
4 56BA1470	.178E-01	.270E-02	.107E-02	.126E-02	.330E-03	.116E-01	.101E-01	.810E-02	.130E-01	.465E-02
4 56BA1500	.187E-05	.298E-07	.715E-08	.979E-08	.120E-08	.665E-07	.401E-06	.298E-06	.643E-06	.676E-07
4 57LA1490	.281E-02	.511E-03	.166E-03	.225E-03	.753E-04	.463E-03	.119E-02	.111E-02	.114E-02	.840E-03
TOTAL GROUP	.118E+01	.488E+00	.275E+00	.255E+00	.132E+00	.344E+00	.684E+00	.615E+00	.559E+00	.311E+00
5 30ZN 790	.159E-03	.123E-04	.289E-05	.815E-05	.342E-05	.144E-04	.935E-05	.198E-04	.291E-04	.135E-05
5 31GA 820	.392E-02	.539E-03	.113E-03	.167E-03	.838E-04	.286E-03	.460E-03	.513E-03	.515E-03	.699E-04
5 31GA 830	.257E-02	.180E-03	.365E-04	.588E-04	.204E-04	.136E-03	.300E-03	.269E-03	.381E-03	.230E-04
5 34SE 890	.919E-02	.137E-02	.541E-03	.606E-03	.221E-03	.117E-02	.184E-02	.209E-02	.334E-02	.220E-03
5 34SE 900	.450E-02	.540E-03	.147E-03	.180E-03	.490E-04	.439E-03	.112E-02	.883E-03	.156E-02	.102E-03
5 35BR 910	.431E-01	.121E-01	.187E-02	.418E-02	.141E-02	.637E-02	.978E-02	.113E-01	.117E-01	.175E-02
5 35BR 920	.245E-01	.412E-02	.620E-03	.132E-02	.138E-04	.249E-02	.354E-02	.536E-02	.536E-02	.562E-03
5 36KR 920	.589E-03	.284E-03	.103E-03	.171E-03	.105E-04	.283E-03	.212E-03	.292E-03	.441E-03	.471E-04
5 36KR 950	.672E-02	.701E-03	.875E-04	.309E-03	.708E-04	.738E-03	.195E-02	.166E-02	.261E-02	.133E-03
5 37RB 950	.147E+00	.555E-01	.329E-01	.281E-01	.130E-01	.359E-01	.593E-01	.585E-01	.541E-01	.108E-01
5 38SR 970	.678E-02	.324E-02	.205E-02	.236E-02	.104E-02	.370E-02	.505E-02	.421E-02	.625E-02	.865E-03
5 38SR 980	.447E-02	.133E-02	.833E-03	.945E-03	.348E-03	.178E-02	.304E-02	.266E-02	.437E-02	.453E-03
5 38SR 990	.139E-01	.257E-02	.127E-02	.160E-02	.402E-03	.335E-02	.800E-02	.656E-02	.953E-02	.959E-03
5 38SR1000	.460E-02	.635E-03	.276E-03	.374E-03	.863E-04	.839E-03	.231E-02	.208E-02	.294E-02	.250E-03
5 39Y 981	.582E-01	.562E-01	.377E-01	.395E-01	.307E-01	.381E-01	.435E-01	.454E-01	.355E-01	.187E-01
5 39Y 1000	.104E+00	.490E-01	.230E-01	.292E-01	.147E-01	.329E-01	.591E-01	.650E-01	.445E-01	.190E-01
5 40ZR1050	.114E-02	.160E-03	.126E-03	.167E-03	.309E-04	.283E-03	.116E-02	.109E-02	.144E-02	.323E-03
5 47AG1230	.384E-02	.145E-03	.384E-04	.794E-04	.108E-03	.163E-03	.103E-03	.353E-03	.332E-03	.102E-03
5 49IN1300	.253E-02	.901E-03	.351E-03	.388E-03	.227E-04	.592E-03	.144E-02	.129E-02	.905E-03	.373E-03
5 50SN1350	.107E-03	.215E-04	.839E-05	.594E-05	.292E-07	.301E-04	.201E-03	.122E-03	.210E-03	.235E-04
5 51SB1370	.130E-02	.150E-03	.456E-04	.362E-04	.708E-06	.145E-03	.935E-03	.736E-03	.887E-03	.189E-03
5 52TE1390	.149E-02	.171E-03	.514E-04	.634E-04	.280E-05	.239E-03	.112E-02	.904E-03	.137E-02	.221E-03
5 53I 1410	.273E-01	.345E-02	.270E-02	.110E-02	.101E-03	.304E-02	.123E-01	.110E-01	.127E-01	.457E-02
5 53I 1430	.511E-04	.789E-06	.930E-07	.138E-06	.506E-08	.831E-06	.705E-05	.619E-05	.812E-05	.819E-06
5 55CS1450	.472E-01	.659E-02	.300E-02	.238E-02	.510E-03	.622E-02	.168E-01	.162E-01	.171E-01	.835E-02
5 55CS1460	.688E-02	.573E-03	.193E-03	.167E-03	.292E-04	.546E-03	.217E-02	.198E-02	.214E-02	.119E-02
5 55CS1470	.411E-03	.797E-05	.115E-05	.171E-05	.211E-06	.795E-04	.597E-04	.483E-04	.665E-04	.111E-04
5 56BA1490	.303E-05	.105E-06	.249E-07	.354E-07	.516E-08	.160E-06	.766E-06	.600E-06	.106E-05	.163E-06
5 57LA1500	.801E-03	.706E-04	.205E-04	.277E-04	.858E-05	.763E-04	.248E-03	.234E-03	.235E-03	.164E-03
TOTAL GROUP	.526E+00	.201E+00	.108E+00	.113E+00	.630E-01	.140E+00	.236E+00	.241E+00	.221E+00	.696E-01
6 32GE 850	.346E-02	.454E-03	.578E-04	.152E-03	.562E-04	.363E-03	.694E-03	.617E-03	.968E-03	.727E-04
6 32GE 860	.643E-03	.473E-04	.101E-04	.142E-04	.321E-05	.438E-04	.120E-03	.946E-04	.176E-03	.615E-05
6 33AS 870	.236E-01	.409E-02	.807E-03	.115E-02	.434E-03	.234E-02	.403E-02	.452E-02	.535E-02	.583E-03
6 34SE 910	.109E-02	.916E-04	.112E-04	.271E-04	.410E-05	.785E-04	.197E-03	.196E-03	.353E-03	.132E-04
6 35BR 930	.228E-02	.840E-03	.294E-02	.234E-03	.562E-04	.622E-03	.621E-02	.157E-02	.194E-02	.123E-03
6 36KR 940	.193E-01	.337E-02	.124E-02	.163E-02	.471E-03	.380E-02	.765E-02	.651E-02	.109E-01	.723E-03
6 37RB 960	.972E-01	.208E-01	.682E-02	.990E-02	.438E-02	.146E-01	.300E-01	.301E-01	.249E-01	.487E-02
6 37RB 970	.462E-01	.705E-02	.191E-02	.311E-02	.977E-03	.593E-02	.146E-01	.133E-01	.160E-01	.157E-02
6 37RB 980	.461E-02	.415E-03	.975E-04	.160E-03	.446E-04	.335E-03	.109E-02	.110E-02	.120E-02	.112E-03
6 37RB 990	.108E-03	.420E-05	.796E-06	.142E-05	.201E-06	.414E-05	.210E-04	.187E-04	.233E-04	.126E-05
6 49IN1310	.776E-03	.254E-03	.989E-04	.883E-04	.168E-05	.224E-03	.782E-03	.648E-03	.689E-03	.162E-03
6 49IN1320	.247E-03	.773E-04	.518E-04	.191E-04	.153E-06	.579E-04	.347E-03	.258E-03	.272E-03	.515E-04
6 53I 1420	.200E-02	.904E-04	.376E-04	.246E-04	.192E-05	.886E-04	.471E-02	.442E-03	.460E-03	.105E-03
TOTAL GROUP	.202E+00	.376E-01	.141E-01	.165E-01	.643E-02	.285E-01	.705E-01	.594E-01	.633E-01	.840E-02
TOTAL	.269E+01	.128E+01	.769E+00	.724E+00	.387E+00	.923E+00	.158E+01	.149E+01	.141E+01	.690E+00

TABLE XII

AVERAGE DELAYED NEUTRON GROUP ENERGIES ALL 105 SPECTRA[a]

NUCLIDE	GROUP 1	GROUP 2	GROUP 3	GROUP 4	GROUP 5	GROUP 6	TOTAL
TH232F	2.007E+02	3.870E+02	4.058E+02	4.406E+02	3.882E+02	5.505E+02	4.162E+02
	(308)	(480)	(464)	(442)	(442)	(442)	(447)
TH232H	2.007E+02	3.914E+02	4.147E+02	4.512E+02	4.090E+02	9.775E+02	4.668E+02
U233T	2.007E+02	4.007E+02	4.242E+02	4.468E+02	3.958E+02	6.770E+02	4.139E+02
	(308)	(480)	(464)	(442)	(442)	(442)	(447)
U233F	2.007E+02	3.797E+02	4.232E+02	4.421E+02	3.970E+02	5.027E+02	3.991E+02
U233H	2.007E+02	3.376E+02	4.241E+02	4.426E+02	3.981E+02	4.914E+02	3.941E+02
U235T	2.007E+02	4.239E+02	4.126E+02	4.239E+02	3.803E+02	5.446E+02	4.164E+02
	(308)	(480)	(464)	(442)	(442)	(442)	(450)
U235F	2.007E+02	4.200E+02	4.143E+02	4.319E+02	4.022E+02	4.967E+02	4.180E+02
U235H	2.007E+02	3.631E+02	4.218E+02	4.314E+02	4.071E+02	4.961E+02	4.033E+02
U236F	2.007E+02	4.358E+02	4.032E+02	4.305E+02	4.196E+02	5.196E+02	4.237E+02
U238F	2.007E+02	4.566E+02	3.809E+02	4.145E+02	4.055E+02	5.222E+02	4.184E+02
	(325)	(474)	(496)	(418)	(401)	(401)	(432)
U238H	2.007E+02	4.438E+02	3.986E+02	4.151E+02	4.285E+02	4.963E+02	4.223E+02
NP237F	2.007E+02	4.517E+02	4.045E+02	4.242E+02	4.139E+02	5.017E+02	4.216E+02
PU239T	2.007E+02	4.822E+02	4.019E+02	4.110E+02	3.956E+02	6.735E+02	4.275E+02
	(447)	(501)	(447)	(418)	(418)	(418)	(449)
PU239F	2.007E+02	4.645E+02	3.985E+02	4.096E+02	4.088E+02	4.841E+02	4.176E+02
PU239H	2.007E+02	3.678E+02	4.153E+02	4.240E+02	4.004E+02	4.760E+02	3.945E+02
PU240F	2.007E+02	4.739E+02	3.910E+02	4.061E+02	4.073E+02	4.935E+02	4.198E+02
	(447)	(501)	(447)	(418)	(418)	(418)	(447)
PU241T	2.007E+02	4.900E+02	3.743E+02	3.980E+02	4.042E+02	5.975E+02	4.235E+02
	(447)	(501)	(447)	(418)	(418)	(418)	(443)
PU241F	2.007E+02	4.900E+02	3.772E+02	3.960E+02	4.152E+02	5.033E+02	4.201E+02
PU242F	2.007E+02	4.778E+02	3.809E+02	3.956E+02	4.014E+02	5.042E+02	4.166E+02
CF252S	2.007E+02	5.060E+02	3.370E+02	3.491E+02	4.086E+02	4.966E+02	4.002E+02

[a]VALUES IN PARENTHESIS ARE ENDF/B-V AND ARE INDEPENDENT OF INCIDENT NEUTRON FISSION ENERGY.

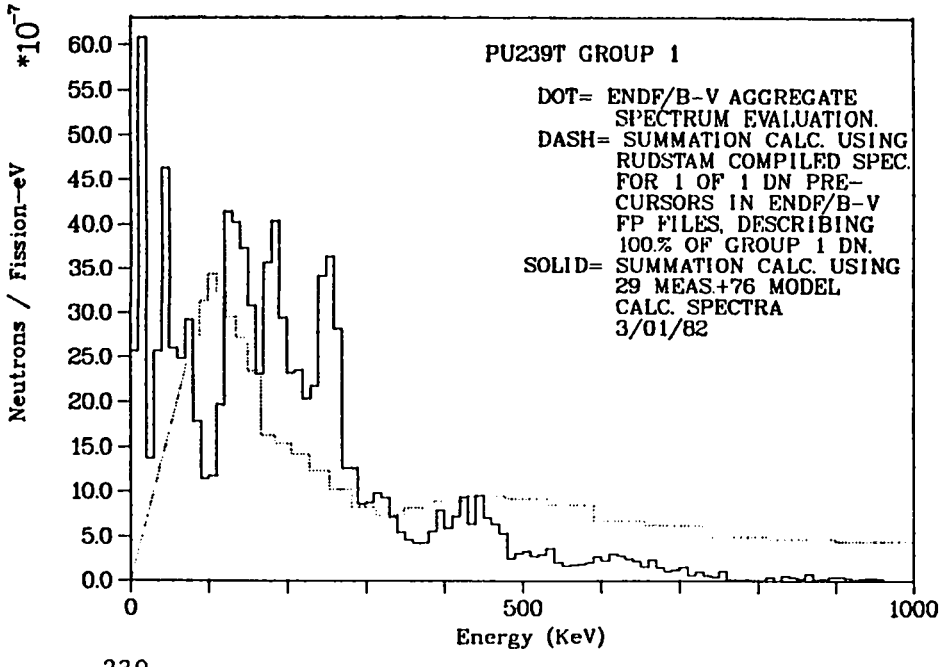

Fig. 41. ^{239}Pu-thermal normalized delayed neutron spectra (Group 1).

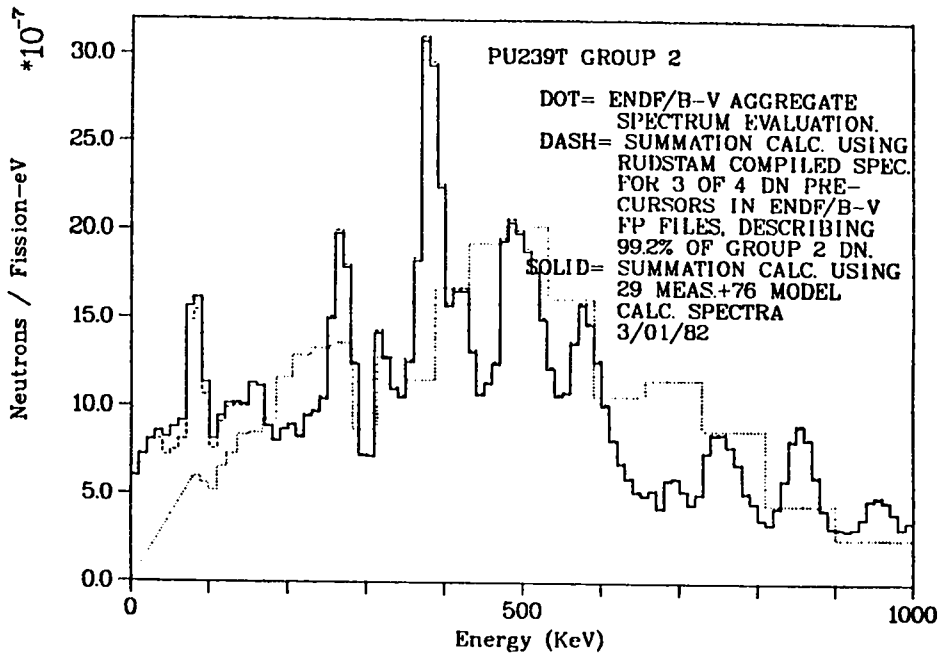

Fig. 42. ^{239}Pu-thermal normalized delayed neutron spectra (Group 2).

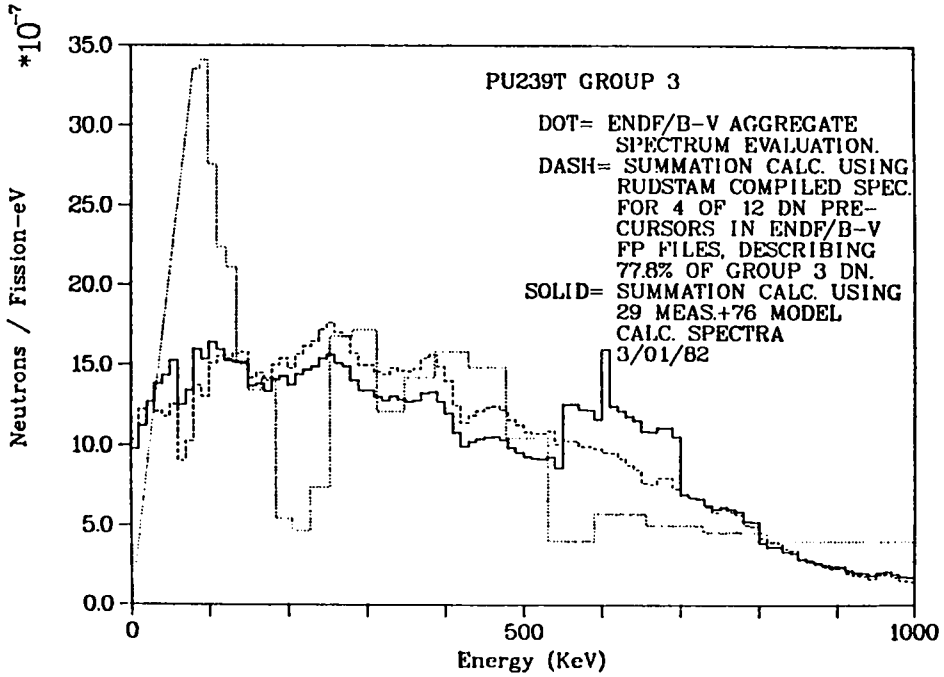

Fig. 43. ^{239}Pu-thermal normalized delayed neutron spectra (Group 3).

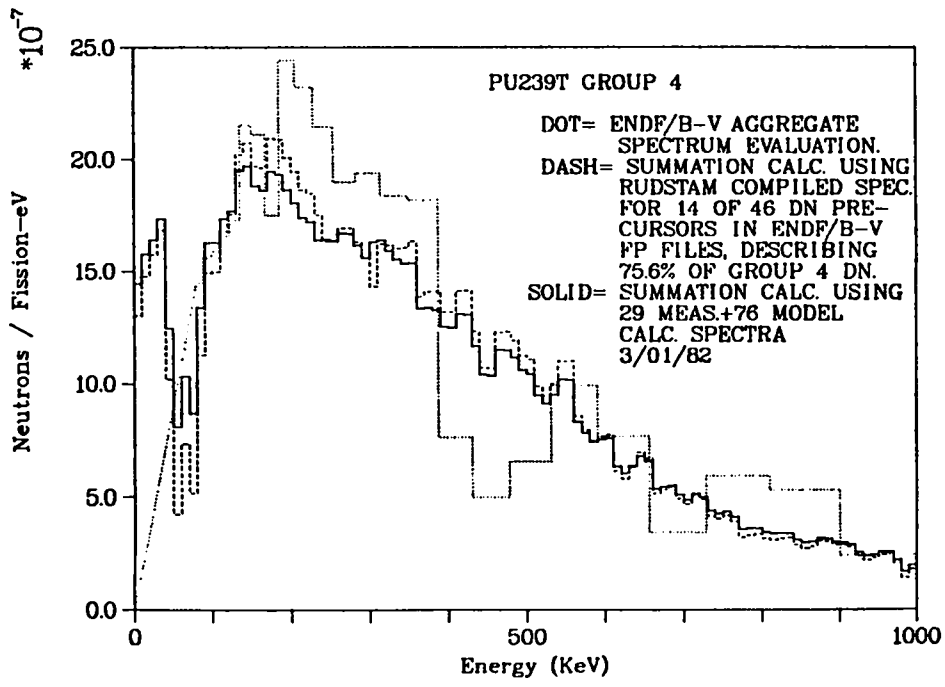

Fig. 44. ^{239}Pu-thermal normalized delayed neutron spectra (Group 4).

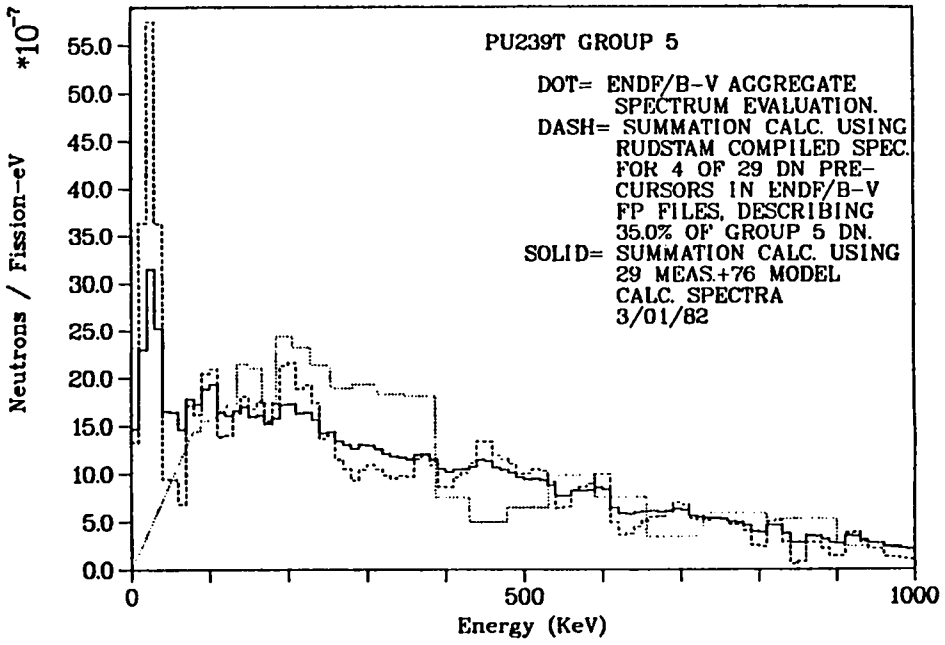

Fig. 45. ^{239}Pu-thermal normalized delayed neutron spectra (Group 5).

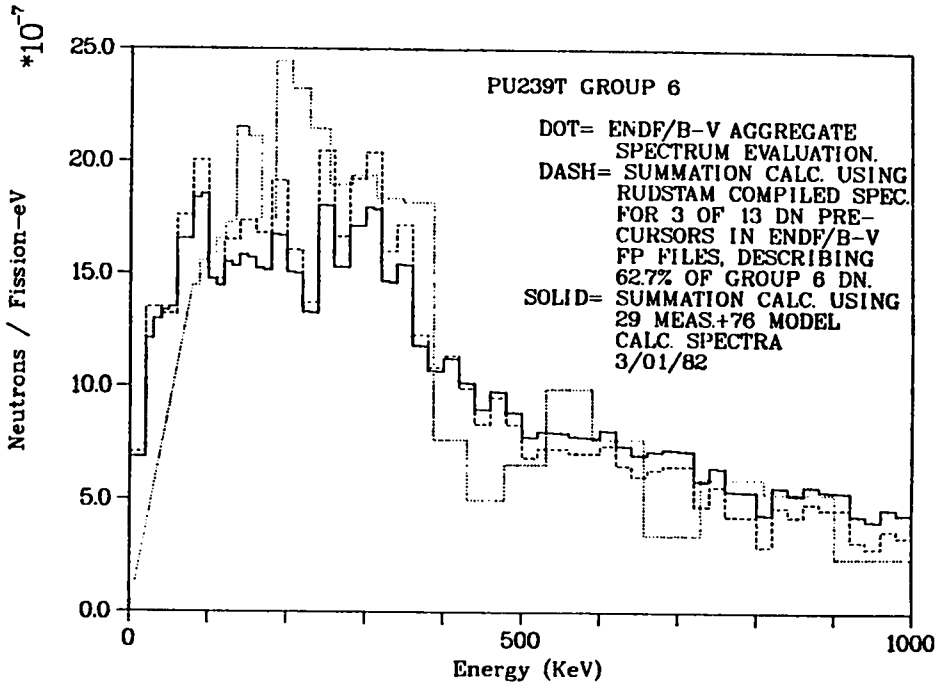

Fig. 46. ^{239}Pu-thermal normalized delayed neutron spectra (Group 6).

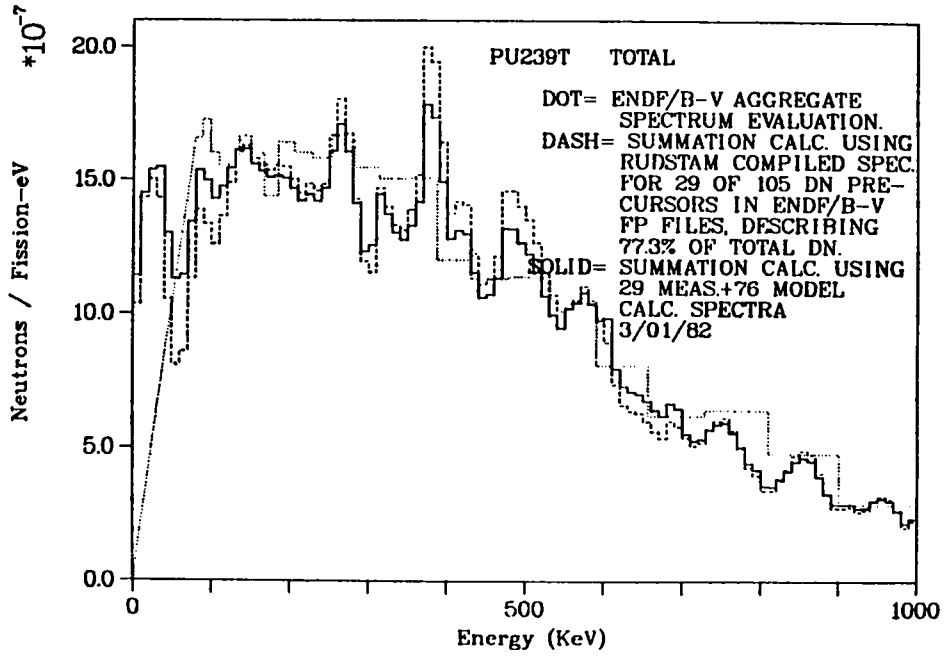

Fig. 47. ^{239}Pu-thermal normalized delayed neutron spectra (Total).

C. CRAY Code Conversions (T. R. England)

The CINDER-10 code uses several non-FORTRAN routines and is based on a 60-bit word length. This code was successfully converted to the CRAY computer (64 bits) during the current reporting period. Several other codes have also been converted and others are in progress.

D. Calculating Fission-Product Decay-Energies and Spectra Using Adjusted Data (D. C. George, R. J. LaBauve, and T. R. England)

A simple computer code ADENA calculates a best estimate of fission-product beta and gamma decay energies and spectra in 19 or fewer energy groups from a mixture of ^{235}U and ^{239}Pu fuels. The calculation uses aggregate, adjusted data derived from a combination of several experiments[73-77] and the ENDF/B-V[78] fission product file. The motivation for creating the adjusted data base is implied by the conclusions of Ref. 79, which compared experimental measurements of fission-product decay energy with summation calculations based on several different fission-product data files. These conclusions indicate that at present the best estimates of decay-energy spectra will result from calculations that use aggregate data derived, where possible, from experiments and augmented by the ENDF/B-V data outside the experimental region (i.e., for cooling times less than 2.2 s and greater than 2×10^5 s for gamma-decay energy or 10^4 s for beta).

Preparatory to producing the adjusted data base, summation calculations using ENDF/B-V data input to the CINDER-10 code[80] were performed and the resultsulting aggregate fission-product decay-energy spectra were fit to the equations,

$$f(t) = \sum_{i=1}^{n} \alpha_i e^{-\lambda_i t} \quad \text{(MeV/fis-s)} \tag{5}$$

using methods described in Refs. 81 and 82. The process produced sets of alpha (α), lambda (λ) parameter pairs that will subsequently be referred to as the ENDF/B-V fits. All fits are produced for beta- and gamma-ray decay, for both ^{235}U and ^{239}Pu fuels, for all decay-energy groups, over the full cooling time range of 10^{-2} s to 10^9 s.

In creating the adjusted data base, three cooling time regions were considered. For times inside the experimental region, the experimental points were used. For times greater than the experimental times, the ENDF/B-V fits

were used with Eq. (5) to calculate several points up to 10^9 s. For times below the experimental region, the ENDF/B-V fits were shifted to coincide with the short cooling time experimental points, and several points were read off the shifted curves. These sets of combined points were input to FITPULS,[82] which calculated sets of parameter pairs (α,λ) constituting the adjusted pulse fits. FITPULS uses a nonlinear least squares procedure taking the ENDF/B-V fits as starting values. Thus, the adjusted fits reflect the basic ENDF shape, as can be seen in Fig. 48, which shows the ENDF/B-V fit, the final adjusted fit, and the experimental points that have been transformed to equivalent pulse values.

These adjusted fits were incorporated into the code ADENA, which uses them to calculate the fission product decay-energy spectra using the equation,

$$F(T,t) = \sum_{i=1}^{n} \frac{\alpha_i}{\lambda_i} e^{-\lambda_i t} \left(1 - e^{-\lambda_i T}\right) \quad \text{(MeV/fis)} \qquad (6)$$

which is an integration of the pulse Eq. (1) over the irradiation time T. For applications involving long irradiation times, a correction to account for the effects of neutron absorption is included.[81]

In order to check the adjusted fits and as a sample application, ADENA was used to calculate the Los Alamos experiment[77] in which ^{235}U was irradiated with thermal neutrons for 20 000 s and aggregate fission-product gamma-ray decay-energy spectra were measured. As can be seen in Fig. 49, which shows the ADENA calculation and the experimental results for a cooling time of 1218 s, the calculation agrees quite well with experiment. For long cooling times and high gamma-ray energies the experimental error is very large; it is in this region that the adjusted fits rely more heavily on the ENDF/B-V data.

The code ADENA avoids the need for the large data base and code system used to produce the adjusted fits and can be used for a wide variety of reactor operational and safety-related computations where aggregate fission-product decay spectra are needed. A report describing this work is in preparation.

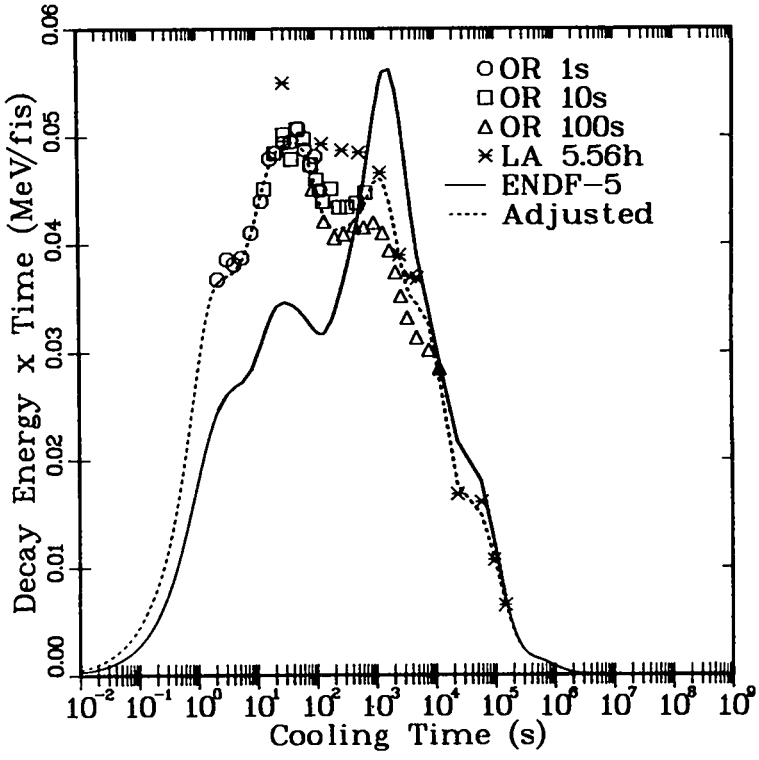

Fig. 48. Gamma-ray decay energy for Group 7 (0.8-1.0 MeV) from ^{235}U thermal fission showing ENDF/B-V fit, final adjusted fit, and transformed pulse values of the experimental points

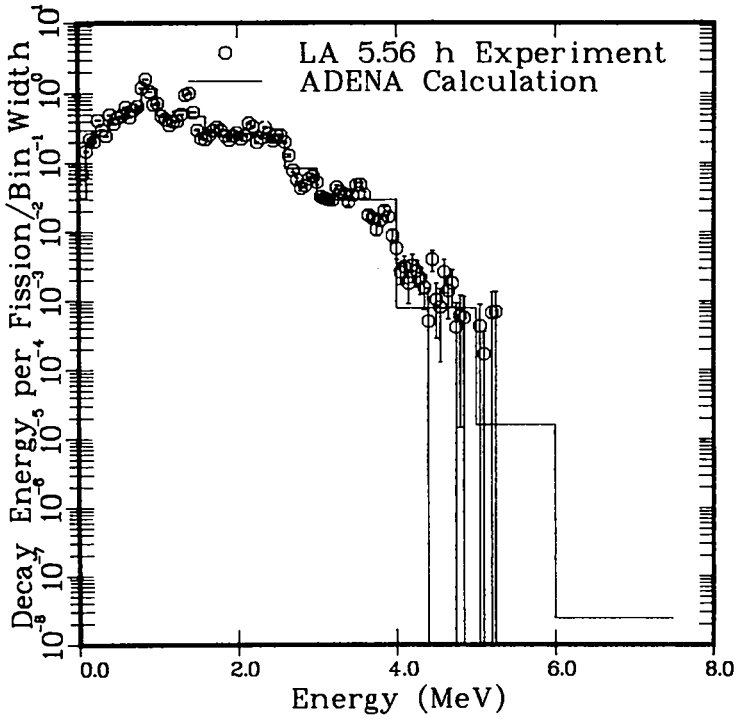

Fig. 49. Comparison of gamma-ray decay energy measured by the Los Alamos 5.56-hour irradiation experiment after a cooling time of 1218 s with an ADENA calculation.

E. Calculated Neutron Sources in Pu Process Solutions [W. B. Wilson, R. T. Perry (Penn. State U.), D. G. Madland, N. Ensslin (Q-1), and J. E. Stewart (Q-1)]

A proposed technique for monitoring ^{240}Pu concentrations in flowing aqueous Pu-process solutions uses a coincidence neutron detector and electronics to separate fission prompt neutron pairs and triplets from the total neutron count. Neutrons originate in the spontaneous fission (SF) decays and the $^{17,18}O(\alpha,n)$ reactions of decay alphas from Pu and Am nuclides. Each neutron source, depending upon spectrum, is multiplied by neutron-induced fission. System modeling requires the accurate description of the magnitude and spectrum of all source contributions. We have calculated the neutron sources within three aqueous Pu process solutions, ranging in Pu content from 2.54 grams Pu/liter to 109.2 grams Pu/liter. The compositions of these solutions are given in Table XIII.

The thresholds for (α,n) reactions on all constituents other than $^{17,18}O$ exceed the 5.55-MeV maximum alpha-particle energy encountered here. We have evaluated the $^{17,18}O(\alpha,n)$ cross sections in an earlier work[83] using the data of Bair and Willard,[84] Bair and Haas,[85] Bair and del Campo,[86] and Hansen et al.,[87] following largely the recommendations of Ombrellaro and Johnson.[88] The calculations of Ref. 83 required the polynomial approximations of alpha-particle stopping cross-section data of Ziegler[89] and Northcliffe and Schilling[90] for Pu, O, and other elements. These have been supplemented by polynomial approximations to the H and N data of Ziegler for use in these calculations, in which the contribution to the stopping cross section of the trace constituent Am is assumed to be the same as that of an equal amount of Pu. These polynomial stopping cross sections and the evaluated $^{17,18}O(\alpha,n)$ cross sections were used with the atom densities of Table XIII and methodology of Ref. 83 to calculate the neutron production by each alpha particle of each nuclide. The accumulated (alpha, n) neutron source associated with each nuclide is given in Table XIV.

The spectra of (α,n) neutrons for these solutions have not been measured or calculated. The spectra for $^{17,18}O(\alpha,n)$ neutrons produced by alpha particles of the same source nuclides (for example, ^{238}Pu) have been examined for cases in which alpha particles slow in different materials (for example, PuO_2). The spectrum of $^{17,18}O(\alpha,n)$ neutrons produced by ^{238}Pu alpha particles in one of the solutions at hand would be the same as those produced in the same reactions of ^{238}Pu alpha particles if, in both cases, the alpha particles react at

TABLE XIII

SOLUTION CONSTITUENTS

CONSTITUENT	CASE 1 2.54 GRAMS PU/L ATOMS/L	ATOM FRAC	CASE 2 21.5 GRAMS PU/L ATOMS/L	ATOM FRAC	CASE 3 109.2 GRAMS PU/L ATOMS/L	ATOM FRAC
1- H	6.2459+25	6.2540-01	6.2459+25	6.2253-01	6.2519+25	6.0699-01
7- N	1.7639+24	1.7662-02	1.8671+24	1.8610-02	2.4651+24	2.393 -02
8- O	3.5641+25	3.5688-01	3.5950+25	3.5832-01	3.7738+25	3.6640-01
O-17	1.354 +22	1.356 -04	1.366 +22	1.362 -04	1.434 +22	1.393 -04
O-18	7.271 +22	7.280 -04	7.334 +22	7.310 -04	7.699 +22	7.476 -04
94-PU	6.398 +21	6.406 -05	5.4156+22	5.3978-04	2.7505+23	2.670 -03
PU-238	3. +18	3. -08	1.5 +19	1. -07	8. +19	1. -06
PU-239	5.743 +21	5.750 -05	4.8622+22	4.846 -04	2.4697+23	2.398 -03
PU-240	6.00 +20	6.01 -06	5.072 +21	5.06 -05	2.575 +22	2.50 -04
PU-241	4.5 +19	4.5 -07	3.77 +20	3.8 -06	1.90 +21	1.8 -05
PU-242	7. +18	7. -08	7.0 +19	7. -07	3.5 +20	3. -06
95-AM-241	1.5 +19	1.5 -07	1.25 +20	1.2 -06	6.2 +20	6.0 -06

TABLE XIV

SUMMARY OF CALCULATED (ALPHA,N) AND SPONTANEOUS-FISSION NEUTRON SOURCE STRENGTHS IN AQUEOUS PLUTONIUM PROCESS SOLUTIONS

QUANTITY	NEUTRONS PER SECOND PER LITER OF SOLUTION CASE 1 2.54 GRAMS PU/L	CASE 2 21.5 GRAMS PU/L	CASE 3 109.2 GRAMS PU/L
(ALPHA,N) NEUTRONS			
DUE TO PU-238	4.02+1 *	2.00+2	1.05+3
DUE TO PU-239	2.19+2	1.84+3	9.20+3
DUE TO PU-240	8.47+1	7.13+2	3.56+3
DUE RO PU-241	5.78-2	4.84-1	2.36+0
DUE TO PU-242	1.44-2	1.43-1	7.05-1
DUE TO AM-241	4.06+1	3.37+2	1.64+3
TOTAL	3.84+2	3.09+3	1.55+4
S.F. NEUTRONS			
DUE TO PU-238	3.06+0	1.53+1	8.17+1
DUE TO PU-239	4.92-2	4.16-1	2.12+0
DUE TO PU-240	2.17+2	1.84+3	9.33+3
DUE TO PU-241	0.	0.	0.
DUE TO PU-242	4.82+0	4.82+1	2.41+2
DUE TO AM-241	7.09-3	5.91-2	2.93-1
TOTAL	2.25+2	1.90+3	9.65+3
TOTAL NEUTRONS			
DUE TO PU-238	4.33+1	2.16+2	1.13+3
DUE TO PU-239	2.19+2	1.84+3	9.21+3
DUE TO PU-240	3.02+2	2.55+3	1.29+4
DUE TO PU-241	5.78-2	4.84-1	2.36+0
DUE TO PU-242	4.83+0	4.83+1	2.42+2
DUE TO AM-241	4.06+1	3.37+2	1.65+3
TOTAL	6.10+2	4.99+3	2.51+4

* READ AS 4.02E+01

the same spectrum of alpha-particle reaction energies. We have calculated the normalized reaction spectra of alpha particles with initial energy 5.5 MeV emitted in each of the three solutions and in PuO_2 and H_2O. The equivalence of these distributions, given in Table XV, show that the 5.5-MeV alpha particles of ^{238}Pu that react with $^{17,18}O$ in any of the solutions do so at nearly the same energies as the ^{238}Pu 5.5-MeV alpha particles in H_2O and PuO_2. Since the same reactions occur at nearly the same energies in all cases compared, the spectrum of neutrons produced in the reactions are therefore essentially equivalent. Lessor and Schenter[91] have calculated the (α,n) neutron spectra of $^{238}PuO_2$, $^{239}PuO_2$, and $^{240}PuO_2$. We suggest in Table XVI the application of these spectra to the description of (α,n) neutrons in the three solutions. Because of the similarity in the alpha-particle decay spectra of ^{238}Pu and ^{241}Am, the (α,n) neutron spectrum associated with $^{238}PuO_2$ may be used to represent the $^{17,18}O(\alpha,n)$ neutron spectrum due to ^{241}Am alpha particles.

The SF neutron source is, of course, dependent only on the abundance of nuclides decaying by SF and their respective SF decay parameters -- $\bar{\nu}$(SF) and SF half-life or SF decay branching fraction. The calculated SF neutron source from each nuclide is given in Table XIV for each solution.

Because of the features of the Monte Carlo neutron tranport program to be used in transporting the source neutrons in future studies, the desired representation for the prompt SF neutrons is the Watt spectrum,[92] given by

$$n(E) = Ce^{-E/A} \sinh(\sqrt{BE}). \qquad (7)$$

The delayed SF neutrons may be neglected because of their relatively small contributions. The SF neutron spectrum of ^{240}Pu has been described with a Watt spectrum in Ref. 93. The SF neutron spectrum of ^{242}Pu has been given in Ref. 94 using an improved functional expression; Watt spectrum parameters for ^{242}Pu SF, though not reported, were also calculated. The Watt spectrum parameters describing SF neutrons of ^{238}Pu were recently generated, and the set of parameters A and B, defining the significant SF neutron spectra, are given in Table XVII.

The magnitude and spectra of all significant (α,n) and SF neutron sources in the three solutions have thus been defined. A report describing the details of the data and calculations is in preparation.

TABLE XV

NORMALIZED NEUTRON PRODUCTION IN $O^{17}+O^{18}$ BY 5.5-MeV ALPHA PARTICLES

ALPHA BIN	ALPHA PARTICLE ENERGY	FRACTION PRODUCED BY ALPHAS IN BIN				
		CASE 1 2.54 G/L	CASE 2 21.5 G/L	CASE 3 109. G/L	PUO2	H2O
1	1.000 MEV- 1.100 MEV	0.000000	0.000000	0.000000	0.000000	0.000000
2	1.100 MEV- 1.200 MEV	0.000001	0.000001	0.000001	0.000001	0.000001
3	1.200 MEV- 1.300 MEV	0.000000	0.000000	0.000000	0.000000	0.000000
4	1.300 MEV- 1.400 MEV	0.000003	0.000003	0.000003	0.000004	0.000003
5	1.400 MEV- 1.500 MEV	0.000011	0.000011	0.000011	0.000012	0.000011
6	1.500 MEV- 1.600 MEV	0.000038	0.000038	0.000038	0.000041	0.000038
7	1.600 MEV- 1.700 MEV	0.000012	0.000012	0.000012	0.000013	0.000012
8	1.700 MEV- 1.800 MEV	0.000030	0.000030	0.000030	0.000032	0.000030
9	1.800 MEV- 1.900 MEV	0.000152	0.000152	0.000152	0.000162	0.000152
10	1.900 MEV- 2.000 MEV	0.000098	0.000098	0.000098	0.000104	0.000098
11	2.000 MEV- 2.100 MEV	0.000165	0.000165	0.000166	0.000175	0.000165
12	2.100 MEV- 2.200 MEV	0.000907	0.000907	0.000908	0.000959	0.000907
13	2.200 MEV- 2.300 MEV	0.000432	0.000432	0.000433	0.000456	0.000432
14	2.300 MEV- 2.400 MEV	0.000676	0.000676	0.000677	0.000710	0.000676
15	2.400 MEV- 2.500 MEV	0.002450	0.002451	0.002454	0.002567	0.002451
16	2.500 MEV- 2.600 MEV	0.007361	0.007362	0.007370	0.007690	0.007364
17	2.600 MEV- 2.700 MEV	0.001716	0.001717	0.001719	0.001788	0.001717
18	2.700 MEV- 2.800 MEV	0.008439	0.008440	0.008448	0.008773	0.008443
19	2.800 MEV- 2.900 MEV	0.005497	0.005498	0.005502	0.005692	0.005499
20	2.900 MEV- 3.000 MEV	0.009791	0.009793	0.009800	0.010121	0.009795
21	3.000 MEV- 3.100 MEV	0.004140	0.004141	0.004144	0.004266	0.004142
22	3.100 MEV- 3.200 MEV	0.010416	0.010418	0.010424	0.010704	0.010420
23	3.200 MEV- 3.300 MEV	0.012071	0.012073	0.012080	0.012379	0.012076
24	3.300 MEV- 3.400 MEV	0.014380	0.014382	0.014389	0.014711	0.014385
25	3.400 MEV- 3.500 MEV	0.008952	0.008953	0.008957	0.009133	0.008955
26	3.500 MEV- 3.600 MEV	0.029609	0.029612	0.029624	0.030142	0.029618
27	3.600 MEV- 3.700 MEV	0.030025	0.030028	0.030039	0.030503	0.030033
28	3.700 MEV- 3.800 MEV	0.028692	0.028695	0.028703	0.029079	0.028699
29	3.800 MEV- 3.900 MEV	0.046161	0.046164	0.046175	0.046687	0.046171
30	3.900 MEV- 4.000 MEV	0.030653	0.030654	0.030661	0.030943	0.030658
31	4.000 MEV- 4.100 MEV	0.023607	0.023608	0.023612	0.023772	0.023611
32	4.100 MEV- 4.200 MEV	0.032359	0.032360	0.032364	0.032527	0.032361
33	4.200 MEV- 4.300 MEV	0.049949	0.049951	0.049953	0.050106	0.049954
34	4.300 MEV- 4.400 MEV	0.056483	0.056482	0.056484	0.056548	0.056485
35	4.400 MEV- 4.500 MEV	0.045166	0.045166	0.045166	0.045150	0.045168
36	4.500 MEV- 4.600 MEV	0.053034	0.053033	0.053030	0.052900	0.053033
37	4.600 MEV- 4.700 MEV	0.061803	0.061800	0.061794	0.061548	0.061798
38	4.700 MEV- 4.800 MEV	0.038385	0.038384	0.038379	0.038162	0.038382
39	4.800 MEV- 4.900 MEV	0.043881	0.043880	0.043872	0.043547	0.043876
40	4.900 MEV- 5.000 MEV	0.051509	0.051505	0.051495	0.051037	0.051501
41	5.000 MEV- 5.100 MEV	0.035384	0.035383	0.035373	0.034999	0.035378
42	5.100 MEV- 5.200 MEV	0.061215	0.061210	0.061194	0.060465	0.061202
43	5.200 MEV- 5.300 MEV	0.062961	0.062955	0.062936	0.062095	0.062946
44	5.300 MEV- 5.400 MEV	0.064758	0.064753	0.064729	0.063773	0.064742
45	5.400 MEV- 5.500 MEV	0.066632	0.066625	0.066601	0.065525	0.066614

TABLE XVI

APPLICABLE SPECTRA FOR (ALPHA,N) NEUTRONS

SOURCE NUCLIDE	% OF (ALPHA,N) NEUTRON PRODUCTION CASE 1	CASE 2	CASE 3	APPLICABLE SPECTRUM
PU-238	10.5	6.5	6.8	LESSOR&SCHENTER,BNWL-B-109(6/71),FIG4,238PU-02
PU-239	56.9	59.5	59.5	LESSOR&SCHENTER,BNWL-B-109(6/71),FIG5,239PU-02
PU-240	22.0	23.1	23.0	LESSOR&SCHENTER,BNWL-B-109(6/71),FIG6,240PU-02
PU-241	.02	.02	.02	NEGLECT OR SUBSTITUTE
PU-242	.004	.005	.005	NEGLECT OR SUBSTITUTE
AM-241	10.6	10.9	10.6	LESSOR&SCHENTER,BNWL-B-109(6/71),FIG4,238PU-02

TABLE XVII

APPLICABLE SPECTRA FOR SPONTANEOUS-FISSION NEUTRONS

SOURCE NUCLIDE	% OF (S.F.) NEUTRON PRODUCTION CASE 1	CASE 2	CASE 3	APPLICABLE SPECTRUM
PU-238	1.4	0.8	0.8	MADLAND(81):WATT;A=0.847832MEV,B=4.411724/MEV
PU-239	0.02	0.02	0.02	NEGLECT OR SUBSTITUTE
PU-240	96.5	96.6	96.6	MADLAND(81):WATT;A=0.7989087MEV,B=4.902689/MEV
PU-241	0.	0.	0.	NO S.F.DECAY MODE
PU-242	2.1	2.5	2.5	MADLAND(81):WATT;A=0.8191567MEV,B=4.587376/MEV
AM-241	0.003	0.003	0.003	NEGLECT OR SUBSTITUTE

REFERENCES

1. G. M. Hale, "Peripheral Effects in R-Matrix Theory," in Los Alamos National Laboratory report LA-8874-PR, p. 1 (July 1981).

2. S. T. Perkins and D. E. Cullen, Nucl. Sci. Eng. 77, 20 (1981).

3. P. G. Young and L. Stewart, "Evaluated Data for n + ^{9}Be Reactions," Los Alamos Scientific Laboratory report LA-7932-MS (ENDF-283) (July 1979).

4. R. E. MacFarlane, D. W. Muir, and R. M. Boicourt, "The NJOY Nuclear Data Processing System, Volume I: User's Manual," Los Alamos National Laboratory report LA-9303-M (ENDF 329) (May 1982).

5. P. G. Young, "Variance-Covariance Analysis of n + ^{7}Li Reactions," Los Alamos National Laboratory report LA-8874-PR, p. 2 (July 1981).

6. P. G. Young, Trans. Am. Nucl. Soc. 39, 272 (1981).

7. D. M. Hetrick and C. Y. Fu, "GLUCS: A Generalized Least-Squares Program for Updating Cross-Section Evaluations with Correlated Data Sets," Oak Ridge National Laboratory report ORNL/TM-7341 (ENDF-303) (1980).

8. D. R. Harris, W. A. Reupke, and W. B. Wilson, "Consistency Among Differential Nuclear Data and Integral Observations: The ALVIN Code for Data Adjustment, for Sensitivity Calculations, and for Identification of Inconsistent Data," Los Alamos Scientific Laboratory report LA-5987 (December 1975).

9. R. O. Lane, A. S. Langsdorf, Jr., J. E. Monahan, and A. J. Elwyn, Ann. Physics 12, 135 (1961).

10. H. H. Knitter and M. Coppola, "Measurements of Neutron Scattering from ^{7}Li," Proc. Conf. on Neutron Cross Sections and Tech., Washington, D.C., 1968, Vol. II, p. 287). (NBS Special Pub. 299.)

11. H. D. Knox, R. M. White, and R. O. Lane, Nucl. Sci. Eng. 69, 223 (1979).

12. H. D. Knox and R. O. Lane, Nucl. Phys. A359, 131 (1981).

13. H. H. Hogue, P. L. von Behren, D. W. Glasgow, S. G. Glendinning, P. W. Lisowski, C. E. Nelson, F. O. Purser, and W. Mornow, "Elastic and Inelastic Scattering of 7- to 14-MeV neutrons from Lithium-6 and Lithium-7," Nucl. Sci. Eng. 69, 22 (1979).

14. P. W. Lisowski, G. F. Auchampaugh, D. M. Drake, M. Drosg, G. Haouat, N. W. Hill, and L. Nilsson, "Cross Sections for Neutron-Induced, Neutron-Producing Reactions in ^{6}Li and ^{7}Li at 5.96 and 9.83 MeV," Los Alamos Scientific Laboratory report LA-8342 (October 1980).

15. G. L. Morgan, "Cross Sections for the ^{7}Li(n,xn) and ^{7}Li(n, n'γ) Reactions Between 1 and 20 MeV," Oak Ridge National Laboratory report ORNL/TM-6247 (1978).

16. D. G. Foster, Jr. and E. D. Arthur, "Average Neutronic Properties of Prompt Fission Products," in Los Alamos National Laboratory report LA-9168-MS (February 1982).

17. E. D. Arthur, "Deformed Optical Model Analysis of n + ^{169}Tm Reaction," in Los Alamos National Laboratory report LA-9060-PR, p. 6 (December 1981).

18. P. A. Moldauer, "Optical Model of Low Energy Neutron Interactions with Spherical Nuclei," Nucl. Phys. 47, 65 (1963).

19. D. R. Nethaway, "Measurement of the ^{168}Tm(n,2n) Cross Section," presented at 11th Interlaboratory Radio/Chemistry Working Group Meeting, Livermore, California, March 1982 (Los Alamos informal report LA-UR-762).

20. E. D. Arthur and C. A. Philis, "New Calculations of Neutron-Induced Cross Sections on Tungsten Isotopes," in Los Alamos Scientific Laboratory report LA-8630-PR, p. 2 (December 1980).

21. E. D. Arthur, "Gamma-Ray production Cross Section Calculations for the Tungsten Evaluation," and E. D. Arthur, P. G. Young, A. B. Smith, C. A. Philis, "$^{181\ 183\ 184\ 186}$W Evaluations," in Los Alamos National Laboratory report LA-8757-PR, pp. 3 and 6 (March 1981).

22. W. E. Kinney and F. G. Perey, "Tungsten Neutron Elastic- and Inelastic-Scattering Cross Sections from 4.34 to 8.56 MeV," Oak Ridge National Laboratory report ORNL-4803 (1973).

23. H. Vonach, A. Chalupka, F. Wenninger, G. Staffel, "Measurement of the Angle-Integrated Secondary Neutron Spectra from the Interaction of 14 MeV Neutrons with Medium and Heavy Nuclei," Proc. Symp. on Neutron Cross-Sections from 10 to 50 MeV, Brookhaven National Laboratory, 1980, BNL-NCS-51245, Vol. 1, p. 343.

24. J. K. Dickens, T. A. Love, and G. L. Morgan, "Gamma-Ray Production due to Neutron Interactions with Tungsten for Incident Neutron Energies between 1. and 20 MeV," Oak Ridge National Laboratory report ORNL-4847 (1973).

25. M. B. Savin, In. A. Khoklov, I. N. Paramonova, V. A. Chirkin, V. N. Lunin, and N. N. Zalialov, "Total Gamma-Ray Production Cross Sections from the Interaction of 1-10 MeV Neutrons with Tungsten Nuclei," Proc. 4th All Union Conf. Neutron Physics, Kiev, 1978, Vol. 2, p. 103.

26. D. M. Drake, J. C. Hopkins, C. S. Young, and H. Condé, "Gamma-Ray Production Cross Sections for Fast Neutron Interactions with Several Elements," Nucl. Sci. Eng. 40, 194 (1970).

27. E. D. Arthur, "Improvements of the Fission Channel in COMNUC," in Los Alamos National Laboratory report LA-9262-PR, p. 9 (March 1982).

28. C. L. Dunford, "A Unified Model for Analysis of Compound Nucleus Reactions," Atomics International Report AI-AEC-12931 (1970).

29. E. D. Arthur, "Use of the Statistical Model for the Calculation of Compound Nucleus Contribution to Inelastic Scattering on Actinide Nuclei," presented at Specialists' Meeting on "Fast Neutron Scattering on Actinide Nuclei," November 1981, OECD, Paris, France.

30. A. Gilbert and A. G. W. Cameron, "A Composite Nuclear Level Density Formula with Shell Corrections," Can. J. Physics 43, 1446 (1965).

31. H. C. Britt, "Experimental Survey of the Potential Energy Surfaces Associated with Fission," Proc. Int. Conf. on Physics and Chemistry of Fission, Jülich, Germany, 1979, 1 AEA-SM-241/A1, Vol. 1, p. 3 (1980).

32. A. S. Jensen, "Recent Developments in the Theory of the Nuclear Level Density," Proc. Int. Conf. Neutron Phys. and Nucl. Data, Harwell, England, 1978, p. 378.

33. A. Gavron, H. C. Britt, P. D. Goldstone, and J. B. Wilhelmy, "Complexity of the Potential-Energy Surface for Fission of ^{238}U," Phys. Rev. Lett. 38, 1457 (1977).

34. E. D. Arthur, "Determination of Deformed Optical Model Parameters for Neutron Reactions on ^{235}U and ^{239}Pu," in Los Alamos National Laboratory report LA-8874-PR, p. 15 (July 1981).

35. G. Haouat, Ch. Lagrange, J. Lachkar, J. Jary, Y. Patin, and J. Sigaud, "Fast Neutron Scattering Cross Sections for Actinide Nuclei," Proc. Int. Conf. Nucl. Cross Sections for Technology, 1980, NBS Special Publication 594, p. 672.

36. A. B. Smith and P. T. Guenther, "On Neutron Inelastic-Scattering Cross Sections of ^{232}Th, ^{233}U, ^{235}U, ^{238}U, ^{239}Pu and ^{240}Pu," Argonne National Laboratory report ANL/NDM-63 (January 1982).

37. R. C. Thompson, J. R. Huizenga, Th. W. Elze, "Collective States in ^{233}U, ^{235}U, ^{237}Np, and ^{239}Pu Excited by Inelastic Deuteron Scattering," Phys. Rev. C-13, 638 (1976).

38. D. G. Madland and P. G. Young, "Neutron-Nucleus Optical Potential for the Actinide Region," Proc. Int. Conf. Neutron Physics and Nuclear Data, 1978, p. 349.

39. Th. W. Elze and J. R. Huizenga, "Collective States of ^{232}Th, ^{238}U, and ^{242}Pu," Nucl. Phys. A 187, 545 (1972).

40. D. K. Olsen, G. L. Morgan, and J. W. McConnell, "Measurement of ^{238}U-(n,n'γ)U Cross Sections," Proc. Int. Conf. Nucl. Cross Sections for Technology, 1980, NBS Special Publication 594, p. 677.

41. A. Mittler, G. P. Couchell, W. A. Schier, S. Ashar, J. H. Chang, and A. T. Y. Wang, "Neutron Inelastic Scattering Cross Sections of ^{238}U via (n,n'γ)," Proc. Int. Conf. Nucl. Cross Sections for Technology, 1980, NBS Special Publication 594, p. 680.

42. D. G. Madland and J. R. Nix, "New Calculation of Prompt Fission Neutron Spectra and Average Prompt Neutron Multiplicities," Los Alamos pre-print LA-UR-81-2968 (October 1, 1981); accepted for pub. in Nucl. Sci. Eng.

43. D. G. Madland, "New Fission Neutron Spectrum Representation for ENDF," in Los Alamos National Laboratory report LA-9285-MS (ENDF-321) (May 1982).

44. D. G. Madland, "Calculation of the Prompt Neutron Spectrum and $\bar{\nu}_p$ for the Spontaneous Fission of ^{252}Cf," Trans. Am. Nucl. Soc. 38, 649 (1981).

45. A. H. Wapstra and K. Bos, "The 1977 Atomic Mass Evaluation," Atomic Data and Nuclear Data Tables 19 , 177 (1977).

46. W. D. Myers, Droplet Model of Atomic Nuclei (IFI/Plenum Data Co., New York, 1977).

47. P. Möller and J. R. Nix, "Atomic Masses and Nuclear Ground-State Deformations Calculated with a New Macroscopic-Microscopic Model," Atomic Data and Nuclear Data Tables 26, 165 (1981).

48. R. L. Walsh and J. W. Boldeman, "Fine Structure in the Neutron Emission $\nu(A)$ from ^{252}Cf Spontaneous Fission Fragments," Nucl. Phys. A276, 189 (1977).

49. R. E. MacFarlane, D. W. Muir, R. M. Boicourt, "Resonance Reconstruction in NJOY," in Los Alamos National Laboratory report LA-9262-PR, pp. 32-38 (March 1982).

50. R. E. MacFarlane, "An Improved Calculation of Heating and Radiation Damage," in Los Alamos National Laboratory report LA-8874-PR, pp. 22-23 (July 1981).

51. R. E. MacFarlane, "ENDF/B-IV and -V Cross Section Libraries for Thermal Power Reactor Analysis," Proc. Int. Conf. on Nucl. Cross Sections for Technology, Knoxville, Tennessee, October 1979 (Nat. Bureau of Standards Publication 594, September 1980).

52. D. W. Muir and R. J. LaBauve, "COVFILS - A 30-Group Covariance Library Based on ENDF/B-V," Los Alamos National Laboratory report LA-8733-MS (ENDF-306) (March 1981).

53. R. D. O'Dell, "Standard Interface Files and Procedures for Reactor Physics Codes, Version IV," Los Alamos Scientific Laboratory report LA-6941-MS (September 1977).

54. R. E. MacFarlane, D. W. Muir, and R. M. Boicourt, "The NJOY Nuclear Data Processing System, Volume II: The NJOY, RECONR, BROADR, HEATR, and THERMR Modules," Los Alamos National Laboratory report LA-9303-MS (ENDF-324) (May 1982).

55. R. D. O'Dell, "Standard Interface Files and Procedures for Reactor Physics Codes, Version IV," Los Alamos Scientific Laboratory report LA-6941-MS (September 1977).

56. F. G. Perey, "The Data Covariance Files for ENDF/B-V," Oak Ridge National Laboratory report ORNL/TM-5938 (ENDF-249) (1977).

57. R. Kinsey, "ENDF-102, Data Formats and Procedures for the Evaluated Nuclear Data Files, ENDF," Brookhaven National Laboratory report BNL-NCS-50496 (ENDF-102) 2nd Ed. (ENDF/B-V) (1979).

58. P. G. Young, "Variance-Covariance Analysis of n + ^{7}Li Reactions, in Los Alamos National Laboratory report LA-8874-PR, pp. 2-10 (July 1981).

59. R. J. LaBauve, D. C. George, and D. G. Madland, "S-n Calculations for D-20 Sphere," in Los Alamos National Laboratory report LA-8874-PR, pp. 31, 37 (July 1981).

60. D. G. Madland, R. J. LaBauve, R. E. MacFarlane, and P. G. Young, "New Fission Neutron Spectrum Representation of Evaluated Nuclear Data Files," Los Alamos National Laboratory report LA-9060-PR, pp. 15, 19 (December 1981).

61. R. J. LaBauve, D. G. Madland, R. E. MacFarlane, P. G. Young, and R. M. Boicourt, "Integral Cross Sections in Three Representations of the Cf-252 Spontaneous Fission Spectrum," in Los Alamos National Laboratory report LA-9060-PR, pp. 23, 33 (December 1981).

62. R. J. LaBauve, D. G. Madland, L. Stewart, and R. M. Boicourt, "Comparisons of Integral Cross Sections Calculated in Several Representations of the U-235 Thermal and Cf-252 Spontaneous Fission Spectra with Experiment," in Los Alamos National Laboratory report LA-9262-PR, pp. 42-45 (March 1982).

63. R. J. LaBauve and D. G. Madland, "Comparison of Measured and Calculated Integral Cross Sections for the Thermal Fission Spectrum of U-235," presented at June 1982 ANS mtg., Los Angeles, CA.

64. J. A. Grundl, "A Study of Fission-Neutron Spectra with High-Energy Activation Detectors. Part II: Fission Spectra," Nucl. Sci. Eng. 31, 191-206 (1968).

65. B. A. Magurno, "Status of the Dosimetry File for ENDF/B-V," Proc. Advisory Group Mtg. Nuclear Data for Reactor Dosimetry, INDC(nds)-103M, (Nuclear Data Section 1, Int. Atomic Energy Agency, 1979), p. 1.

66. J. M. Adams, "Comparisons of U-235 and Pu-239 Fast Neutron Fission Spectra," NEANDC(UK)170L/NEACRP L176 (1977).

67. T. R. England, W. B. Wilson, R. E. Schenter, and F. M. Mann, "Aggregate Delayed Neutrons and Spectral Calculations Using Preliminary Precursor Data Evaluated for Inclusion in ENDF/B-VI," Symp. on Beta-Delayed Neutron Emission at 183rd Annual Mtg. Am. Chem. Soc., Las Vegas, Nevada, April 1982.

68. S. A. Cox, "Delayed Neutron Data - Review and Evaluations," Argonne National Laboratory report ANL/NDM-5 (April 1984).

69. T. R. England, R. E. Schenter, and F. Schmittroth, "Delayed Neutron Calculations using ENDF/B-V Data," Proc. ANS/APS Int. Conf. Nucl. Cross Sections for Technology, Knoxville, Tennessee, October 1979, NBS Special Publication 594, issued September 1980.

70. Letter transmitting delayed neutron spectra data (G. Rudstam to T. R. England, September 21, 1981) used in G. Rudstam, "Six-Group Representation of the Energy Spectra of Delayed Neutrons from Fission," Nucl. Sci. Eng. 80, 238-255 (February 1982).

71. F. M. Mann, C. Dunn, and R. E. Schenter, "Beta Decay Properties from a Statistical Model," Trans. Am. Nucl. Soc. 39, 880 (1981). [See also Phys. Rev. C 25, No. 1, 524 (January 1982).]

72. R. J. Tuttle, "Delayed-Neutron Data for Reactor-Physics Analysis," Nucl. Sci. Eng. 56, 37-71 (1975).

73. J. K. Dickens, T. A. Love, J. W. McConnell, J. F. Emery, K. J. Northcutt, and R. W. Peelle, "Delayed Beta- and Gamma-Ray Production Due to Thermal-Neutron Fission of ^{235}U, Spectral Distributions for Times After Fission Between 2 and 14 000 sec: Tabular and Graphical Data," Oak Ridge National Laboratory report NUREG/CR-0162, ORNL/NUREG-39 (August 1978).

74. J. K. Dickens, T. R. England, T. A. Love, J. W. McConnell, J. F. Emery, K. J. Northcutt, and R. W. Peelle, "Delayed Beta- and Gamma-Ray Production Due to Thermal-Neutron Fission of ^{239}Pu: Tabular and Graphical Spectral Distributions for Times After Fission Between 2 and 14 000 sec," Oak Ridge National Laboratory report NUREG/CR-1172, ORNL/NUREG-66 (January 1980).

75. J. L. Yarnell and P. J. Bendt, "Decay Heat from Products of ^{235}U Thermal Fission by Fast-Response Boil-Off Calorimetry," Los Alamos Scientific Laboratory report LA-NUREG-6713 (September 1977).

76. J. L. Yarnell and P. J. Bendt, "Calorimetric Fission Product Decay Heat Measurements for ^{239}Pu, ^{233}U, and ^{235}U," Los Alamos Scientific Laboratory report NUREG/CR-0349, LA-7452-MS (September 1978).

77. E. T. Jurney, P. J. Bendt, and T. R. England, "Fission Product Gamma Spectra," in Los Alamos Scientific Laboratory report LA-7620-MS (January 1979).

78. Fission-Product Decay Library of the Evaluated Nuclear Data File, Version V (ENDF/B-V). [Available from and maintained by the National Nuclear Data Center (NNC) at Brookhaven National Laboratory.] NOTE: spectral files in these compilations are based primarily on data evaluated at INEL.

79. R. J. LaBauve, T. R. England, D. C. George, "Integral Data Testing of ENDF/B Fission Product Data and Comparisons of ENDF/B With Other Fission Product Data Files," in Los Alamos National Laboratory report LA-9090-MS, (ENDF-320), (December, 1981).

80. T. R. England, R. Wilczynski, and N. L. Whittemore, "CINDER-7: An Interim Report for Users," Los Alamos Scientific Laboratory report LA-5885-MS (April 1976). [CINDER-10, the version used in this report is unpublished; it is described in Los Alamos Scientific Laboratory report LA-6472-PR, p. 60 (1976) and in Los Alamos Scientific Laboratory report LA-6266-PR, p. 13 (1976).]

81. R. J. LaBauve, T. R. England, D. C. George, and M. G. Stamatelatos, "The Application of a Library of Processed ENDF/B-IV Fission-Product Aggregate Decay Data in the Calculation of Decay-Energy Spectra," Los Alamos Scientific Laboratory report LA-7483-MS (September 1978).

82. R. J. LaBauve, D. C. George, and T. R. England, "FITPULS, A Code for Obtaining Analytic Fits to Aggregate Fission-Product Decay-Energy Spectra," Los Alamos Scientific Laboratory report LA-8277-MS (March 1980).

83. R. T. Perry and W. B. Wilson, "The (α,n) Neutron Production by Alpha Particles in PuO_2, UO_2, and Th_2 Fuels," in Los Alamos Scientific Laboratory report LA-8524-PR, p. 20 (September 1980).

84. J. K. Bair and H. B. Willard, "Level Structure in Ne^{22} and Si^{30} from the Reactions $O^{18}(\alpha,n)Ne^{21}$ and $Mg^{26}(\alpha,n)Si$," Phys. Rev. 128, 299 (1962).

85. J. K. Bair and F. X. Haas, "Total Neutron Yield from the Reactions $^{13}C(\alpha,n)^{16}O$ and $^{17}\,^{18}O(\alpha,n)^{20}\,^{21}Ne$," Phys. Rev. C7, 1356 (1973).

86. J. K. Bair and J. Gomez del Campo, "Neutron Yields from Alpha-Particle Bombardment," Nucl. Sci. Eng. 71, 18 (1979).

87. L. F. Hansen, J. D. Anderson, J. W. McClure, B. A. Pohl, M. L. Stelts, J. J. Wesolowski, and C. Wong, "The (α,n) Cross Sections on ^{17}O and ^{18}O Between 5 and 12.5 MeV," Nucl. Phys. A98, 25 (1967).

88. P. A. Ombrellaro and D. L. Johnson, "Subcritical Reactivity Monitoring: Neutron Yields from Spontaneous (α,n) Reactions in FFTF Fuel," Hanford Engineering Development Laboratory report HEDL TME 78-39 (June 1978).

89. J. F. Ziegler, Helium Stopping Powers and Ranges in All Elemental Matter, Vol. 4 of The Stopping and Ranges of Ions in Matter Series (Pergamon Press, New York, 1977).

90. L. C. Northcliffe and R. F. Schilling, "Range and Stopping Power Tables for Heavy Ions," Nucl. Data Tables A7, 233 (1970).

91. D. L. Lessor and R. E. Schenter, "Neutron Spectra From (α,n) Reactions in Plutonium Compounds Calculated from Hauser-Feshbach Reaction Theory," Battelle Pacific Northwest Laboratories report BNWL-B-109 (June 1971).

92. R. Kinsey, Ed., "Data Formats and Procedures for the Evaluated Nuclear Data File, ENDF," Brookhaven National Laboratory report ENDF-102, p. 5.4 (October 1979).

93. D. G. Madland, "Calculation of Watt Distribution Parameters for Spontaneous and Neutron-Induced Fission," in Los Alamos National Laboratory report LA-8757-PR, p. 17 (March 1981).

94. D. G. Madland, "Calculation of Prompt Fission Neutron Spectra for $^{242}Pu(sf)$ and $^{252}Cf(sf)$," in Los Alamos National Laboratory report LA-8757-PR, p. 16 (March 1981).

☆U.S. GOVERNMENT PRINTING OFFICE: 1982-0-576-020/134

Printed in the United States of America
Available from
National Technical Information Service
US Department of Commerce
5285 Port Royal Road
Springfield, VA 22161

Microfiche (A01)

Page Range	NTIS Price Code	Page Range	NTIS Price Code	Page Range	NTIS Price Code	Page Range	NTIS Price Code
001-025	A02	151-175	A08	301-325	A14	451-475	A20
026-050	A03	176-200	A09	326-350	A15	476-500	A21
051-075	A04	201-225	A10	351-375	A16	501-525	A22
076-100	A05	226-250	A11	376-400	A17	526-550	A23
101-125	A06	251-275	A12	401-425	A18	551-575	A24
126-150	A07	276-300	A13	426-450	A19	576-600	A25
						601-up*	A99

*Contact NTIS for a price quote.

Los Alamos